Synchronization and Control of Chaotic Systems. Spatio-Temporal Structures and Applications to Communications.

Universidad de Santiago de Compostela
Departamento de Fisica de la Materia Condensada
Grupo de Fisica No Lineal
Inés Pérez Mariño

Junio 1999

Acknowledgements

El trabajo descrito en esta memoria constituye el resultado de1 esfuerzo realizado durante casi cinco años de investigatión, en los cuales se han visto involucradas, en mayor o menor medida, muchas personas a las que me gustaría darles las gracias.

En primer lugar, expresar mi agradecimiento a los directores de este trabajo: al Prof. Vicente Perez Villar, por admitirme en su grupo y brindarme así la oportunidad de introducirme en el mundo de la investigación, y al Prof. Vicente Perez Munuzuri, por encarrilar mi trabajo dejandome al mismo tiempo investigar libremente, por confiar siempre en mis posibilidades y por sus siempre atinados consejos.

Al Prof. Celso Grebogi por considerarme una más en su grupo de caos de la Universidad de Maryland en College Park, su orientación y guia en mi trabajo. También agradezco al Prof. Epa Rosa nuestras provechosas discusiones y todas las horas que me ha dedicado con sus comentarios. La experiencia de haber trabajado con ellos result6 y continua siendo altamente fructifera.

Al Prof. Manuel Matías de la Universidad de Salamanca, con quien he colaborado en gran medida durante mis primeros años de investigación, y a quien agradezco las importantes aportaciones teóricas que han dado lugar a buena parte de esta tesis. También me gustaría mencionar a Esteban Sanchez por su colaboración en el montaje experimental de este trabajo.

A Nieves, con quien he trabajado muy directamente, que siempre ha estado a mi lado ayudándome y apoyandome en todo lo posible, con la que he pasado muy buenos momentos y compartido algunas preocupaciones. A Diego, con quien he comentado muchas ideas y dudas durante este último año.

A Hector, Carlos y Monica, por las horas dedicadas al laboratorio de electronica para conseguir que los circuitos funcionaran lo mejor posible.

A mis compaiieros de1 grupo de Fisica No Lineal: Moncho, Alberto, Julio, Maite, Juan, Pedro, Chus, Manuel, Irene, Ivan, Adolfo, Bea y Edu, que con su buen humor han creado siempre un ambiente de trabajo muy agradable.

A muchos otros compañeros de la Universidad de Santiago y, en especial, a Pili,

Angel y Encina, que siempre han estado ahí para escucharme y con los que he compartido muy buenos ratos.

A los que durante meses fueron mis companeros en College Park: Carl, Takashi, Murilo, y, particularmente, a Antonio, Santi y Mit, que siempre estuvieron dispuestos a ayudarme y a escuchar mis dudas y preocupaciones.

Al grupo de Serial y Sistemas de Comunicaciones de la Universidad de A Coruña, por permitirme usar su laboratorio de informatica.

A Joaquin, a quien más he dado la vara de todos, por toda la paciencia que ha tenido conmigo y con la tesis, que ha estado a mi lado en las duras y en las maduras, ofreciendome su cariño, sus consejos y su apoyo incondicional.

Y, como no, agradecer a mi familia, siempre presente, todo su apoyo y cariño durante estos años.

Abstract

The field of dynamical systems and especially the study of chaotic systems has been considered as one of the important breakthroughs in science in this century. While this area is still relatively young, there is no question that it is becoming more and more important in a variety of scientific disciplines. Thus, this work starts with an historical overview about nonlinear dynamics and chaotic behavior (Chapter 1) that introduces the motivation for the results presented in the subsequent chapters.

The first part of the present thesis (Chapter 2 and Chapter 3) is devoted to the phenomenon of synchronization among coupled chaotic systems. This topic results very interesting since it could appear to be almost in contradiction with the definition of chaos which includes the rapid decorrelation of nearby orbits due to the instabilities throughout the phase space. In particular, Chapter 2 is devoted to show different categories of connections among identical chaotic systems that can lead to synchronized motions of the oscillators, and in Chapter 3 we analyze the stability of the global synchronized state in open linear arrays or in rings of chaotic oscillators. We will also pay attention to some stable spatio-temporal structures (periodic rotating waves and chaotic rotating waves) that can arise when a instability appears in the global synchronized state of a ring of chaotic oscillators. The interaction between these structures when two rings are interconnected is investigated as well. Numerical simulations have been carried out with assemblies of Lorenz oscillators and Chua's oscillators, whereas experiments have been carried out in a board of Chua's oscillators.

The second part of the thesis (Chapter 4 and Chapter 5) deals with possible applications of chaotic systems to the communications field. In Chapter 4 we show some advantageous features that chaotic behavior can incorporate to conventional digital communication systems and some different schemes that have already been proposed. In Chapter 5 we introduce a simple control technique to encode binary sequences of information in a chaotic Lorenz waveform as well as two different methods to reconstruct damaged parts of this chaotic waveform when it is transmitted through a communication channel. Both methods exploit the redundancy provided

by the determinism of chaotic signals. Finally, it is shown how these reconstruction methods allow not only to reconstruct damaged parts of the transmitted signal but they can also be used to increase the rate of the information transmission by means of a time division multiplexing scheme.

Finally, in Chapter 6, conclusions and outlooks of this work are presented.

Contents

List of Figures

List of Tables

Chapter 1

Introduction.

Isaac Newton brought to the world the idea of modeling the motion of physical systems with equations. It was necessary to invent calculus along the way, since fundamental equations of motion involve velocities and accelerations, which are derivatives of position. His greatest single success was his discovery that the motion of the planets and moons of the solar system resulted from a single fundamental source: the gravitational attraction of the bodies. The circular, elliptical, and parabolic orbits of astronomy were no longer fundamental determinants of motion, but approximations to laws specified with differential equations. Subsequent generations of scientists extended the method of using differential equations to describe how physical systems evolve. Such sets of equations are called dynamical systems. The theory of dynamical systems describes phenomena that are common to physical and biological systems throughout science. It has benefited greatly from the collisison of ideas from mathematics and these sciences. The goal of scientists and applied mathematicians is to find nature's unifying ideas or laws and to fashion a language to describe these ideas.

A very active research field in modern physics is that of nonlinear dynamics and, more recently, the subfield of chaotic dynamics. Although chaotic dynamics had been known to exist for a long time, its importance for a broad variety of applications began to be widely appreciated only within the last decade or so. Concurrently, there has been enormous interest both within the mathematical community and among engineers and scientists. The field continues to develop rapidly in many directions, and its implications continue to grow.

Chaotic dynamics may be said to have started at the turn of the century with the work of the French mathematician Henri Poincare (1892), who discovered that certain mechanical systems whose time evolution was governed by Hamilton's equations could display chaotic motion. Poincare's motivation was partly provided by the problem of the orbits of three celestial bodies experiencing mutual gravitational attraction (e.g., a star and two planets). By considering the behavior of orbits arising from *sets* of initial points (rather than focusing on individual orbits), Poincare was able to show that very complicated (now called chaotic) orbits were possible.

Poincare's techniques were applicable to a wide variety of physical systems. Important further contributions were made by Birkhoff, Cartwright and Littlewood, Levinson, Kolmogorov and his students, among others. Some of them are: the use of the discrete dynamics as a means of understanding the more difficult dynamics arising from differential equations carried out by Birkhoff in the 1920s; curious attractors, first discovered in the solutions of *physical* differential equations by Cartwright and Littlewood and by Levinson in the 1940s; the subsequent discovery of numerous physical strange attractors; the complementary situation of persisting oscillatory, non-chaotic dynamics (Fermi-Pasta-Ulam and Kolmogorov, in the 1950s) and its relationship to chaos in conservative system (the Kolmogorov-Arnold-Moser theorem), etc.. However, at first, knowledge of the area of nonlinear dynamics remained largely confined to the mathematical community, and it had to wait until the 1950s when these ideas started to be applicated to a wide variety of disciplines, such as physics, chemistry, biology, neurology, astronomy, geophysics, meteorology, economics,.

One important year was 1963, when the meteorologist E.N. Lorenz found that even a simple set of three coupled, first order, nonlinear differential equations can lead to completely chaotic trajectories. Lorenz's paper, the general importance of which is recognized today, was also not widely appreciated until many years after its publication. He discovered one of the first examples of deterministic chaos in dissipative systems. Starting in the mid-1970s, and stimulated by the availability of digital computers, this situation rapidly changed, as the broad impact and occurrence of chaos in the sciences and engineering began to be widely recognized. It has been demonstrated that chaos is relevant to problems in fields as diverse as ecology, chemistry, fluid mechanics, solid state devices, biology, and celestial mechanics. Some important works were carried out by the physicist Feigenbaum, who have rekindled

interest in low dimensional discrete dynamical systems, and by Ruelle, Takens and Newhouse, who have played an important role in the study of deterministic chaos in hydrodynamic systems, among others. It was recognized that chaos is not an exclusive type of behavior in nonlinear systems. The motion appears to be chaotic as soon as it is locally unstable and globally bounded. In many cases, motions of such kind correspond better to the oscillatory behavior of real life systems.

More recently, the study of chaotic dynamics has entered a new phase. In addition to the original pursuits of demonstrating chaos in a wide range of situations, and studying the properties of chaotic dynamics, many researchers are interested in utilizing the basic knowledge of the theory of chaos either to analyze chaotic experimental time series data [l, 2], or else to use the presence of chaos to achieve some practical goal. Thus, the interest in studying chaotic phenomena was recently revived, when evidence was found that chaotic models describe the financial time series better than the conventional random walk models [183]. Moreover, chaotic models were reported to be useful for financial time series prediction and for trading, along with other fashionable techniques such as neural networks and genetic algorithms.

At the beginning of the present decade (1990) two different discoveries have changed the point of view of the field of nonlinear dynamics, in particular the point of view of the chaotic behavior, leading to a new perspective. The first work is related to the possibility of controlling chaos, as shown by Ott, Grebogi and Yorke [166] at Maryland, while the second one regards the practical demonstration that certain chaotic systems can synchronize, by Pecora and Carroll [174, 175] at the Office of Naval Research. Both possibilities would apparently defy common sense regarding what is known for chaotic systems, and this is related also to the fact that the words *control* and *synchronization* appear to be in contradiction with the word chaos. Controlling a system implies the imposition of some desired behavior on it, while chaotic systems are characterized by their unpredictable behavior, as determined by their sensitive dependence on the initial conditions. This latter property also implies that two identical systems would quickly uncorrelate even when purposely started with identical initial conditions, at least from a practical point of view.

The paper by Ott *et al.* [166] puts forth a strategy for controlling systems whose uncontrolled orbits are chaotic, and points out that this can be done applying small perturbations to the system. The basic idea is to determine some of the low

period unstable periodic orbits or steady states embedded in the attractor, and then use feedback to stabilize one of these, chosen as to yield improved performance. Subsequent research on control of chaos by means of the stabilization of unstable orbits has been carried out [57, 213, 100, 64, 59, 190, 230, 66, 184]. One of the earliest was the work by Ditto et al. [57] on a gravitationally buckling magnetoelastic ribbon. This was rapidly followed by Singer et al. [213] on thermally driven fluid convection, Hunt [l00] on an electrical circuit, Garfinkel et al. [64] on chaotically oscillating rabbit cardiac tissue, Gills *et al.* [66] on a laser system and Petrov *et al.* [184] on the Belousov-Zhabotinsky chemical reaction. It is also remarkable the work by Dressler and Nitsche [59] who discuss how this strategy of stabilizing unstable orbits can be implemented using delay coordinate embedding. A more complete treatment of the theory, including delay coordinates, is given in the paper by Romeiras *et al.* [190], which is based on the pole *placement technique,* well known in control theory. Another way of controlling chaos was proposed by Hayes *et al.* [88]. The idea is to control the dynamics of a chaotic oscillator so that it follows a given sequence in some associated symbolic dynamics. Since this sequence can be controlled, it can be used in the field of communications to transmit information.

The paper by Pecora and Carroll [174] considers how identical, or almost identical chaotic systems can be synchronized by a chaotic reference signal so that the two systems follow the same chaotic orbit. R. He and P.G. Vaidya [93] showed how this synchronization can be understood in many representative cases by the existence of a global Lyapunov function of the difference signals.

One possible use of the ability to synchronize chaotic systems is in secure communications [log, 32, 45, 46, 131]. The idea is to mask the information-bearing signal to be transmitted with a chaotic signal that exhibits broadband features. This is an alternative to more classical noise-masking methods, in which one uses a purely stochastic signal to mask the information to be transmitted. One should note, however, that some recent studies [210, 179] have shown that more sophisticated masking techniques should be used because otherwise the transmitted signal would be easily unmasked by using the deterministic properties of a chaotic signal.

Chapter 2

Synchronization of Coupled Chaotic Oscillators.

2.1 Synchronization of Coupled Oscillators.

Systems of discretely-coupled cells with transference of mass, energy or electric charge often serve as standard models for investigating the phenomena occurring in the transformation and transport processes in living cells, tissues, neuron networks, physiological systems and ecosystems, as well as in all forms of chemical, biochemical and biological reactors and combustion systems [83, 67, 156, 232, 233, 245, 231, 232, 123, 148, 116,49, 150]. An important and early work was carried out by Winfree [231], who discovered that a class of coupled oscillators with different internal frequencies suddenly synchronized to a common frequency when the coupling between oscillators exceeded a critical value. Winfree and others suggested that these models could give insight into the behavior of coupled biological rhythms, such as swarms of fireflies that flash in synchrony, synchronous firing of cardiac pacemaker cells, groups of women whose menstrual cycles become synchronized, etc. [232].

Coupled dynamical systems are typically synthesized from simpler, low-dimensional systems to form new and more complex organizations. This is often done with the intent of realistically modeling spatially extended systems, with the belief that dominant features of the underlying constituents will be retained. From an application point of view this building up approach can also be used to create a novel

system whose behavior is more flexible or richer than that of the constituents, but whose analysis and/or control remains tractable. These and other motivations have led to numerous studies of coupled systems in a wide range of disciplines. Even an abbreviated list of coupled oscillator references is prohibitively long. Representative works are in optical [234, 24, 165, 212], chemical [122, 16, 242], condensed matter [61, 220], biological [232, 117, 60, 150, 42], neural network [216, 120, 132, 160], and other [9, 162, 69, 33] systems.

Synchronization is a universal phenomenon that can occur when two or more nonlinear oscillators are coupled. The ability of nonlinear oscillators to synchronize with each other is a basis for the explanation of many processes of nature and, therefore, synchronization plays a significant role in science. Numerous applications in mechanics, electronics, communication, measurements, and in many other fields have shown that synchronization is extremely important in engineering. For example, in the design of microwave systems the power of many devices may be combined through synchronization so that power increases quadratically with the number of oscillators. In this case, the oscillators must have not only the same frequency, but also a small phase difference. Similar needs are found in electrical power generators, coupled lasers, Josephson junction arrays, etc. Another important application of synchronization is related to a network of clocks distributed geographically in different locations, where it is necessary to have the same time for all clocks. For these applications, synchronization is usually achieved by using phase-locked loops [206,105]. These have become so widely used that it is rare to find a piece of electronic equipment without them. In addition to the specific synchronization applications mentioned above, more examples are found in computers, radar, television sets, communication networks, instruments for signal tracking from satellites, etc.

Usually, synchronization is understood as the ability of coupled self-excited oscillators with different frequencies to switch their behavior from the regime of independent oscillations characterized by beats to the regime of cooperative stable periodic oscillations, as the strength of coupling is increased. As a result of synchronization, the oscillators change their frequencies in such a way that these frequencies become identical or related via a rational factor. Depending upon the properties of oscillators considered, there are different explanations as to why these oscillators synchronize. For instance, one can distinguish between the mechanism for synchronization of relaxation oscillators that produce sharp pulses and the mechanism

for synchronization of oscillators that generate smooth waveforms. However, one should keep in mind that the separation of these mechanisms is not precise, and they can be considered as limiting cases of a general mechanism, where resonances and actions of dissipative forces are very important.

2.2 Synchronization of Coupled Chaotic Systems.

Chaotic phenomena arise ubiquitously in natural systems and in man-made devices. Past work has focussed mainly on the discovery and characterization of chaotic behavior ocurring in situations where there is no goal-oriented intervention, i.e., control. Recently, ideas and techniques have been proposed to utilize the rich properties of chaos to achieve certain objectives. For instance, the broad-band nature of chaotic signals makes them tempting for their use in secure communications or spread-spectrum applications. Futhermore, the fact that such signals emanate from a deterministic dynamical system lends to the hope that one will also be able to control them sufficiently for many uses. Taken as isolated systems, oscillators exhibiying a chaotic behavior chaotic appear to offer many impediments to anyone to put them to use. The willingness to make chaotic systems part of a more complex (and interesting) system opens up a new direction for the applications of chaos. These applications are best viewed as synthesis of dynamical systems.

The possibility of two or more chaotic systems oscillating in a coherent and synchronized way is not an obvious one. One of the main features associated with the definition of chaotic behavior is the sensitive dependence on initial conditions. Then one may conclude that synchronization is not feasible in chaotic systems because it is not possible in real systems to reproduce exactly identical initial conditions. Thus, even an infinitesimal deviation in any one of the parameters or initial conditions will eventually result in the divergence of nearby starting orbits. In this context, the fact of achieving synchronization of chaotic systems through suitable coupling can be considered as a fascinating concept.

Over the last decade, a number of different types of synchronization have appeared: identical synchronization [174], phase synchronization [124, 193], lag synchronization [194], and generalized synchronization [200, 201], to mention only a few. This is in addition to the classic examples of synchronization in periodic

systems [20]. Many of these have been experimentally observed in a single system [223]. Synchronization is often categorized on the basis of whether the coupling mechanism is uni-directional or bi-directional. Stable synchronization with uni-directional coupling has been called synchronization by an external force (for frequency synchronization) and master-slave synchronization (Pecora and Carroll [174]). It has recently been shown that, if the synchronized systems are identical then there is no essential difference between uni-directional and bi-directional synchronization [103].

The phenomenon of synchronization of identical or nearly identical *chaotic* systems coupled in an array has recently received a great deal of attention [119, 104, 94, 234, 182, 14, 157, 96, 237, 97, 65, 176, 225, 128, 112, 238, 47, 142, 145] although the behavior was shown to exist some years ago, both theoretically and experimentally [63, 239, 6, 229, 234, 198, 196, 174]. Chaotic synchronization of two continuous-time dynamical systems was experimentally discovered in 1985 [5] at both identical and slightly different system parameters. After a rather general definition of synchronized chaos was given by Afraimovich [6], which includes the case of nonidentical oscillations, a number of analytical, experimental and numerical results about stability of synchronized chaotic oscillations and self-oscillations were obtained for coupled nonlinear oscillators with periodic forcing [6, 228], Lorenz's equations [227], electronic circuits [11, 229],. ...

The two seminal papers, *Controlling Chaos* by Ott, Grebogi and Yorke (OGY) [166] and Sy*nchronization in Chaotic Systems* by Pecora and Carroll [174], published in the year 1990 opened up a wide range of applications outside the traditional scope of chaos and nonlinear dynamics research. Both papers immediately received a great deal of attention, and led to the establishment of two active areas of research [209, 58, 35, 101, 195, 169]: synchronization and control of chaotic systems. Synchronization is in many ways related to control [1]. The two ideas of synchronizing and controlling chaotic motions have common roots in the notion of driving a nonlinear system to restrict its motion onto a subspace of the total phase space of the dynamical system. In each case one selects parameter regimes or external forcing to achieve this collapse of the full space to a selected subspace. In controlling chaos we seek to move the free running system into more regular or more chaotic motions by adding dynamics to the original system in the form of time varying parameters or external driving of other forms. In synchronization we seek subspaces of the coupled

system space in which a special kind of motion which relates the coupled system takes place. It was known from the start that the techniques of chaos control have their origins in control theory. On the other hand, synchronization of chaos has evolved somewhat in its own right. However, recent progress [237, 115, 19] casts the problem of chaos synchronization in the framework of nonlinear control theory. This unifies the study of chaos control and chaos synchronization under the same rubric.

In the analysis of synchronized chaotic motions one has to distinguish between the instability for perturbations within the synchronization manifold [187] and transverse to it. The regime of identical chaotic oscillations is stable when the synchronized trajectories are stable for the perturbations in the transverse direction to this manifold [187]. The two most frequently used criteria for stability of synchronized chaotic motions are the Lyapunov function criterion [227, 197, 237, 7] and the analysis of transversal (conditional) Lyapunov exponents calculated from the linearized equations for the perturbations transversal to the synchronization manifold [63, 174, 15, 94]. The criterion based on the analysis of Lyapunov functions for the vector field of perturbations transversal to the manifold enables one, in some cases, to prove that all trajectories in the phase space of the coupled systems are attracted by the manifold of synchronized motions. Despite the fact that this criterion guarantees the onset of synchronization, it is not a general method since there is no procedure for constructing the Lyapunov function for an arbitrary system. In many practical cases, Lyapunov functions cannot be found, even for systems that possess a stable manifold of synchronized motions for a broad range of parameters of coupled systems, and of the coupling itself.

In contrast with Lyapunov functions, the analysis of transversal Lyapunov exponents is quite straightforward and can be easily employed, even for rather complicated systems. However, it has been pointed out [185, 14, 168, 26, 96] that, in practice, the negativeness of Lyapunov exponents does not always guarantee that there are not unstable invariant sets in the synchronous state [14] or areas on the attractor that are locally unstable [65, 176, 202], both of which can cause attractor bubbling and bursting of the system away from synchronization when there is noise or parameter mismatch. In spite of this fact, it is noticeable that the transversal Lyapunov exponents criterion may help to find a master stability function [178], which, as it has been recently proved, solves the problem of synchronous stability for any linear coupling of oscillators.

There exist several possibilities for linking chaotic systems so that they become synchronized. Thus, one can connect them by using linear diffusive coupling, as initially suggested by F'ujisaka and Yamada [63], or by driving coupling, introduced by Pecora and Carroll [174]. These two possibilities will be described in the next subsections.

2.2.1 Synchronizing Chaotic Systems by Linear Diffusive Coupling.

The linear diffusive coupling, suggested by Fujisaka and Yamada [63], was implemented in practice by a number of authors, using both mutual and unidirectional coupling [197, 182, 199, 189, 96]. In this case it is guaranteed that if one couples all the variables there is some threshold value for the coupling such that one gets synchronized behavior [94] (although the practical determination of this threshold may be subtle [96]). An important work in this context of linear diffusive coupling was carried out by Rul'kov et al. [197], who have experimentally studied the evolution of two coupled electronic circuits connected by means of a resistor R. This study was carried out not only with identical chaotic oscillators, but also when small differences between the self-oscillators exist. Synchronization can be obtained in both cases. Rul'kov et al. have demonstrated, by using dissipative coupled nonlinear circuits with individual chaotic behaviors, that the local and global stability boundaries of the synchronization regime of chaos can be located at different coupling parameters values. This is connected with the bifurcations of some attractors in the global regions of the phase space. Note that the introduction of a coupling between chaotic self-oscillators can lead not only to more complex behavior or to the synchronization of the chaotic oscillations, but also to the appearance of simple types of attractors like, for example, limit cycles. This result bears similarity with the case of coupled cell cultures of Dictyostelium amoebae suspensions [84]. The experiments showed the ocurrence of rather regular oscillations where different possible chaotic cells were coupled, providing thus a fraction of cells that behave in a periodic manner. The cells shared a common intermediate chemical which is like the resistor in Rul'kov's experiment.

Chaotic synchronization in one dimensional arrays of identical and slightly different chaotic circuits diffusively coupled has also been studied [182, 243, 50]. It

has been found that the role of the coupling is always to stabilize the system, and then synchronize it. For example, computer simulations and experimental results of an array of Chua's circuits has been carried out **[182],** considering arrays of identical and slightly different oscillators. In the first case, the oscillators synchronize and synchronize in phase, i.e, each one repeats exactly the same behavior as the rest of them. When the oscillators are not identical, they can also synchronize but not in phase with each other. The last situation is shown to form structures in the phase space of the dynamical variables.

2.2.2 Synchronizing Chaotic Systems by Driving.

If one gives some thought to communications, especially with signals whose future behavior is difficult or impossible to predict over the course of the transmission, one realizes that some sort of synchronization between sender and receiver would be very useful. Synchronizing chaotic systems seems, at first, quite problematic. Identical chaotic systems will diverge in their behavior if each one is started on a slightly different phase space point, which is surely to be the case in any real system. It is, however, possible to set up two remote chaotic systems with identical components and synchronize them by transmitting the corresponding signals from one to the other. In addition, transmission need only be one way; that is, one system is driving the other, but not vice versa. In 1990 Pecora and Carroll discovered a way to accomplish this feat that is relatively straightforward and deceptively simple [174]. They take a complete chaotic system and choose a subsystem within it. Then, they make a replica of this subsystem. The original system is called the drive and the duplicated subsystem is called the response. Figure 2.1 depicts an schematic of the drive-response system proposed by Pecora and Carroll.

The response is just like the drive except that it is missing one or more variables. The missing variables are sent from the drive to the response, inputting the variable wherever it is needed in the response system. If a *stable* response subsystem has been chosen, then the response's dynamic variables will converge to their counterparts in the drive and will remain synchronized with them (amplitude and phase always equal) as long as the drive continues to be supplied to the response (see Fig. 2.2). The key idea is to have a stable subsystem. Stability here is in the sense of Lyapunov [133]. A measure of the stability of the subsystem is given by the conditional Lyapunov

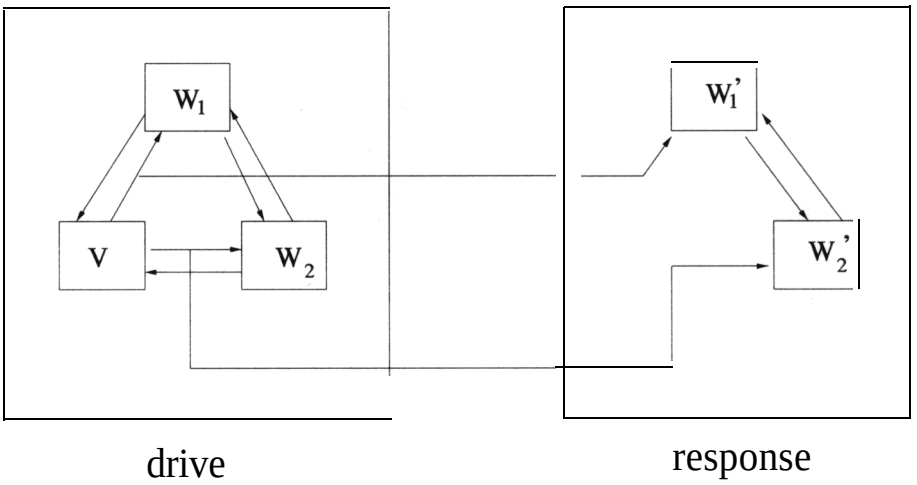

Figure 2.1: Schematic for creating a synchronizing chaotic system proposed by Pecora and Carroll.

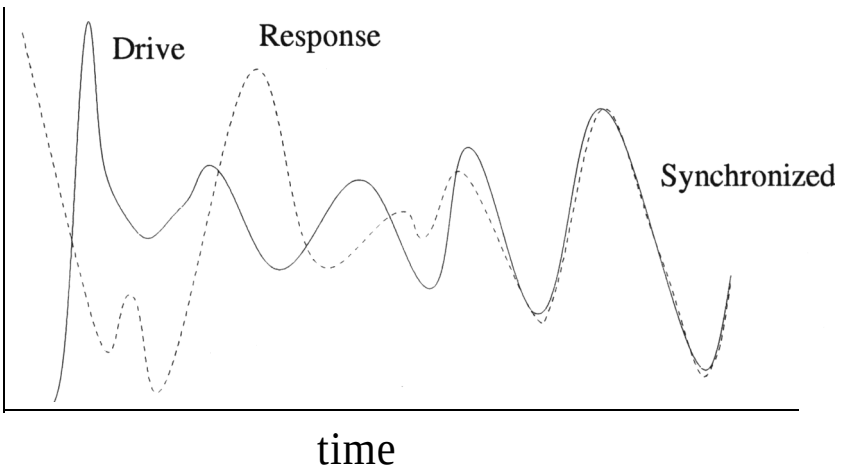

Figure 2.2: Convergence of the response to the drive.

exponents of that system [175]. These are not usually a subset of the usual Lyapunov exponents of the full system (the drive) and must be calculated separately.

It is possible to see mathematically where these conditional exponents come from. We can write the drive system of ordinary differential equations (ODE's) as $\dot{\mathbf{x}} = d\mathbf{x}/dt = \mathbf{F(x)}$. The system can be broken into two subsystems by a partition of the original vector x into two subvectors x = (v, w), where x is *n*-dimenional, w is m-dimensional, and v is n – m dimensional. Then, the original equations of motion are

$$\begin{aligned} \dot{\mathbf{v}} &= \mathbf{g}(\mathbf{v}, \mathbf{w}) \\ \dot{\mathbf{w}} &= \mathrm{h}(\mathrm{v}, \mathrm{w}) \end{aligned} \tag{2.1}$$

where **F = (g, h).** An auxiliary equation is added for the duplicated subsystem

$$\dot{\mathbf{w}}' = \mathbf{h}(\mathbf{v}, \mathbf{w}') \quad (2.2)$$

The variables of the response w' will converge to the drive values w if the difference $\mathbf{A}\mathbf{w} = \mathbf{w}' - \mathbf{w} \to \mathbf{0}$ as the entire system (drive + response) evolves. Substracting Eq. (2.1) from Eq. (2.2) we get an equation for the dynamics of **Aw** (neglecting higher order terms in **Aw)**

$$\dot{\Delta\mathbf{w}} = \mathbf{D}\mathbf{h}(\mathbf{v}, \mathbf{w})\Delta\mathbf{w} \quad \mathbf{(2.3)}$$

where **Dh** is the matrix of derivatives of **h** with respect to w. Equation (2.3) is a basic equation for much of the discussion on synchronizing chaotic systems. The conditions on stability are simple to understand using it (although they are not trivial). For example, if **Dh** is a constant over the attractor, then the solution to Eq. (2.3) is well known to be $\Delta\mathbf{w}(t) = exp(\mathbf{D}\mathbf{h}t)\Delta\mathbf{w}(0)$. Then, depending on the eigenvalues of **Dh** (assuming **Dh** is diagonalizable) **Aw** will either converge to zero (synchronization) or not (asynchronous situation).

A more robust and rigorous definition can be given in terms of the Lyapunov exponents. Namely, when the Lyapunov exponents for Eq. (2.3) are all negative, the systems will synchronize. Note that the full system for $\dot{\mathbf{x}}$ has a set of Lyapunov exponents, but the exponents for Eq. (2.3) are not usually a subset of the Lyapunov exponents of the full system. The exponents for Eq. (2.3) are called conditional Lyapunov exponents, because they depend on the drive v. Synchronization can occur only when the subsystem's Lyapunov exponents are negative. The criteria of negativity of Lyapunov exponents is a local result and does not always mean that the response will synchronize with the drive when started from any phase space point.

Cascading Synchronized Systems.

Once one gets used to the idea of breaking chaotic systems up and having one driven by other, different configurations appear possible and present some interesting prospects. One of these is the idea of cascading synchronized drive/response systems [32, 31]. Figure 2.3 shows an schematical setup for a three-dimensional dynamical system (it generalizes to any dimension) using the Pecora-Carroll method. Another response is simply added in cascaded form to the original setup of Pecora-Carroll

drive/response. Note that this requires that the drive system have two or more stable subsystems. In this case all the signals in the response systems would actually reproduce the signals in the original drive system, including the transmitted drive.

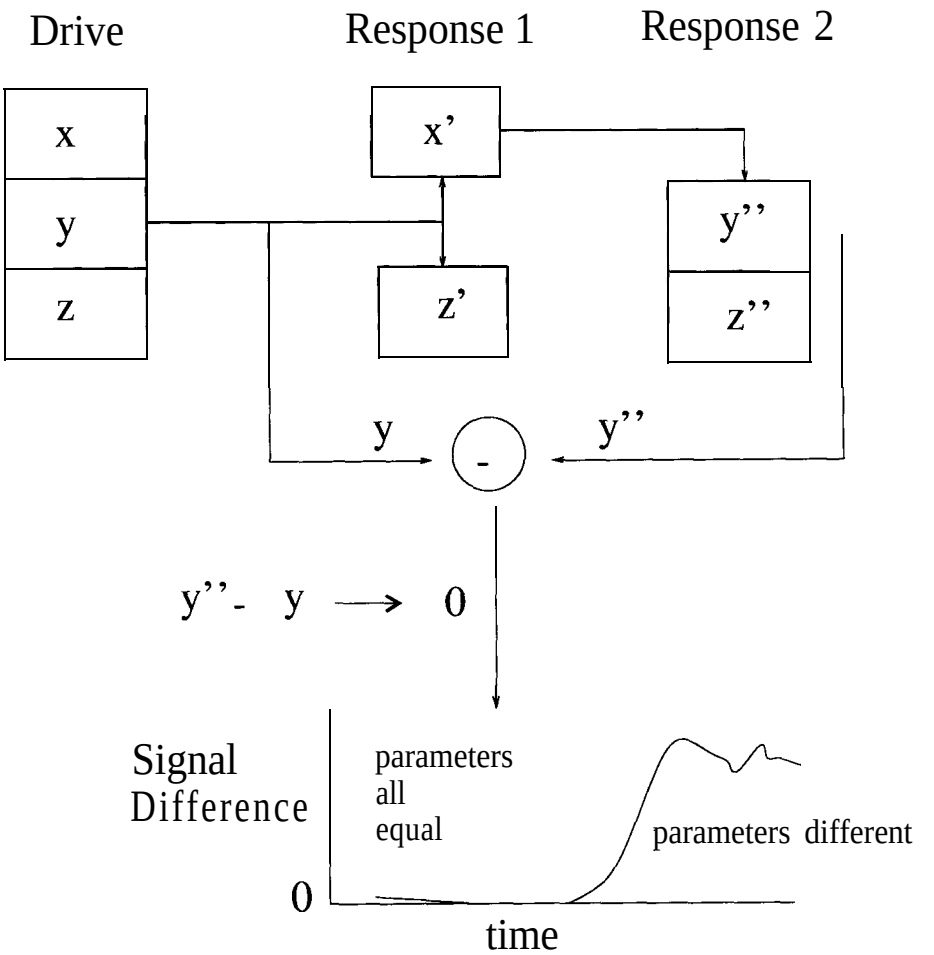

Figure 2.3: Cascading synchronized chaotic systems based on Pecora-Carroll method.

If all the parameters of the drive and cascaded responses are the same, then the reproduced signals will match their counterparts back in the drive. If the parameters in the drive or response are varied the signals in the response will not match those in the drive. These facts about signal matching suggest several possibilities for communications. One is to modulate the drive signal and compare it to the reproduction coming out the *back* end of the cascaded responses. This would allow the modulation to be detected. Another, more elegant method would be to modulate a parameter in the drive and detect it by noticing that the difference between the incoming and reproduced drive signals varies from null. One can even set up a mechanism to vary the appropiate parameter in the responses to match the drive

values as they change by keeping the drive-reproduced-drive difference to zero. Carroll **[32, 31]** has shown how to do this as well as other variations in the cascaded setup.

Another interesting variation on the cascaded setup was presented by Oppenheim et al. [164, 45], who further expanded the applications of synchronizing chaotic systems by demonstrating how synchronized chaotic systems could be used in a scheme for private communication. This scheme is also a cascading arrangement in which the original drive is reproduced in a particular system, namely the Lorenz. It turns out that this system has a great ability to clean up the incoming signal and reproduce only the original drive signal from the Lorenz system. One can take advantage of this fact and use the new clean drive to expose signals masked by the original drive or to clean out noise in the original drive channel. This is a rather remarkable result and may hold for some other cascaded arrangements. For example, Kocarev et al. [109] have applied the Oppenheim/Cuomo scheme to the double-scroll circuit.

Modified Method for Synchronizing and Cascading Chaotic Systems.

As said in the previous sections, Pecora and Carroll [174, 175] have considered the situation of unidirectional coupling, in which a chaotic signal from a drive system is used to force a second response system. In the Pecora-Carroll method a subsystem of the drive, that is common between the two systems, is used to make the response synchronize with the drive. Güémez and Matias introduced a modification of this one-way synchronization method, such that one does not need to split the system in subsystems [78, 81]. Therefore, both drive and response have the same dimensionality. The main idea behind the method is to generalize the coexistence of different signals in the same chaotic oscillator, allowing the driving signal to enter at one or more terms in the evolution equations of the response. This yields the same result obtained within the original Pecora-Carroll method with a cascade of two subsystems. The main advantage of this method is that the dynamical evolution of the driving signal in the response is not suppresed, and, thus, one can consider more general arrangements of the connected systems, such as arrays of chaotic units. Since with a single connection one has nontrivial output for all the variables, it is possible to connect many low-dimensional systems in different ways, including simultaneous connections.

Chapter 3

Synchronization of Spatio-Temporal Systems.

3.1 Introduction.

The theory of complex systems, such as neural assemblies or lattices of chaotic oscillators has generated many new problems including the synchronization or regularization of the cooperative behavior of systems consisting of chaotic elements, regular spatial patterns in chaotic lattices, and so on. Analysis of complex systems are quite novel for nonlinear dynamicists who set absolutely new problems that necessitate new approaches. As an illustration, two of such problems generated by neurophysiology can be considered. Briefly, one would like to understand the key features that make possible

- the birth of regular, predictable behavior in a complex system consisting of elements with chaotic individual dynamics, and
- the construction of fast systems from slow elements.

It no longer seems surprising that a chaotic system, which is a completely deterministic, relatively simple dynamical system is able to exhibit complex, irregular and unpredictable temporal behavior. A much more challenging issue is the apparent self-organization which comes up in some networks of such chaotic elements. It is

quite surprising how it is possible for complex systems with a large number of degrees of freedom to produce regular patterns and regular rhythms. This phenomenon is frequently encountered in biological systems where chaotic elements work together to produce functional activity associated with living animals and directed responses to sensory inputs which produce cooperative motor functions.

It has only recently been demonstrated that many oscillating neurons are dynamical systems operating in a regime which possesses low-dimensional strange attractors [8, 152, 87, 3, 29, 68]. The experimental studies and many additional modeling studies listed above merely demonstrate that the behavior of individual neurons which are part of small and large neural assemblies generate chaos. At the same time, networks of neurons, as a whole, behave in a predictable fashion. Small neural networks such as central pattern generators (CPGs) produce regular rhythmic motor patterns that control muscles. An increasing number of new experiments have appeared confirming the fact that the dynamics of neural assemblies are more regular than that of an individual neuron [141, 86]. This also appears to be the case for neurons in the human cortex [28], where structures consisting of a large number of neurons coupled *all-to-all* play the role of individual elements in the assembly.

It is important to clarify that this regular behavior is not the most common behavior that can arise when chaotic elements are coupled dissipatively. Intuition gained in the analysis of other chaotic elements coupled dissipatively such as coupled electrical oscillators, autocatalytic chemical reactions with diffusion, and so forth, suggests that the behavior of an assembly can function as a simple yet still chaotic unit [6, 30]. Indeed, the electrical coupling that is proportional to the mismatch of the variables in coupled oscillators, $\epsilon(x_1(t) - x_2(t))$ where ϵ is the magnitude of coupling, tends to drive the error signal to zero. If the dissipative coupling is strong compared to the growth rate of spreading chaotic trajectories, then the chaotic oscillators are completely synchronized and function as a unit. For weak coupling, on the other hand, the regime of chaotic synchronization $x_1(t) \equiv x_2(t)$ is unstable, and the dynamics of the pair becomes more complicated. Namely, the number of positive Lyapunov exponents is doubled, the dimension of the limiting chaotic set grows, and so forth. Such electrical (dissipative) couplings are encountered in neural networks too, although couplings through chemical synapses are more typical. Synaptic couplings exhibit the two typical nonlinear features of threshold and saturation. Such a coupling changes significantly the dynamics of spikes and

may lead to a complete suppresion of chaos [3].

As mentioned above, another very challenging problem is the understanding of the mechanism of fast operation in systems consisting of slow elements. This can be realized, in particular, in complex systems consisting of strongly nonlinear elements possesing essentially nonisochronous individual dynamics. One good example is the brain itself, that is able to perform various tasks in a short time, although the neurons on which these tasks rely are relatively slow. How is this possible?.

Neuroethological studies have identified that the specialized computational systems of some animals are able to process temporal information with a resolution that exceeds by orders of magnitude that of individual neurons. This phenomenon, called *hyperucuity* [192], is very important due to the high accuracy achieved by these animals in vital tasks. Some examples are the auditory system of the barn owl [114], the electric wave detecting system of some electric-emitting fishes [98] and the sonar system of echolocating bats [222]. The idea is that a small neural assembly may exhibit a transition to a fast collective oscillatory state that is in the desired microsecond scale.

Barn owls, *Tyto alba*, are night predators that rely almost exclusively on auditory clues to locate their preys. They are able to analyze information arriving at both ears to locate objects in azimuth and elevation, [114] through the separate analysis of interaural time differences and intensities, respectively [108,151]. This information converges then to higher stages so that owls are able to detect interaural time differences as short as 10 microseconds, that imply a resolution better than one degree in azimuth. Analogously, electric fishes of the genus *Eigenmunniu* have a very sophisticated system that they use in the so-called jamming avoidance response. These fishes use self-generated electric fields for object detection and navigation, but this system fails if another electric fish is using a similar frequency, as the superposition wave, a beat, has an almost zero amplitude for some finite time. The fish responds to this situation by shifting away its frequency using a quite sophisticated phase-comparison system, that, remarkably, can resolve time differences as small as 0.4 microseconds [192].

The open question is: which is the mechanism used by these animals to achieve this remarkable microsecond resolution from the use of slow neurons operating in the scale of miliseconds [106]?. The work developed in this chapter is based on structures

that arise from instabilities in the uniform synchronized state of small assemblies of chaotic nonlinear analog oscillators. We will see that some of these structures (called rotating waves) involve a fast collective behavior (faster than the associated to the isolated oscillators). This is a phenomenon analogous to the one that ocurrs in the real systems described above and could help to understand them a bit more.

In Section 3.2 a description of the numerical and experimental setup is presented. The nonlinear oscillators we will use to simulate assemblies of chaotic systems are the Lorenz oscillator and the Chua's oscillator. Thus, in Section 3.3 we show the results obtained when considering open linear arrays of chaotic oscillators, while Section 3.4 is devoted to circular geometries.

3.2 Setup.

3.2.1 Numerical Setup.

Different geometries of coupling chaotic oscillators are described in the next subsections. The coupling between oscillators has been chosen in such a way that yields synchonization when two oscillators are considered. As it was said before, the nonlinear oscillators chosen for the computer simulations have been the Lorenz oscillator and the Chua's oscillator (see Appendix A), two classical paradigms for chaotic behavior. These two dynamical systems have played a prominent role in the modeling, investigation and understanding of new dynamic nonlinear phenomena, especially chaotic behavior [127, 40].

The purpose of Lorenz was to analyze the unpredictable behavior of the weather. He first expanded a set of nonlinear partial differential equations (Navier-Stokes equation under Boussinesq approximation) by Fourier transformations and then truncated them by retaining only three modes [126, 224]. The resulting equations are generally called the Lorenz equation, which in dimensionless form is represented by the following third-order ordinary differential equations

$$\begin{aligned} \dot{x} &= \sigma(y - x) \\ \dot{y} &= R x - y - x z \\ \dot{z} &= x y - b z, \end{aligned} \tag{3.1}$$

where, roughly speaking, the variable x measures the rate of convective overturning, the variable y measures the horizontal temperature variation, and the variable z measures the vertical temperature variation. The parameters σ and R are proportional to the Prandtl and the Rayleigh number, respectively.

Although the origin of the Lorenz equation is in the meteorological field, many authors have derived Eq. (3.1) from other physical systems: Haken has used the Lorenz equation to model the irregular spiking phenomena in lasers [82]. Malkus and Yorke to study the problem of convection in a toroidal region [135, 241], Knobloch has derived that equation from a disc dynamo [107], Pedlosky and Frenzen from a study of the dynamics of a weakly unstable, finite amplitude, baroclinic wave (two-layer model). The Lorenz equation has also been used to describe the dynamics of the simplest laser model (e.g. the Shimizu-Morioka System [208]).

On the other hand, Chua's aim [39] was to actually build a real physical electronic circuit capable of reproducing chaotic phenomena previously known from different analytical models, including the Lorenz equation. To simplify practical considerations and to provide rigorous mathematical proof of the existence of a chaotic attractor in Chua's circuit, Chua chose a 33segment piecewiselinear function of one variable as the nonlinearity in Chua's equation (see Appendix A), in contrast to Lorenz, who had needed two polynomial functions of two variables as the nonlinearity in the Lorenz equation (see Eq. (3.1)). It is because of its simplicity, robustness, and low cost that Chua's circuit has become a favorite tool for analytical, numerical and experimental study of chaos. Notice that it became the first real physical object in which chaos was proved analytically [36, 37], numerically [134], as well as experimentally [244].

Lorenz Oscillator.

We are going to consider an array of N identical Lorenz oscillators coupled through partial unidirectional injection of a signal produced by one oscillator into the next one [78], either forming an open linear geometry or a closed loop. Thus, the dynamical behavior of each Lorenz system is governed by the following set of dimensionless differential equations,

$$\left.\begin{aligned} \dot{x}_j &= \sigma(y_j - x_j) \\ \dot{y}_j &= R\bar{x}_j - y_j - x_j z_j \\ \dot{z}_j &= x_j y_j - b\ z_j \end{aligned}\right\} \quad j = 0, \ldots, N-1\ , \tag{3.2}$$

where the coupling enters through $\overline{x}_j$, defined as $\overline{x}_j = x_{j-1}$, with $\overline{x}_0 = x_0$ in the case of an open linear array and with $\overline{x}_0 = x_{N-1}$ in the case of a circular one. An illustration about the influence of the variables of one oscillator on the following one is shown in Fig. 3.1, in which the dashed line has sense only when considering a ring geometry.

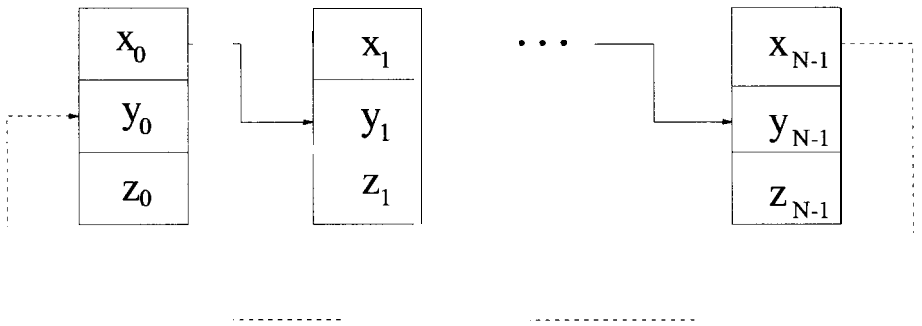

Figure 3.1: Influence of the variables of one Lorenz oscillator on the following one in the array. The dashed line corresponds to a ring geometry.

The values of the parameters are the standard ones, namely, (a, R, b) = (10,28,8/3). In this way, for any set of initial conditions all Lorenz systems are in a chaotic regime when they are uncoupled. The set of equations (3.2), together with suitable boundary conditions are integrated by using a stable fixed-step fourth-order Runge-Kutta method with a stepsize of At = 0.001 time units (t.u.). The isolated systems are allowed to evolve without coupling for an amount of time such that the system dynamics take place in the chaotic attractor. Then, the oscillators are connected in the form described by Eq. (3.2).

Chua's Oscillator.

We are also going to consider arrays of chaotic Chua's systems [134] that are coupled through driving, in particular, through the variant of the Pecora-Carroll method [174] introduced by Güémez and Matías [78]. This way of coupling will be used for open linear arrays as well as for closed loops.

The dynamics of an array with N units can be modeled by a system of 3N first-order autonomous nonlinear differential equations, that in explicit resealed

dimensionless form (including coupling) are written as,

$$\left.\begin{aligned} \dot{x}_j &= \alpha[y_j - x_j - f(\overline{x}_j)] \\ \dot{y}_j &= x_j - y_j + z_j \\ \dot{z}_j &= -\beta\, y_j - \gamma z_j \end{aligned}\right\} \quad j = 0, \ldots, N-1 \tag{3.3}$$

where $\alpha = C_2/C_1$, $\beta = C_2/(L G^2)$, and $\gamma = (C_2 r_0)/(L\ G)$. The three-segment piecewise-linear characteristic of the nonlinear resistor (Chua's diode) is given by,

$$f(x) = \left\{ bx + \frac{1}{2}(a-b)[|x+1| - |x-1|] \right\} \tag{3.4}$$

where a and b are the slopes of the inner and outer regions, respectively, of $f(x)$. Driving is introduced through $f(\overline{x}_j)$, and $\overline{x}_j = x_{j-1}$ for $j \neq 0$, while for $j = 0$ and depending on the type of arrangement, one has $\overline{x}_0 = x_0$ for open linear arrays, while for closed loops $\overline{x}_0 = x_{N-1}$. Figure 3.2 illustrates the influence of the variables of one oscillator on the following one for the case of an open linear array as well as for a ring geometry of Chua's circuits.

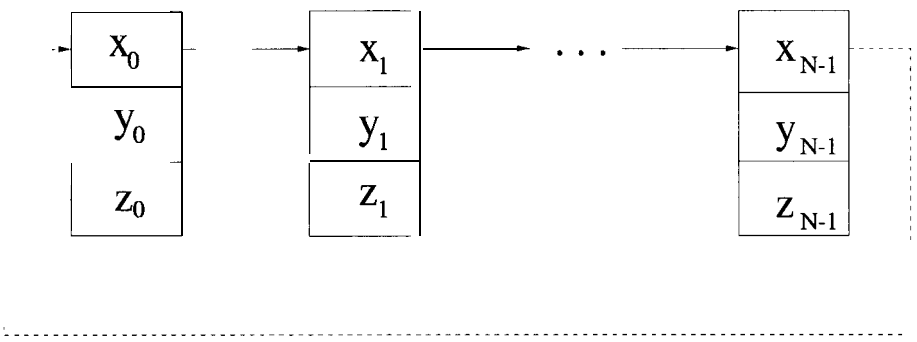

Figure 3.2: Influence of the variables of the circuits on the following ones for an array of Chua's oscillators coupled in an open linear geometry and in a closed loop. In the latter case the variables of the last circuit affect the dynamics of the first one. This influence is represented by the dashed line.

Apart from studying the behavior of an isolated array of Chua's circuits, either with an open linear geometry or a circular one, the interaction between two different rings of Chua's oscillators has also been considered. Two rings, each one consisting of N Chua's circuits, have been connected cell-to-cell in a diffusive way and, as before, each circuit inside each ring is coupled unidirectionally by driving through the nonlinear element. If we label with the superindex i the corresponding ring and

with the subindex j the position of each circuit inside the ring, the dynamics of each oscillator can be represented by the following dimensionless evolution equations

$$\begin{aligned} \dot{x}_j^i &= \alpha[y_j^i - x_j^i - f(\bar{x}_j^i)] + D\,(x_j^{i+1} - x_j^i) \\ \dot{y}_j^i &= x_j^i - y_j^i + z_j^i \\ \dot{z}_j^i &= -\beta\, y_j^i - \gamma\, z_j^i \end{aligned} \tag{3.5}$$

where $j = 0,..,(N-1)$ runs over the number of elements in the ring, $i = 0,1$ runs over the number of coupled rings and D represents the coupling constant between rings. Notice that the operations on the j indices and i indices are modulo N and modulo 2, respectively.

When considering two rings of oscillators coupled in the way described above, two different configurations can be obtained depending on the equal or different sense of the driving connections in each ring. Therefore, two different configurations have been analyzed,

- cells within a ring were unidirectionally coupled in the same direction as shown in Fig. 3.3: parallel coupling,

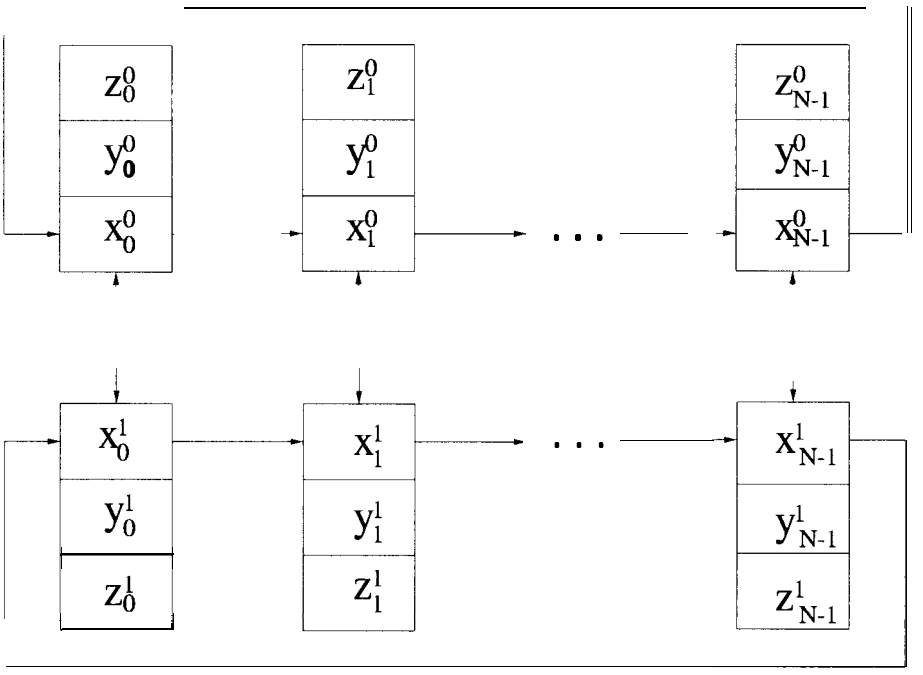

Figure 3.3: Parallel coupling.

- cells within a ring were unidirectionally coupled in opposite directions as shown in Fig. 3.4: antiparallel coupling.

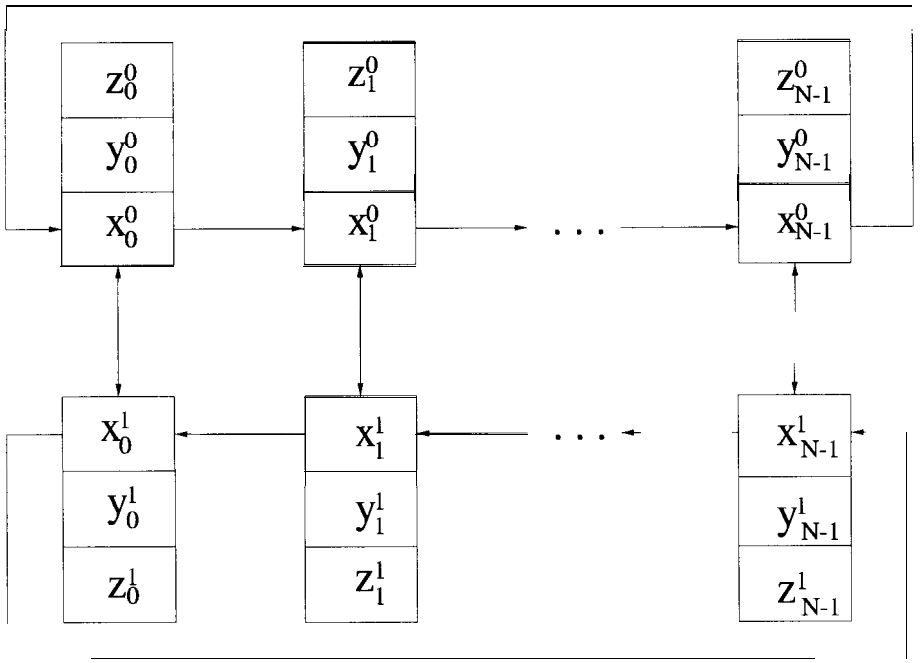

Figure 3.4: Antiparallel coupling.

Thus, for parallel coupling $\overline{x}_j^i = x_{j-1}^i$ for both $i = 0, 1$, while in the case of antiparallel coupling this variable will be different for the two rings: for one of them, say $i = 0$, $\overline{x}_j^0 = x_{j-1}^0$, while for the other one $\overline{x}_j^1 = x_{j+1}^1$.

The set of parameters used most of the time for the numerical calculations has been either $(\alpha, \beta, \gamma, a, b)$ = (10,14.87,0.06,-1.27,-0.68) or $(\alpha, \beta, \gamma, a, b)$ = (10,12.1,0.22, -1.26, -0.79). The former has been chosen because it represents the standard values and the latter because it is the set of values of the experimental setup. The set of equations (3.3), together with the suitable boundary conditions, zero-flux for linear arrays and periodic for closed loop arrays (or rings), have been integrated by using a stable fixed-step fourth-order Runge-Kutta method with a stepsize of At = 0.001 ***t.u.*** (1 ***t.u.*** = 0.1 μs for these values of the parameters). In all numerical simulations, the isolated systems have been allowed to evolve without coupling for an amount of time such that the system dynamics take place in the double-scroll (chaotic) attractor. Then, the circuits are connected with the desired topology in the form described by Eq. (3.3) or Eq. (3.5).

3.2.2 Experimental Setup.

Experiments have been performed in a board containing twenty Chua's circuits in chaotic regime. The nonlinear element of these Chua's circuits has been modified according to the design shown in Section A. 1. The components of the circuits are defined by (C_1, C_2, L, r_0, R) = (10 nF, 100 nF, 10 mH, 20 Ω, 1.1 kΩ), (which corresponds with the dimensionless set of parameters $(\alpha, \beta, \gamma, a, b)$ = (10, 12.1, 0.22, -1.26, -0.79)). The tolerances of the components employed are: 10 % for inductances, 5 % for capacitances and 1% for resistances. In most of the experiments, the circuits have been sampled with a digital oscilloscope (Hewlett-Packard 54601) with a maximum sampling rate of 20 millions of samples per second, 8 bit A/D resolution, and a record length of 4000 points. However, in some cases, we have used a different digital oscilloscope (Hewlett-Packard 54645D) with zoom in order to visualize transient phenomena otherwise too fast to be observed with a more conventional oscilloscope.

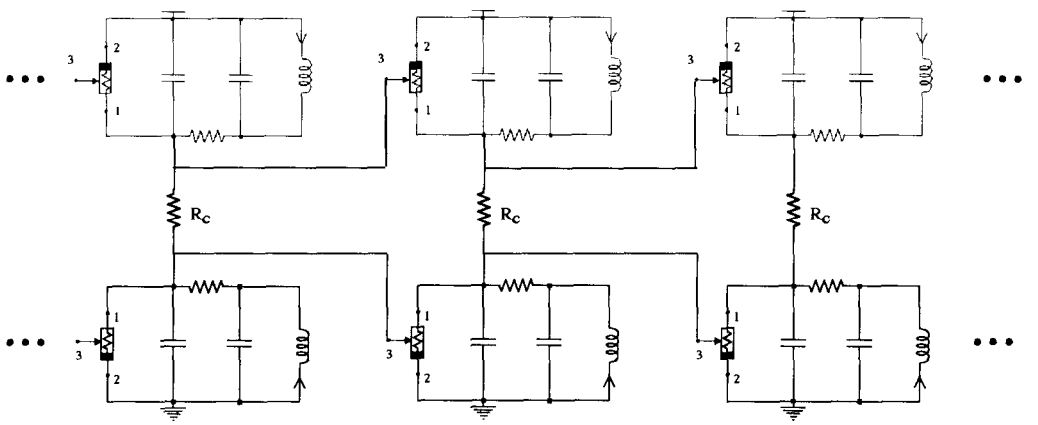

Figure 3.5: Chua's circuits coupled in two different ways: mutual diffusive coupling and unidirectional driving coupling.

The board has been constructed in such a way that circuits can be connected

either by driving and/or by diffusive coupling. Both connections are represented in Fig. 3.5. The driving coupling is carried out by connecting the node 1 of the driving circuit with the node 3 of the response one (see Fig. A.3). The diffusive coupling, only used to study the interaction between two different rings, is carried out with a resistor, R_c, that connects the node 1 of the i-th circuit in the first ring with the node 1 of the i-th circuit in the second ring. In this case, the evolution equations for each circuit are

$$\begin{aligned} C_1 \frac{dV_{1,j}^i}{dt} &= \frac{V_{2,j}^i - V_{1,j}^i}{R} - g(\overline{V_{1,j}^i}) + \frac{(V_{1,j}^{i+1} - V_{1,j}^i)}{R_c} \\ C_2 \frac{dV_{2,j}^i}{dt} &= \frac{V_{1,j}^i - V_{2,j}^i}{R} + I_{L,j}^i \\ L \frac{dI_{L,j}^i}{dt} &= -V_{2,j}^i - I_{L,j}^i r_0 \,, \end{aligned} \tag{3.6}$$

where $j = 0, \ldots, (N-1)$ runs over the number of elements in each ring and i = 0,1 runs over the number of coupled rings. Coupling within each ring enters in the nonlinear element, as the corresponding term, $g(V_{1,j})$, is not driven, in principle, by the voltage across capacitor C_1 of the j-th circuit, but by the voltage across capacitor C_1 of a different circuit of the same ring. The precise driving circuit depends on the type of coupling: parallel or antiparallel. The relationship between the dimensionless coupling constant D from Eq. (3.5) and the physical parameter R_c from Eq. (3.6) is $D = \alpha R/R_c$. Thus, strong coupling is given by low values of R_c (high values of the coupling constant D), and weak coupling is given by high values of R_c (low values of D).

Notice that when considering open linear arrays, the first element of the array corresponds to a non-modified circuit (obtained just by connecting together node 3 and node 1 of that circuit).

3.3 Open Linear Arrays of Chaotic Oscillators.

3.3.1 Numerical Results.

When the elements of an open linear array of N Lorenz oscillators are coupled as described in Section 3.2.1, synchronization is observed after some transient time in which each oscillator has to adapt its own dynamics.

Figure 3.6 represents the variable x of three Lorenz oscillators from an array of N = 20 before and after coupling. Synchronization does not happen instantaneously, but, instead, it takes place as a synchronization *wave* spreads through the system. Therefore, the oscillators in the array synchronize with the first one consecutively, in such a way that the first oscillator imposes its behavior to the whole array. As shown in Fig. 3.6, the two first oscillators practically synchronize at the instant when connection is carried out and there is hardly time in which the oscillators are not doing the same. However, moving forward through the array we can observe the existence of a transient time, that gives rise to oscillations not confined to the own boundaries of the attractor. Observe, in Fig. 3.6, the behavior of the eighteenth oscillator before synchronization is achieved. This happens approximately at 40 time units.

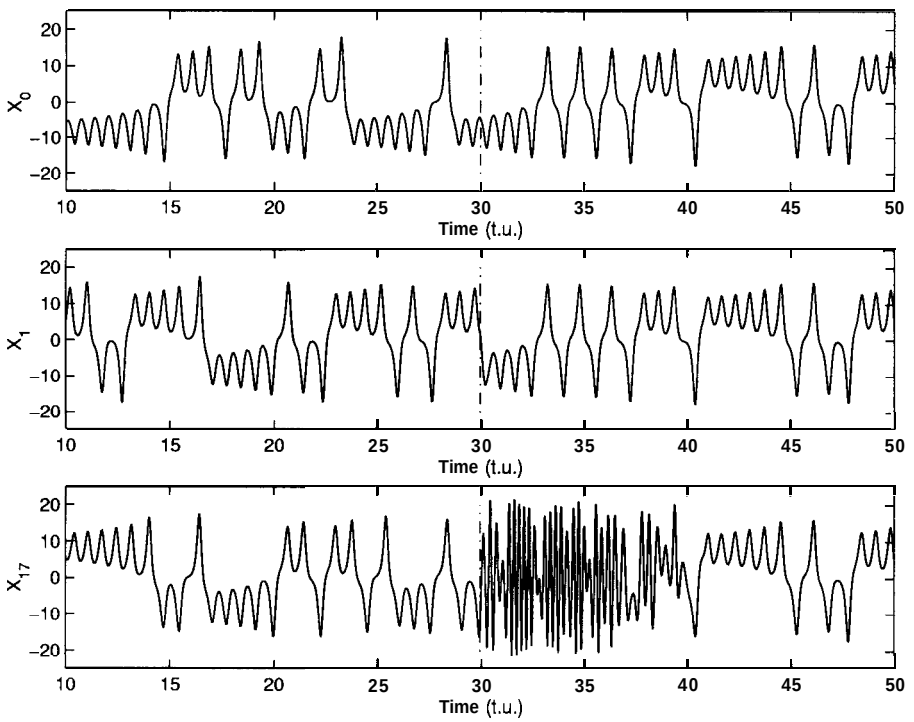

Figure 3.6: Temporal evolution of the variable x of the first, second and eighteenth Lorenz oscillators, namely, x_0, x_1, x_{17}, respectively, before and after coupling. Notice that coupling is carried out at time equal to 30 t.u. and that standard parameters have been used.

Leaving aside the behavior of the oscillators before synchonization, we can focus our attention on the characterization of the properties of the synchronization wave. Figure 3.7 shows the synchronization time (amount of time needed by the cells to be considered as synchronized [182, 12, 174, 175, 197, 18, 10]), called T_s, as a function

of the length of the array (measured in number of oscillators) for two different sets of parameters: (a, $R, b) = (10, 28, 8/3)$ and (a, $R, b) = (18,28,8/3)$. For each set of parameters we observe a linear relationship between the synchronization time and the number of oscillators in the array. Therefore, the synchronization wave can be characterized by a constant velocity. The value of this velocity is given by the inverse of the slope of the straight lines in Fig. 3.7. In particular, for (a, $R, b) = (10,28,8/3)$ the value of the velocity is, approximately, 1.33 osc./t.u. (oscillators per time unit) while for (a, $R, b) = (18,28,8/3)$ this approximated value is 2.94 osc./t.u..

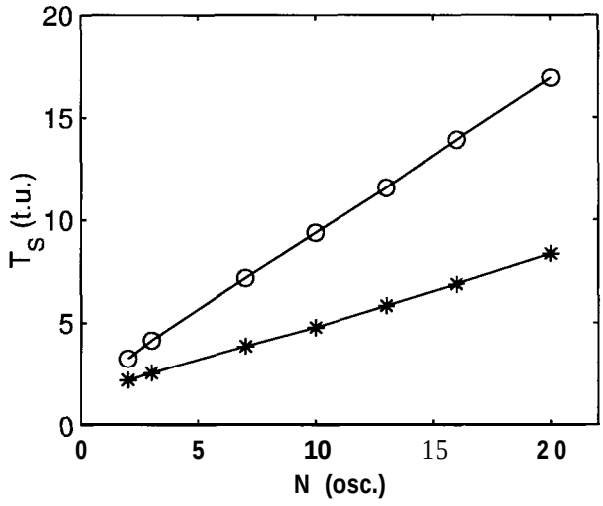

Figure 3.7: Representation of the synchronization time as a function of the number of Lorenz oscillators in the array for two different sets of parameters: (a, $R, b) = (10,28,8/3)$ ('o') and (a, $R, b) = (18,28,8/3)$ ('*').

Notice that synchronization is being considered in the numerical simulations when the condition $(x_{N-1} - x_0)^2 + (y_{N-1} - y_0)^2 + (z_{N-1} - z_0)^2 < 10^{-3}$ is satisfied.

At difference to the case of classical waves in linear systems or autowaves in dissipative media [121], chaotic synchronization waves may carry *information* through the array of cells. This information can be encoded in the first element of the array (using, for example, the method in Section 4.2.1 or the one that will be described in Chapter 5) and so be transmitted through the array. Thus, the study of this synchronization wave can provide some insight into the transmission of signals in Cellular Neural Networks (CNNs) [38] or be useful for signal processing applications.

The same behavior is obtained in numerical simulations when considering an array of Chua's circuits coupled as described in Section 3.2.1. In Fig. 3.8 we can

see synchronization of three chaotic circuits: the first, the second and the fifth from an array of N = 20. As in the previous case, we let the circuits evolve for a certain time before connecting them and we observe that the two first oscillators synchronize almost instantaneously whereas the rest of the circuits in the array spend a transient time proportional to the distance from the first oscillator. Thus, we observe again the existence of a synchronization wave that propagates through the array with a constant velocity [128, 129, 130]. Now, however, the transient time each circuit spends before synchronization is longer than in the Lorenz case. Therefore, bigger oscillations in the transient regime already appear in the first oscillators in the array, although, as it may be expected, these ocillations grow up as we move forward through the array. In an approximated way, the duration of the transient behavior obtained for the fifth Chua's circuit coincides with that of the eighteenth Lorenz oscillator (compare Fig. 3.8 with Fig. 3.6).

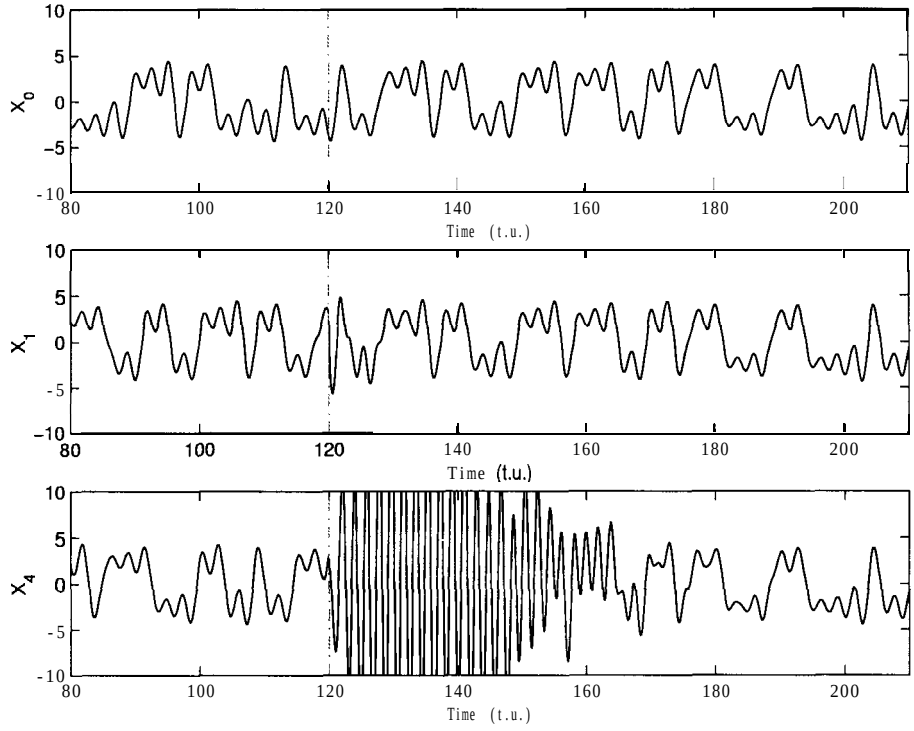

Figure 3.8: Temporal evolution of the variable x of the first, second and fifth oscillators, namely, x_0, x_1, x_4, respectively, before and after coupling. The coupling among circuits is carried out at time equal to 120 t.u., and the set of used parameters is (a, β, γ, a, b) = (10.0,12.1,0.22, -1.26, -0.79).

Figure 3.9 represents the dependence of the synchronization time on the length of the array for two different sets of parameters: $(\alpha, \beta, \gamma, a, b)$ =

(10.0,12.1,0.22,-1.26,-0.79) and $(\alpha, \beta, \gamma, a, b)$ = (10,14.87,0.06,-1.27, -0.68). There exists a linear relationship between these two magnitudes, what implies a constant velocity of the synchronization wave. For $(\alpha, \beta, \gamma, a, b)$ = (10.0,12.1,0.22, -1.26, -0.79) the approximated value of this velocity is 0.0543 osc./t.u. whereas for (a, β, γ, a, b) = (10,14.87,0.06, -1.27, -0.68) this value is 0.0246 osc./t.u.. Now synchronization has been considered when $(x_{N-1}-x_0)^2+(y_{N-1}-y_0)^2+(z_{N-1}-z_0)^2$ < 10-s.

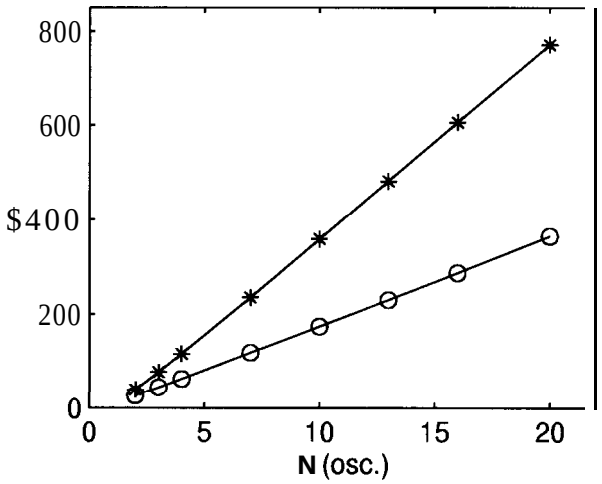

Figure 3.9: Representation of the synchronization time versus the number of Chua's circuits in the array, for two different set of parameters: $(\alpha, \beta, \gamma$, a, $b)$ = (10.0,12.1,0.22,-1.26,-0.79) ('o') and $(\alpha, \beta, \gamma, a, b)$ = (10,14.87,0.06,-1.27,-0.68) ('*').

3.3.2 Experimental results.

Chaotic synchronization has also been obtained experimentally in an array of ten Chua's circuits. This feature is not obvious at all, because one could expect that the tolerances inherent to electronic components would make this phenomenon to deteriorate along the array. However, the tolerances used in the experimental setup (see Section 3.2.2) are small enough so they do not affect the synchronization phenomenon.

The experiments have been performed in the board described in Section 3.2.2. In order to measure the synchronization time we need to incorporate to the setup an automatic mechanism made up of some relays (one for each circuit) and a switch, in such a way that all circuits are coupled at the same time. This mechanism

introduces some noise into the system and, thus, as we move forward through the array, synchronization is harder to achieve.

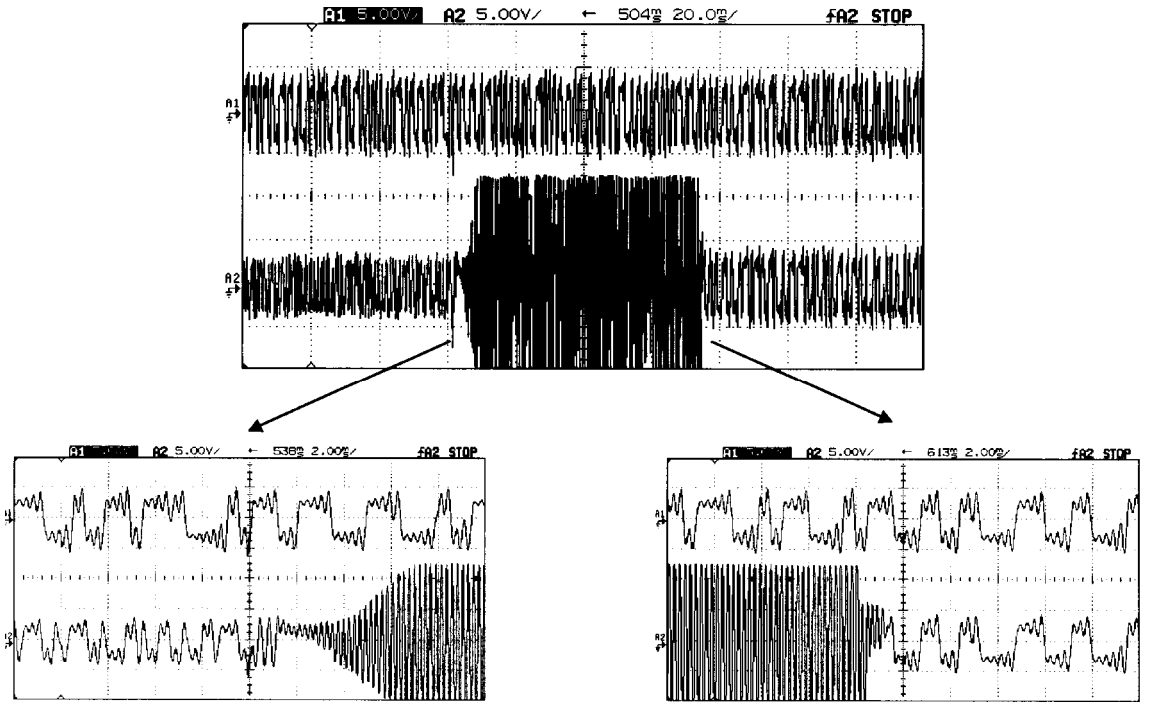

Figure 3.10: Temporal evolution of the voltage at the capacitor C_1 for the first and fourth circuits of the array before and after coupling them. A transient behavior can be observed before synchronization is achieved. In the zoom on the left we are plotting the temporal evolution of these circuits around the coupling instant, 538 ms, while the zoom on the right represents the evolution around the synchonization instant, 613 ms.

In order to find out how long two circuits take to synchronize we have used a digital oscilloscope HP54645D with zoom, which allows to broaden some desired zones of a prerecorded image. Figure 3.10 shows two different zooms of an image in which the signals from the first and fourth circuit of an array are plotted. One zoom represents the temporal evolution of such circuits around the instant of connection and the other one represents the same around the synchronization moment. The coupling among circuits occurs at time equal to 538 ms (see left zoom in Fig. 3.10) and the synchronization is achieved at time 613 ms (see right zoom in Fig. 3.10). Therefore, the synchronization time (duration of the transient behavior) in an array of four Chua's circuits is around 75 ms. Notice that in the transient time the circuits move on the external limit cycle characteristic of the Chua's circuits in which the

variable V_1 oscillates between +12 volt and -12 volt.

In order to know the relationship between the synchronization time and the length of the array 50 experimental realizations for different array lengths have been carried out. The results are shown in Fig. 3.11, where the linear relationship between these two magnitudes shown in numerical simulations is experimentally confirmed. The error bars represent the standard deviation of 50 realizations with respect to the average value. The velocity of the synchronization wave for the values of the components described in Section 3.2.2 is approximately equal to 0.0747 osc./ms.

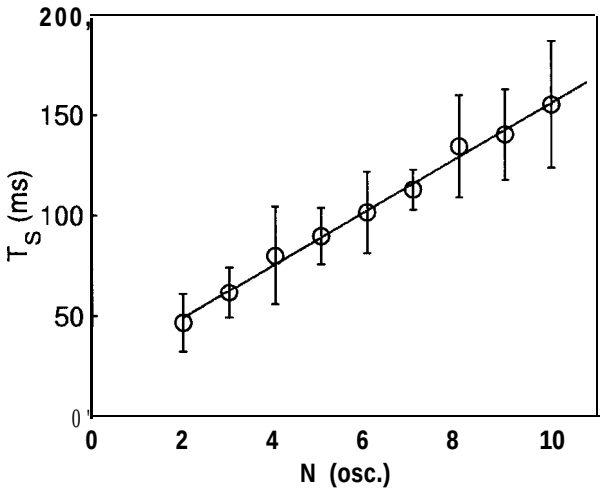

Figure 3.11: Synchronization time obtained experimentally as a function of the length of an array of Chua's circuits. The components of the electronic circuits are $(C_1, C_2, L, r_0, \mathrm{R}) = (10\,\mathrm{nF}, 100\,\mathrm{nF}, 10\,\mathrm{mH}, 20\,\Omega, 1.1\,\mathrm{k}\Omega)$.

3.3.3 Theoretical Analysis.

Synchronization means that the dynamics of the compound system collapse onto an invariant manifold in the global phase space of the coupled systems, called the synchronization manifold.

A theoretical analysis about the synchronization of two consecutive oscillators can be carried out by considering the evolution of perturbations that bring the system outside the synchronization manifold. At a local level this can be done by studying the time evolution of small perturbations that are transverse to this manifold, i.e., by performing a linear stability analysis of these perturbations. This analysis will yield

a linear equation of the form

$$\dot{\delta\mathbf{x}} = \dot{\mathbf{x}}_1 - \dot{\mathbf{x}}_0 = \mathbf{Z}\,\delta\mathbf{x} + O((\delta\mathbf{x})^2), \tag{3.7}$$

where 6x = $x_i - \mathbf{x_0}$ and the relevant information about the synchronized behavior of the two oscillators is contained in the matrix **Z.** Therefore, we are going to calculate this matrix for the two first oscillators, $\mathbf{x}_0 = (x_0, y_0, z_0)$ and xi = (x_1, y_1, z_1), of the open array of Chua's circuits.

The evolution equations of the first circuit in dimensionless form are

$$\begin{aligned} \dot{x_0} &= \alpha[y_0 - x_0 - f(x_0)] \\ \dot{y_0} &= x_0 - \mathbf{Yo} + z_0 \\ \dot{z_0} &= -\beta\, y_0 - \gamma\, z_0 \end{aligned} \tag{3.8}$$

and the corresponding ones of the second circuit

$$\begin{aligned} \dot{x_1} &= \alpha[y_1 - x_1 - f(x_0)] \\ \dot{y_1} &= x_1 - y_1 + z_1 \\ \dot{z_1} &= -\beta\, y_1 - \gamma\, z_1 \end{aligned} \tag{3.9}$$

Thus, substracting Eq. (3.9) out of Eq. (3.8) one obtains the following time evolution equations of the differences between the two systems

$$\begin{aligned} \dot{\delta x} &= \alpha[\delta y - \delta x] \\ \dot{\delta y} &= \delta x - \delta y + \delta z \\ \dot{\delta z} &= -\beta\,\delta y - \gamma\,\delta z, \end{aligned} \tag{3.10}$$

which in a more compact form can be written as $\dot{\delta\mathbf{x}} = \mathbf{Z}\ \delta\mathbf{x}$, being 6x = $(\delta x, \delta y,$ 6x) and

$$\mathbf{Z} = \begin{pmatrix} -\alpha & \alpha & 0 \\ 1 & -1 & 1 \\ 0 & -\beta & -\gamma \end{pmatrix} \tag{3.11}$$

Notice that this matrix is identical to the Jacobian matrix corresponding to an isolated Chua's circuit except by the terms that are cancelled because of the connections that are carried out. Thus, the former can be calculated from the latter just by setting to zero the entries corresponding to the connection in the linearized approximation to the flow [78, 79]. The connection enters through the nonlinear element f(x) in Eq. (3.9), and this is the reason why the matrix (3.11) has only constant coefficients.

In order to know the asymptotic behavior of these two coupled oscillators, it is interesting to solve Eq. (3.7). This can be done by calculating the transverse

Lyapunov spectrum, which can be obtained by taking the real part of the eigenvalues of the matrix (3.11), where one does not need to perform the usual $t \to \infty$ limit, as the coefficients of the matrix are constant for this particular arrangement. Recall that small deviations from the synchronized state behave in the form $\dot{\mathbf{x}}$ = Z x and this implies that

$$\mathbf{x}(t) = \mathbf{x}(0) \exp(\Lambda t), \tag{3.12}$$

where A is obtained by transforming matrix Z to diagonal form, that is, A is the diagonal matrix that contains the transverse Lyapunov exponents. For the type of connection used in these simulations all the transverse Lyapunov exponents are negative, which implies synchronization between the two systems. One may assume that Eq. (3.12) is dominated by the highest transverse Lyapunov exponent Xi, i.e., x(t) = $\mathbf{x}(0) \exp(-|\lambda_1|$ t), that defines arelaxationalprocess in a timescaler = $1/|\lambda_1|$. Thus, the velocity of synchronization between two oscillators is determined by the highest transverse Lyapunov exponent. The bigger the absolute value of the highest transverse Lyapunov exponent is, the quicker the synchronization occurs.

When considering an array of chaotic oscillators the synchronization process is observed gradually. Thus, first of all the two first oscillators synchronize, then a third oscillator synchronizes with the previous ones and so on. What is a little surprising is that each oscillator spends the same amount of time in synchronizing with the previous one, once this previous oscillator has achieved synchronization (constant velocity of the synchronization wave, shown in Fig. 3.9). This is because the time needed for each oscillator to synchronize with the previous one depends only of the value of τ, defined above. Thus, one can associate the velocity of the synchronization of the two first oscillators of the array with the velocity of the synchronization wave V_s.

As it may be expected, the bigger the absolute value of the highest transverse Lyapunov exponent, calculated from two oscillators, is, the bigger the velocity of the synchronization wave will be. It has been found that for an open array of Chua's circuits connected as defined in this section the dependence of this velocity V_s on λ_1 is linear, as shown in Fig. 3.12, that has been obtained from numerical simulations with different values of the parameters.

A similar analysis for linear arrays of Lorenz oscillators in chaotic regime has been recently published [461].

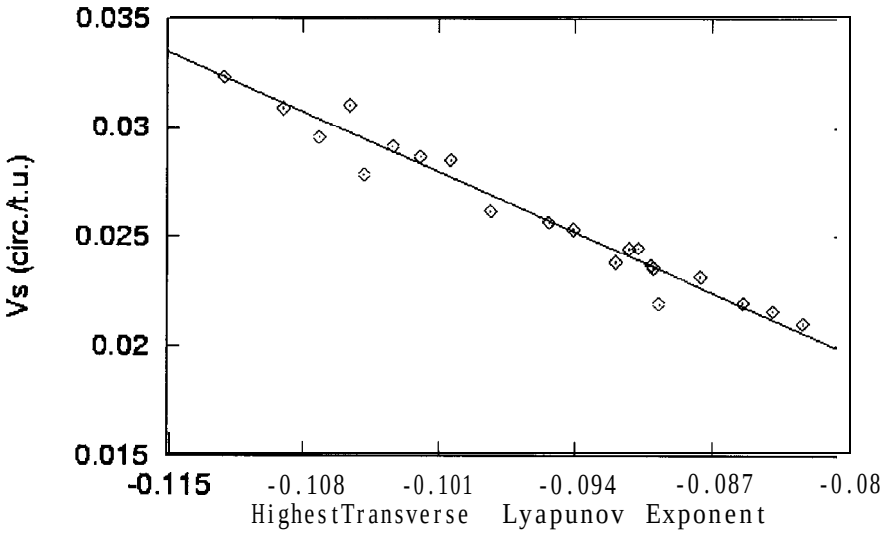

Figure 3.12: Representation of the average velocity of synchronization V_s versus the highest transverse Lyapunov exponent, showing the linear relationship between these two quantities.

3.4 Rings of Coupled Chaotic Oscillators.

Rings of coupled (discrete) cells are relevant in the study of some physiological and biochemical systems. This was the motivation of the seminal work by Turing [226, 156], who used this kind of system in his proposal of a plausible model of morphogenesis. Later, this kind of models were used to study slow-wave activity in the mammalian intestine [125]. One of the most interesting fields where rings of coupled cells have come up as a useful modeling tool is that of neural systems, namely in the context of Central Pattern Generators (CPGs) [86]. These are networks of neurons in the central nervous system capable of producing an autonomous rhythmic output (breathing, walking, running, etc.), i.e., without making use of sensory feedback with the corresponding moving organ. Although current neurophysiological techniques are unable to isolate such circuits among the intricate neural connections of complex animals, there are some strong indirect experimental evidences for their existence (see, e.g., [73, 74, 75, 76, 173, 207, 219]). Irrespective of physiological considerations, CPG-like networks of coupled cells (e.g., electronic circuits) are an attractive option for the design and control of legged robots, because they produce a variety of phase relationships in a stable and natural manner [77]. An interesting study is that of Collins and Stewart [42, 43] that, in the case of animals with a small number of legs, obtained the patterns of oscillations (i.e., the gaits) used by these animals in their

locomotion [221]. They did so by analyzing the periodic states that arise through a symmetric Hopf bifurcation [71] from the trivial stand gait and by using simple symmetric networks of coupled identical cells.

Although rings are a useful way of implementing CPGs, it is impossible to obtain all the gaits (phase relationships) from a single ring of coupled oscillators, whose symmetry, connectivity, etc. are fixed. Thus, it is natural to think of extending the simplest ideas by considering more complex networks of coupled oscillators. A possible extension consists of assemblies of 2 N identical oscillators in which the CPG consists of two rings. The oscillators within a ring have identical unidirectional coupling, while the two rings are coupled transversally by a different type of coupling (bidirectional). In this way one has a probably more realistic representation of CPGs of bilaterally symmetric animals, that, hopefully, will describe more accurately locomotion in these animals. Among the models of identical cells to simulate the behavior of CPGs, it is important to mention the study of Collins and Stewart [42], who considered two coupled rings each comprising three oscillators, and that of Ermentrout and Kopell [118]. Another recent important study was carried out by Golubitsky et al. [72], who proposed a modular symmetric network consisting of two mutually coupled rings, each one made of 2 N identical cells coupled unidirectionally, to reproduce the phase relationships found in gaits of a 2 N-legged animal. In addition, more complex networks have also been studied. One example is the modeling of the human colon [17], that consists of 33 symmetrically coupled three-membered rings.

The study and modeling of CPGs needs to take into account not just the topology and detailed form of connections, but also the local dynamics of the oscillators. Although most of the studies [42, 43, 72] consider a quiescent or periodic local dynamics, it is important to recall that experiments performed in recent years indicate that normal activity of a single, i.e., isolated, neuron is deterministic chaos [87, 152,4]. For this reason, our attention will be focussed on the study of rings of identical chaotic oscillators with unidirectional coupling. It is interesting to emphasize the richness of dynamical behaviors that are possible in this kind of systems. In particular, surprising structures arise when a desynchronizing transition occurs in the global synchronized state. We will show the case of a ring of identical Lorenz oscillators and another one of identical Chua's oscillators. With the particular setup considered in this work, a for Lorenz oscillators a periodic structure is observed when the instability appears,

whereas for Chua's oscillators the observed structure is chaotic. Finally, we will analyze what happens when considering two rings of Chua's oscillators with mutual diffusive coupling between them.

3.4.1 Rings of Lorenz Oscillators.

The behavior of a ring of Lorenz oscillators, initially in a chaotic state and coupled as described in Section 3.2, will be analyzed in this section [143, 138]. Our attention will be focussed on the study of the stability of the global synchonized state. To do this, we will introduce a theoretical analysis based on the transverse Lyapunov exponents, followed by numerical simulations that confirm this theory.

Theoretical Analysis.

The behavior of the ring can be analyzed in a convenient form by means of a linear stability analysis of the oscillators in the system starting from the uniform synchronized state. Let us consider a ring with N identical Lorenz oscillators, coupled in the way described by the set of Eqs.(3.2). This set of equations can be written in a compact form as,

$$\dot{\mathbf{x}}_j = \mathbf{G}_j(\mathbf{x}_0, \ldots, \mathbf{x}_{N-1}) \quad j = 0, \ldots, \text{N-1} \tag{3.13}$$

where $\mathbf{x}_j = (x_j, y_j, z_j)$ is the coordinate vector of the jth Lorenz oscillator in the ring and $\mathbf{G}_j : \Re^{3\times N} \rightarrow \Re^3$ is the function that describes the temporal evolution of the jth oscillator, defined by

$$\mathbf{G}_j(\mathbf{x}_0, \ldots, \mathbf{x}_{N-1}) = (\sigma(y_j - x_j), R\,x_{j-1} - y_j - x_j\,z_j, y_j - b\,z_j), \tag{3.14}$$

where operations over the index j are modulo N. Since a ring of N identical oscillators is considered, the dynamical evolution does not vary from one oscillator to the next. From a mathematical point of view, this means that the functions $\mathbf{G}_j$ are of the shift-invariant type, since the condition

$$\mathbf{G}_j(\mathbf{x}_i, \mathbf{x}_{i+1}, \ldots, \mathbf{x}_{i+N-1}) = \mathbf{G}_{j+1}(\mathbf{x}_{i-1}, \mathbf{x}_i, \ldots, \mathbf{x}_{i+N-2}) \quad i, j = 0, \ldots, N-1 \tag{3.15}$$

is satisfied. All indices are understood to be taken mod N.

The linearization of the system (3.13) around the synchronized state defined by s = $\mathbf{x}_0 = \mathbf{x}_1 = \ldots = \mathbf{x}_{N-1}$ leads to a set of linear variational equations given by

$$\delta\dot{\mathbf{x}}_j = \sum_{i=0}^{N-1} \mathbf{D}_i \mathbf{G}_j(\mathbf{x}_0, \ldots, \mathbf{x}_{N-1})|_{\mathbf{s}} \quad \delta\mathbf{x}_i \quad j = 0, \ldots, N-1 \tag{3.16}$$

where $\delta\mathbf{x}_j = \mathbf{x}_j$ – s with s = $(x_s(t), y_s(t), z_s(t))$ and $\mathbf{D}_i$ is the differential operator acting on coordinates of the ith oscillator. Since the functions $\mathbf{G}_j$ are of the shift-invariant type, (3.15) can be used to express all of the derivatives $\mathbf{D}_i\mathbf{G}_j(\mathbf{x}_0, \ldots, \mathbf{x}_{N-1})|_{\mathbf{s}}$ in terms of derivatives of $\mathbf{G}_0(\mathbf{x}_0, \ldots, \mathbf{x}_{N-1})|_{\mathbf{s}}$. The result is

$$\delta\dot{\mathbf{x}}_j = \sum_{i=0}^{N-1} \mathbf{D}_{i-j} \mathbf{G}_0(\mathbf{x}_0, \ldots, \mathbf{x}_{N-1})|_{\mathbf{s}} \, \delta\mathbf{x}_i \quad j = 0, \ldots, N-1 \tag{3.17}$$

These equations can be placed in the form of a discrete circular convolution by defining the backward sequence

$$\{\mathbf{H}_i\}_{i=0}^{N-1} = \{\mathbf{D}_0\mathbf{G}_0|_{\mathbf{s}}, \mathbf{D}_{N-1}\mathbf{G}_0|_{\mathbf{s}}, \mathbf{D}_{N-2}\mathbf{G}_0|_{\mathbf{s}}, \ldots, \mathbf{D}_1\mathbf{G}_0|_{\mathbf{s}}\}. \tag{3.18}$$

The variational equations then become

$$\delta\dot{\mathbf{x}}_j = \sum_{i=0}^{N-1} \mathbf{H}_{j-i} \, \delta\mathbf{x}_i \qquad j = 0, \ldots, N- \tag{3.19}$$

where

$$\mathbf{H}_0 = \begin{pmatrix} -\sigma & \sigma & 0 \\ -z_s & -1 & -x_s \\ y_s & x_s & -b \end{pmatrix}, \quad \mathbf{H}_1 = \begin{pmatrix} 0 & 0 & 0 \\ R & 0 & 0 \\ 0 & 0 & 0 \end{pmatrix}, \quad \mathbf{H}_2 = \ldots = \mathbf{H}_{N-1} = \mathbf{0}_{3\times 3}. \tag{3.20}$$

Remember that these matrices are evaluated in the synchronized state s. An easier way of seeing the discrete circular convolution (3.19) is by means of the following expression for the global system,

$$\begin{pmatrix} \delta\dot{\mathbf{x}}_0 \\ \delta\dot{\mathbf{x}}_1 \\ \delta\dot{\mathbf{x}}_2 \\ \cdots \\ \cdots \\ \delta\dot{\mathbf{x}}_{N-2} \\ \delta\dot{\mathbf{x}}_{N-1} \end{pmatrix} = \begin{pmatrix} \mathbf{H}_0 & 0 & 0 & 0 & \cdots & 0 & \mathbf{H}_1 \\ \mathbf{H}_1 & \mathbf{H}_0 & 0 & 0 & \cdots & 0 & 0 \\ 0 & \mathbf{H}_1 & \mathbf{H}_0 & 0 & \cdots & 0 & 0 \\ 0 & 0 & \mathbf{H}_1 & \mathbf{H}_0 & \cdots & 0 & 0 \\ \cdots & \cdots & \cdots & \cdots & \cdots & \cdots & \cdots \\ 0 & 0 & 0 & 0 & \cdots & \mathbf{H}_0 & 0 \\ \mathbf{0} & 0 & 0 & 0 & \cdots & \mathbf{H}_1 & \mathbf{H}_0 \end{pmatrix} \cdot \begin{pmatrix} \delta\mathbf{x}_0 \\ \delta\mathbf{x}_1 \\ \delta\mathbf{x}_2 \\ \cdots \\ \cdots \\ \delta\mathbf{x}_{N-2} \\ \delta\mathbf{x}_{N-1} \end{pmatrix} \tag{3.21}$$

and from now on this matrix will be called matrix H. If we define the vector 6x = $(\delta\mathbf{x}_0, \ldots, \delta\mathbf{x}_{N-1})$, this last equation can be written as,

$$\delta\dot{\mathbf{x}} = \mathbf{H}\,\delta\mathbf{x}, \tag{3.22}$$

The structure of this matrix is circulant since it represents a convolution sum. For this reason, the Fourier transform diagonalization method can be applied [163]. Thus, one can put Eq. (3.21) in a more convenient form through the use of the Discrete Fourier Transform (DFT) [226, 94]. Introducing discrete Fourier transforms of the sequence (3.18) and the sequence $\{\delta\mathbf{x}_0, \delta\mathbf{x}_1, \ldots, \delta\mathbf{x}_{N-1}\}$, called $\mathbf{C}^{(k)}$ and $\eta^{(k)}$, respectively, yields

$$\begin{aligned} \mathbf{C}^{(k)} &= \sum_{j=0}^{N-1} \mathbf{H}_j e^{\frac{2\pi i j k}{N}}, \\ \eta^{(k)} &= \sum_{j=0}^{N-1} \delta\mathbf{x}_j e^{\frac{2\pi i j k}{N}}, \end{aligned} \tag{3.23}$$

so the matrix in (3.21) is block-diagonalized by virtue of the convolution theorem for discrete Fourier transforms [163], which says that convolution of sequences implies multiplication of the corresponding Fourier transforms. Thus, the transformed variational equations are given by the Fourier modes

$$\dot{\eta}^{(k)} = \mathbf{C}^{(k)}\eta^{(k)} \quad k = 0, \ldots, N-1, \tag{3.24}$$

that are decoupled. In a global form, this is represented by a block-diagonalized matrix, as shown the following equation,

$$\begin{pmatrix} \dot{\eta}^{(0)} \\ \dot{\eta}^{(1)} \\ \vdots \\ \dot{\eta}^{(N-1)} \end{pmatrix} = \begin{pmatrix} \mathbf{C}^{(0)} & \mathbf{0} & \cdots & \mathbf{0} \\ \mathbf{0} & \mathbf{C}^{(1)} & \cdots & \mathbf{0} \\ \vdots & \vdots & \ddots & \\ \mathbf{0} & \mathbf{0} & \cdots & \mathbf{C}^{(N-1)} \end{pmatrix} \cdot \begin{pmatrix} \eta^{(0)} \\ \eta^{(1)} \\ \vdots \\ \eta^{(N-1)} \end{pmatrix} \tag{3.25}$$

Note that $\eta^{(k)}$ for the Lorenz case is a 3 x 1 dimensional vector. The structure of each block can be written in the form,

$$\mathbf{C}^{(k)} = \begin{pmatrix} -\sigma & \sigma & 0 \\ (Re_k - z_s) & -1 & -x_s \\ y_s & x_s & -b \end{pmatrix}, \tag{3.26}$$

with $e_k = \exp(i\,2\pi\,k/N)$ and being $k = 0, \ldots,$ (N-l) the Fourier modes of the system, with N the number of oscillators in the ring. Notice that the $\mathbf{C}^{(k)}$ matrices have time-dependent (chaotically varying) coefficients, namely x3(t), ys(t) and zS(t). Thus, we have chosen to characterize its stability by determining the corresponding Lyapunov spectrum considering the infinitetime limit of the real part of the eigenvalues of this matrix. This has been done by generalizing Wolf's algorithm [235] to the case of complex vector spaces.

Before proceeding, it is useful to discuss the geometry of the variations $\eta^{(k)}$. The global dynamical system, in which the dynamics of each oscillator is governed by

Eq. (3.2), evolves in $\Re^{3N}$. The synchronization *manifold* $M \subset \Re^{3N}$ is defined by the conditions $\mathbf{x}_0 = \mathbf{x}_1 = \ldots = \mathbf{x}_{N-1}$. Synchronous oscillations of all types (not just chaotic solutions) are constrained to this manifold. The synchronization conditions represent $3(N-1)$ constraint equations. Therefore the dimension of M is $3N - 3(N-1) = 3$, which is the phase space dimension of a single oscillator. The Fourier transform basis $\eta^{(k)}$ provides a convenient decomposition of the variations into variations within the synchronization manifold M and variations transverse to this manifold. The variation $\eta^{(0)}$ is within M and the remaining variations $\eta^{(k)}$, $k = 1, \ldots (N-1)$ are transverse to M and control the stablity of the synchronized state[1]. Stability of the synchronized state is ensured if arbitrary small transverse variations decay to zero. In some cases, as it occurs for the Lorenz oscillators connected in the considered way, the variation $\eta^{(0)}$ obeys the variational equation for a single, isolated oscillator. The $k = 0$ Fourier mode represents the uniform synchronized state of the ring, and the stability of this state can be characterized by analyzing the transverse spectrum, corresponding to Fourier modes with $k \neq 0$, which gives information about the evolution of transversal deviations around this state. The uniform mode $k = 0$ will be stable whenever this spectrum is negative. An instability in the uniform synchronized state will occur whenever one (or more) of the transverse Lyapunov exponents becomes positive.

In order to determine the nature (chaotic or periodic) of the synchronized state ($k = 0$ Fourier mode) is necessary to evaluate the Lyapunov exponents corresponding to the $k = 0$ mode. Particularly, a positive Lyapunov exponent implies chaotic behavior. In fact, the highest Lyapunov exponent associated to the $k = 0$ mode is always positive since $C^{(0)}$ is the error growth of an uncoupled Lorenz system and the parameters of the Lorenz system have been chosen to be in a chaotic regime.

Instead of determining the highest Lyapunov exponent associated to each transverse Fourier mode (each $k \neq 0$) for a given size of the array, namely N, and doing this for different values of N, a more practical procedure is to define the reduced wavenumber $q = k/N$ as a continuous variable in the range [0, 1]. The highest Lyapunov exponent as a function of q, namely $\lambda(q)$, may allow one to characterize the stability of the uniform synchronized state in a convenient way. The function X(q), obtained by generalizing the procedure of Wolf et al. [235] to allow for a

[1]Since the transverse variations are generally complex this statement is technically incorrect, however the real forms of the transverse variations, given by $\chi^k = \frac{1}{2}(\eta^k + \eta^{N-k})$ and $\sigma^k = \frac{1}{(2i)}(\eta^k - \eta^{N-k})$, are transverse to the (real) synchronization manifold M.

complex vector space due to the presence of the complex quantity e_q, is represented in Fig. 3.13 for the case of rings of Lorenz oscillators with standard parameters. A first remark is that $X(q)$ in Fig. 3.13 is symmetric with respect to the line $q = 1/2$. This can be easily explained taking into account that for a given N the $\mathbf{C}^{(k)}$ and $\mathbf{C}^{(N-k)}$ are complex conjugate due to the presence of the term e_q, implying the same property for their spectra of eigenvalues. Therefore the above mentioned symmetry property holds for the real parts of the eigenvalues and also for their limit when $t \to \infty$, $X(q)$. Moreover, an important point to notice is that as $e_0 = 1$ the Lyapunov exponents corresponding to the uniform mode $k = q = 0$ are identical to those of the isolated (uncoupled) chaotic system. Empirically it is found that $\lambda(q = 1/2) < 0$ for all the chaotic systems so far considered (see, Fig. 3.13). Since $\lambda(q = 1/2) < 0$ and $\lambda(q = 0) > 0$, there must exist some value for the number of oscillators in the ring N_c for which the uniform synchronized state becomes unstable, i.e., for which the transverse Lyapunov spectrum (TLS) becomes nonnegative.

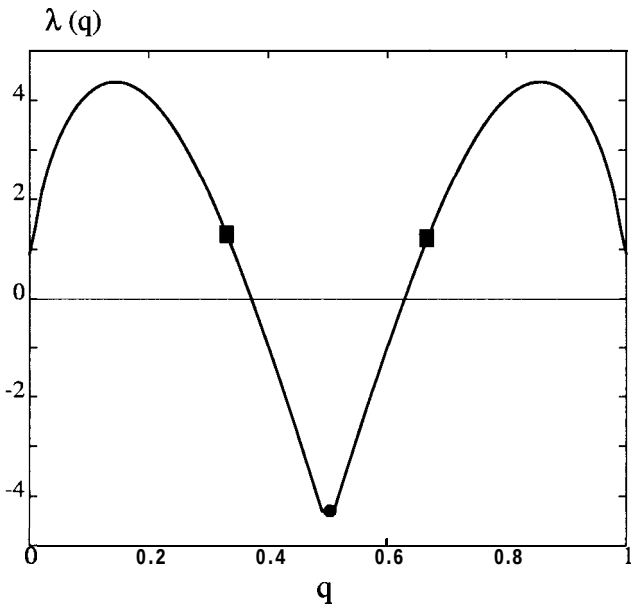

Figure 3.13: Representation of the highest Lyapunov exponent $X(q)$ as a function of $q = k/N$. The circles indicate the highest transverse Lyapnnov exponent for the corresponding transverse Fourier modes in a ring of N = 2 Lorenz oscillators, whereas the squares indicate the same for a ring of N = 3. The values of the parameters are $(\sigma, R, \mathrm{b}) = (10, 28, 8/3)$.

The fact that an instability must appear in the uniform state of a chaotic system at some critical size can be established by using very general arguments [21]. Due to the observed continuity in $X(q)$, there must exist some value of q, namely q_c, such that

$\lambda(q_c)$ = 0 (see Fig. 3.13). The wavenumber q_c indicates the instability of the ring, and the lowest possible value of N for which the k = N q_c condition is fulfilled can be found setting k = 1. Since N is an integer variable, it follows that the critical size of the ring is $N_c\lceil\frac{1}{q_c}\rceil$, where $\lceil\cdot\rceil$ denotes the nearest greater integer. In the case of a ring of Lorenz oscillators with standard parameters, namely (a, R,b) = (10,28,8/3), defined by Eq. (3.2), $q_c \approx 0.37$, and so N_c = 3. In Fig. 3.13 the TLS corresponding to N = 2 and N = 3 are plotted with full circles and squares, respectively, allowing to see in a pictorial way the transition of the TLS from negative to nonnegative. Note that the predictions of this linear stability analysis give useful information only regarding the onset of instability, not so much the final outcome of such instability, that depends also on higher nonlinear terms in the expansion that are neglected in this level of approximation.

Symmetry also determines the behavior of the ring after the onset of the instability. The symmetry induced by the unidirectional character of the coupling makes the eigenvalues of the matrix $C^{(k)}$ to be complex conjugate of the eigenvalues of $\mathbf{C}^{(N-k)}$. One can consider here two possible situations depending on whether the imaginary part of these eigenvalues is zero or not. Of course, the fact that these matrices have time-dependent (chaotically varying) coefficients implies that the instability cannot be characterized analitically. One can, at most, determine instantaneous eigenvalues. As said before, information on the asymptotic behavior of the real part of the eigenvalues can be obtained by determining the Lyapunov spectrum of the corresponding unstable Fourier mode by generalizing the procedure of Wolf *et al.* [235] to the case of a complex space. However, this procedure gives no information about the imaginary part of these eigenvalues. One can obtain some approximate information by replacing the nonconstant coefficients of the matrix $\mathbf{C}^{(k)}$ by their average values when $t \to \infty$, since this yields a problem with constant coefficients from which the real and imaginary parts of the corresponding eigenvalues can be determined. This averaging method has been introduced in and it has been found to be useful in yielding qualitative information about the real or complex character of these eigenvalues. The quality of the approximation can be judged by comparing the real part of these eigenvalues with the transverse Lyapunov exponents, as the former quantity is an approximation to the latter. For the case of a ring of Lorenz systems it can be shown that this procedure yields eigenvalues whose real part is approximately parallel to those numerically determined from Eq. (3.26).

The important point here is that since the matrices $\mathbf{C}^{(1)}$ and $\mathbf{C}^{(N-1)}$ are complex conjugate, at the onset of the instability there will be two eigenvalues, say $\pm i\,w$, that will cross the imaginary axis at the same time, giving rise to a Hopf bifurcation. The theory of Hopf bifurcations in the presence of symmetry [70] says that after the onset of the bifurcation there will be a symmetry-breaking in the system, compared to the symmetry of the homogeneous state. In particular, in the case of the $\mathbf{Z}_n$ symmetry group characteristic of a ring of unidirectionally coupled elements it can be shown [43] that one gets a branch of discrete rotating wave solutions. Instead, in the case that the imaginary part of these eigenvalues is zero, one should not expect to obtain this rotating-wave behavior, and it can be shown that the instability yields simply chaotic uncorrelated behavior among the different oscillators.

The linear analysis gives information about the behavior of the system at the onset of the instability for N $\geq N_c$, but does not say anything about the evolution of these perturbations, that grow as $\exp[\lambda(q)\,t]$. In the case that the oscillators are in a steady state regime the more likely situation is that the system performs a transition to a discrete periodic rotating wave solution [9], as predicted from symmetry arguments [43]. This is what happens in the case of Lorenz systems coupled in a ring geometry as it will be seen immediately below.

Numerical Results.

To confirm this theoretical study based on the linear stability of the global synchronized state, numerical simulations of Eq. (3.2) have been performed. As expected, it was observed that the synchronized chaotic state is stable if the size of the ring is small enough [143], e.g., N = 2 (see Fig. 3.14), while for a certain critical number, N_c = 3, an instability that destroys the uniform chaotic state occurs, leading to a new behavior. In this new behavior (see Fig. 3.15), one actually observes an approximate rotating wave in the sense that a given oscillator is advanced with respect to the oscillator that is driving it by approximately l/N of a period, i.e., neighboring oscillators exhibit a phase difference of 1/3 in our case. Since the behavior of each oscillator is periodic, this rotating wave will be called periodic *rotating wave.*

The frequency of this periodic rotating wave is larger than the frequency corresponding to the average distance between peaks in the chaotic state that

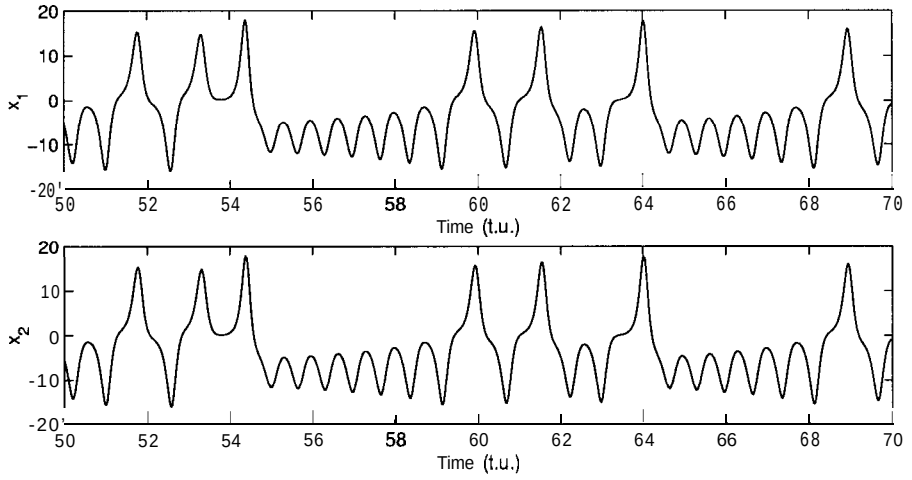

Figure 3.14: Temporal evolution of the variables $x_i, i = 1, 2$ in a ring of $N = 2$ Lorenz oscillators. The values of the parameters are the same as in Fig. 3.13.

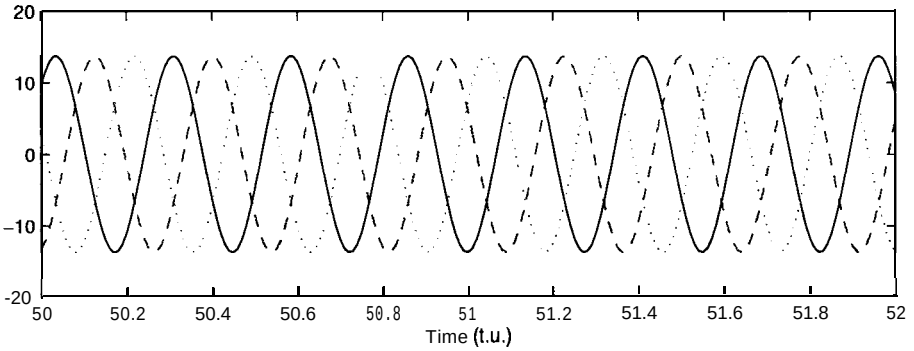

Figure 3.15: Temporal evolution of the variables $x_i, i = 1, \cdots, 3$ in a ring of $N = 3$ Lorenz oscillators. Compare the time scale of this figure with that of Fig. 3.14. The values of the parameters are the same as in Fig. 3.13.

corresponds to an uncoupled Lorenz system[2]. The feature of these rotating waves being faster (at least one order of magnitude faster) than the behavior corresponding to the uncoupled oscillators makes this behavior potentially very attractive. In the context of CPGs it offers a dynamical intrinsic mechanism to generate a fast frequency in the system. This mechanism also might be useful in the design of artificial systems in which one wishes to incorporate this feature of a fast frequency to the system.

Recently, these fast periodic rotating waves have also been found in an experimental setup consisting of unidirectionally coupled Lorenz oscillators [204].

[2]This fact can be noticed by comparing the time scale of Fig. 3.15 with the time scale of Fig. 3.14.

3.4.2 Rings of Chua's Oscillators.

The same type of linear stability analysis discussed for the Lorenz case can be applied here. Now a ring with N Chua's oscillators is considered, where the oscillators are coupled according to Eq. (3.3) and driving is introduced through the nonlinear element in such a way that corresponds to a ring geometry [128, 144, 138]. $\mathbf{x}_j = (x_j, y_j, z_j)$ can be written as,

$$\dot{\mathbf{x}}_j = \mathbf{G}_j(\mathbf{x}_0, \ldots, \mathbf{x}_{N-1}) \quad j = 0, \ldots, N-1 \tag{3.27}$$

where the function $\mathbf{G}_j$ is defined by

$$\mathbf{G}_j(\mathbf{x}_0, \ldots, \mathbf{x}_{N-1}) = (\alpha[y_j - x_j - f(x_{j-1})],\ x_j - y_j + z_j,\ -\beta y_j - \gamma z_j), \tag{3.28}$$

being operations over the index j modulo N and

$$f(x_{j-1}) = \left\{ b x_{j-1} \cdot \frac{1}{2}(a - b)[|x_{j-1} + 1| - |x_{j-1} - 1|] \right\}. \tag{3.29}$$

A linear analysis of small perturbations on the global synchronized state, defined by s = $\mathbf{x}_0 = \mathbf{x}_1 = \ldots = \mathbf{x}_{N-1}$, yields a set of linear variational equations given by,

$$\dot{\delta \mathbf{x}}_j = \sum_{i=0}^{N-1} \mathbf{D}_i \mathbf{G}_j(\mathbf{x}_0, \ldots, \mathbf{x}_{N-1})|_{\mathbf{s}}\, \delta \mathbf{x}_i \quad j = 0, \ldots, N-1 \tag{3.30}$$

where $\delta \mathbf{x}_j = \mathbf{x}_j - \mathbf{s}$ and components of s are (x,(t), $y_s(t), z_s(t)$). Since a ring geometry is considered, the functions $\mathbf{G}_j$ are shift-invariant (see Eq. (3.15)). For this reason, all the derivatives $\mathbf{D}_i \mathbf{G}_j(\mathbf{x}_0, \ldots, \mathbf{x}_{N-1})|_{\mathbf{s}}$ can be expressed in terms of derivatives of $\mathbf{G}_0(\mathbf{x}_0, \ldots, \mathbf{x}_{N-1})|_{\mathbf{s}}$. The result is

$$\dot{\delta \mathbf{x}}_j = \sum_{i=0}^{N-1} \mathbf{D}_{i-j} \mathbf{G}_0(\mathbf{x}_0, \ldots, \mathbf{x}_{N-1})|_{\mathbf{s}}\, \delta \mathbf{x}_i \quad j = 0, \ldots, N-1, \tag{3.31}$$

which can be placed in the form of the discrete convolution

$$\dot{\delta \mathbf{x}}_j = \sum_{i=0}^{N-1} \mathbf{H}_{j-i}\ \delta \mathbf{x}_i, \quad j = 0, \ldots, N-1. \tag{3.32}$$

where

$$\{\mathbf{H}_i\}_{i=0}^{N-1} = \{\mathbf{D}_0 \mathbf{G}_0|_{\mathbf{s}}, \mathbf{D}_{N-1} \mathbf{G}_0|_{\mathbf{s}}, \mathbf{D}_{N-2} \mathbf{G}_0|_{\mathbf{s}}, \ldots, \mathbf{D}_1 \mathbf{G}_0|_{\mathbf{s}}\}. \tag{3.33}$$

This discrete circular convolution can be also represented by the equation

$$\begin{pmatrix} \delta\dot{\mathbf{x}}_0 \\ \delta\dot{\mathbf{x}}_1 \\ \delta\dot{\mathbf{x}}_2 \\ \vdots \\ \delta\dot{\mathbf{x}}_{N-1} \end{pmatrix} = \begin{pmatrix} \mathbf{H}_0 & \mathbf{H}_{N-1} & \mathbf{H}_{N-2} & \cdots & \mathbf{H}_1 \\ \mathbf{H}_1 & \mathbf{H}_0 & \mathbf{H}_{N-1} & \cdots & \mathbf{H}_2 \\ \mathbf{H}_2 & \mathbf{H}_1 & \mathbf{H}_0 & \cdots & \mathbf{H}_3 \\ \vdots & \vdots & \vdots & \vdots & \vdots \\ \mathbf{H}_{N-1} & \mathbf{H}_{N-2} & \mathbf{H}_{N-3} & \cdots & \mathbf{H}_0 \end{pmatrix} \cdot \begin{pmatrix} \delta\mathbf{x}_0 \\ \delta\mathbf{x}_1 \\ \delta\mathbf{x}_2 \\ \vdots \\ \delta\mathbf{x}_{N-1} \end{pmatrix} \tag{3.34}$$

where the structure of the terms is as follows,

$$\mathbf{H}_0 = \begin{pmatrix} -\alpha & \alpha & 0 \\ 1 & -1 & 1 \\ 0 & -\beta & -\gamma \end{pmatrix}, \quad \mathbf{H}_1 = \begin{pmatrix} -\alpha\, f'(x_s) & 0 & 0 \\ 0 & 0 & 0 \\ 0 & 0 & 0 \end{pmatrix}, \quad \mathbf{H}_2 = \ldots = \mathbf{H}_{N-1} = \mathbf{0}_{3\times 3}. \tag{3.35}$$

The coupled problem for the N oscillators of dimension m can be formally decoupled by means of the Discrete Fourier Transform technique to yield a matrix that has N blocks with dimension 3 x 3 (as it has been done for the Lorenz case)

$$\begin{pmatrix} \dot{\eta}^{(0)} \\ \dot{\eta}^{(1)} \\ \vdots \\ \dot{\eta}^{(N-1)} \end{pmatrix} = \begin{pmatrix} \mathbf{C}^{(0)} & \mathbf{0} & \cdots & \mathbf{0} \\ \mathbf{0} & \mathbf{C}^{(1)} & \cdots & \mathbf{0} \\ \vdots & \vdots & \ddots & \vdots \\ \mathbf{0} & \mathbf{0} & \cdots & \mathbf{C}^{(N-1)} \end{pmatrix} \cdot \begin{pmatrix} \eta^{(0)} \\ \eta^{(1)} \\ \vdots \\ \eta^{(N-1)} \end{pmatrix} \tag{3.36}$$

where the structure of each block is the following,

$$\mathbf{C}^{(k)} = \begin{pmatrix} -\alpha[1 + f'(x_s)\, e_k] & \alpha & 0 \\ 1 & -1 & 1 \\ 0 & -\beta & -\gamma \end{pmatrix} \tag{3.37}$$

being $e_k = \exp(i\,2\pi\, k/N)$ and k = 0,. . . , (N − 1) the Fourier modes of the system.

The Fourier mode k = 0 represents the synchronized state, and the matrix $\mathbf{C}^{(0)}$ is the same as that of an isolated Chua's circuit. Thus, since the uncoupled Chua's circuits for the considered values of the parameters and initial conditions (different for each oscillator) are in a chaotic regime, the nature of the synchronized state will be chaotic as well. The other N − 1 matrices allow to determine the stability of the synchronization manifold against transverse perturbations [94] in terms of the corresponding transverse Lyapunov exponents. The Lyapunov exponents are used to analyze the stability of the system, the same as in the Lorenz case, since again the $\mathbf{C}^{(k)}$ matrices have nonconstant, chaotically varying coefficients, namely f'(z).

The highest transverse Lyapunov exponent function plotted as a function of the reduced wave number, $\lambda(q)$, for this scheme of Chua's oscillators (see Fig. 3.16) has

a very similar form to the one obtained for the Lorenz case. As then, this function is symmetric with respect to the line $q = 1/2$, since the eigenvalues of the $\mathbf{C}^{(k)}$ and $\mathbf{C}^{(N-k)}$ are complex conjugate one to each other. On the other hand, once again there exists a certain number of oscillators in the ring, N_c, for which the uniform synchronized chaotic state becomes unstable since $\lambda(q = 0) > 0$ and $\lambda(q = 1/2) < 0$. In particular, for $(\alpha, \beta, \gamma, a, b)$ = (10,14.87,0.06, -1.27, -0.68) this critical number is N_c = 5, which corresponds to $q_c = 0.21$.

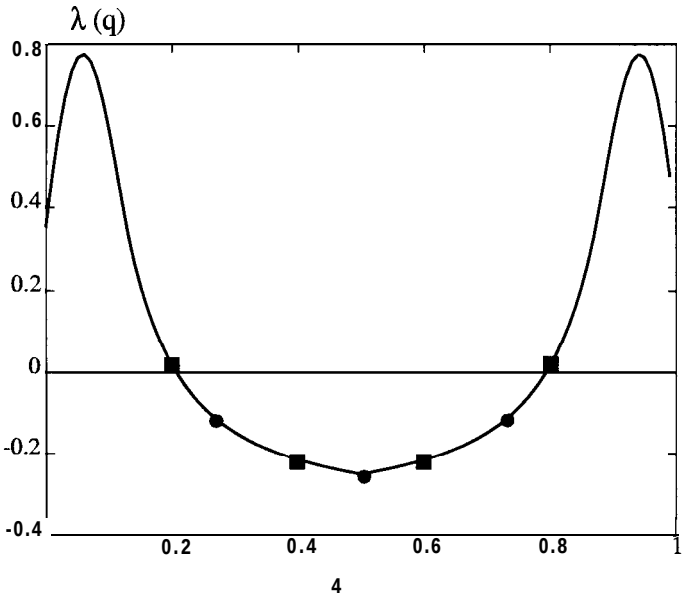

Figure 3.16: Representation of the highest Lyapunov exponent $X(q)$ as a function of $q = k/N$. The circles indicate the highest transverse Lyapunov exponent for the corresponding transverse Fourier modes in a ring of N = 4 Chua's oscillators, whereas the squares indicate the same for a ring of N = 5. The values of the parameters are $(\alpha, \beta, \gamma, a, b)$ = (10,14.87,0.06, -1.27, -0.68).

Symmetry also determines the behavior of the ring after the onset of the instability. We have seen that the eigenvalues of the matrices $\mathbf{C}^{(k)}$ and $\mathbf{C}^{(N-k)}$ are complex conjugate. In order to have qualitative information about the real or complex character of the eigenvalues we can employ the same averaging method used for the Lorenz case. Remember that in that method one replaces the instantaneous time-dependent coefficients of the matrices $\mathbf{C}^{(k)}$ by their average values when $t \to \infty$. As in the Lorenz case, the eigenvalues are complex and the instability will occur through a Hopf bifurcation because the presence of the e_k terms in Eq. (3.37) implies that half of the Fourier modes are complex conjugate to the other half. This means that

when a given mode crosses the instability threshold there will be another mode that also exhibits the same type of crossing. The result is immediate: a Hopf bifurcation occurs, implying the appearance of a discrete rotating wave, in which neighboring oscillators exhibit the reported phase difference.

The theoretical analysis that gives rise to the function $\lambda(q)$ as well as numerical simulations and experiments performed with the electronic setup agree in that the uniform synchronized state is stable when the number of units N in the ring is low enough, and in that starting from a certain size N_c the synchronized state loses stability.

Numerical Results.

Figure 3.17 shows numerical results corresponding to a ring of N = 4 Chua's oscillators, for which the chaotic synchronized solution is still stable, while Fig. 3.18 presents numerical results for N = N_c = 5, size for which the uniform synchronized state of the ring becomes unstable. What can be observed is again a rotating wave, in the sense that a given oscillator is advanced with respect to the previous one by approximately l/N of a period, i.e., $1/5$ in our case. Notice that now the concept of a *period* cannot be defined in a unique way since the behavior of each oscillator is chaotic and the distances between peaks vary chaotically. However, one can define the concept of time shift, that, when optimum, would make the peaks almost coincide, without paying attention to the different height of these peaks. Thus, looking at Fig. 3.18, which contains the representation of the variables $x_1, \ldots, x_5$ for a ring of N = 5 Chua's circuits, one can note that the optimum delay τ is very close to l/5 of the period, as predicted by the theoretical analysis. Regarding the behavior of larger rings, it has been found that the chaotic rotating-wave behavior occurs for rings with N = 5 and N = 6 for the parameters reported up to now, that is, $(\alpha, \beta, \gamma, a, b)$ = (10,14.87,0.06, -1.27, -0.68). For these values of the parameters, when N $\geq$ 7 the ring becomes unstable and the variables of the system explode in an oscillatory fashion. Thus, the observed behavior is that the system remains confined to a neighborhood of the synchronized state for 5 $\geq$ N $\geq$ 6, while the instability dominates the behavior of the system for larger sizes of the ring.

Regarding the dependence of the stability of the ring on the parameters, for

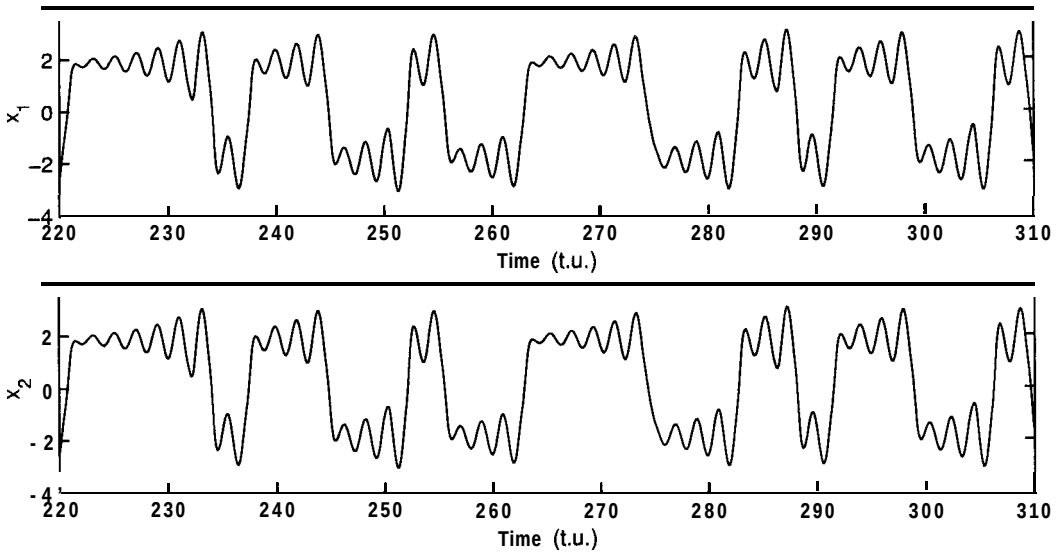

Figure 3.17: Temporal evolution of the variable x of two contiguous oscillator8 in a ring of N = 4 Chua's oscillators. The values of the parameters are the same as in Fig. 3.16.

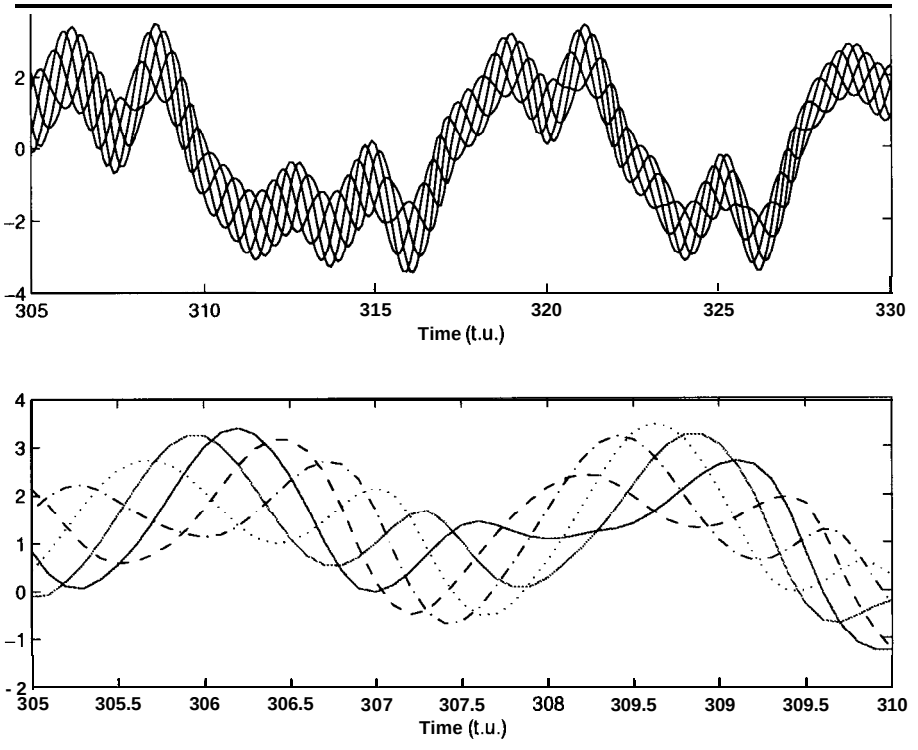

Figure 3.18: Temporal evolution of the variables $x_i, i = 1,. .., 5$ in a ring of N = 5 Chua's oscillators. The values of the parameters are the same as in Fig. 3.16 and Fig. 3.17. The upper plot show8 the chaotic rotating wave structure that arises in the ring. The lower plot is a zoom that allows to observe the time shift between contiguous oscillators. The two solid lines correspond to x_1 and x_2, the dashed line to x_3, the dashed-dotted line to x_4 and the dotted one to x_5.

$(\alpha, \beta, \gamma, a, b)$ = (10,14.87,0.06, – 1.27, -0.68) one has that rings up to N_{max} = 4 are stable in the chaotic uniform state. By varying γ, while keeping fixed the rest of parameters it can be seen that this is true while $\gamma \leq 0.15$, while for $\gamma > 0.15$ the five-membered ring is stable (N_{max} = 5). One cannot consider too high values for γ, because at some point ($\gamma > 0.20$ for the parameters considered here), the Chua's circuit is no longer the usual double-scroll attractor. Thus, if one wishes to obtain stable N-membered rings it is necessary to vary any other parameter, such that it changes the highest eigenvalue of $\mathbf{C}^{(1)}$ in Eq. (3.37). One would suspect that those in the diagonal will have the highest effect. In particular, a six-membered ring has been stabilized for α = 12 and γ = 0.2. Table 3.1 summarizes results described so far.

N_{max}	$(\alpha; \gamma)$
4	$\alpha = 10;\ \gamma \leq 0.15$
5	$\alpha = 10;\ 0.15 < \gamma < 0.2$
6	$\alpha = 12;\ \gamma = 0.2$

Table 3.1: Critical number of chaotic Chua's circuits in a ring, N_{max}, that supports chaotic (uniform) synchronization.

Experimental Results.

The numerical results discussed above have been corroborated by the experiments carried out using the setup described in Section 3.2.2. The values of the components of the oscillators chosen for the setup described in that section, correspond to the adimesional set of values $(\alpha, \beta, \gamma, a, b)$ = (10,12.1,0.22, -1.26, -0.79). Figure 3.19 represents the highest transverse Lyapunov exponent as a function of q = k/N for such adimensional set of values. It can be expected that now synchronization among circuits is obtained when N = 5 while for N = 6 a chaotic rotating wave develops in the system.

Figure 3.20 presents the synchronization phenomenon obtained experimentally for a ring of five oscillators. In such figure, the temporal evolution of the voltage at the capacitor C_1 for two oscillators has been recorded. To see more clearly the synchronization effect we can resort to a representation of the voltage at the capacitor C_1 of one circuit of the ring versus the same magnitude of another different circuit

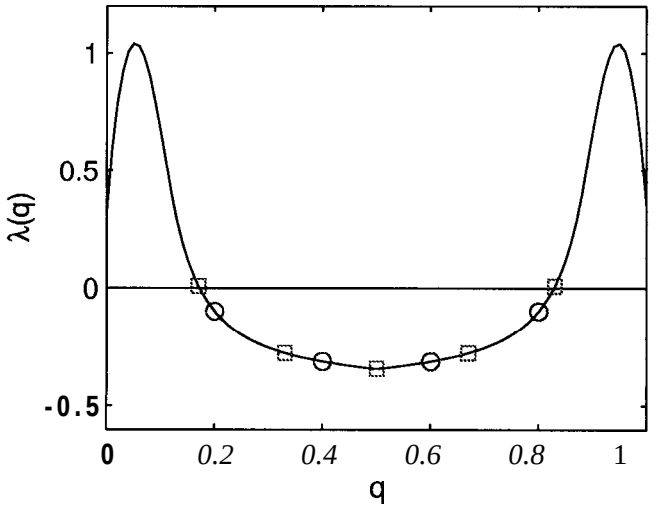

Figure 3.19: Representation of the highest Lyapunov exponent *X(q)* as a function of $q = k/N$. The circles indicate the highest tranverse Lyapunov exponent for the corresponding transverse Fourier modes in a ring of N = 5 Chua's oscillators, whereas the squares indicate the same for a ring of N = 6. The values of the parameters are $(\alpha, \beta, \gamma, a, b)$ = (10,12.1,0.22, -1.26, -0.79).

(see Fig. 3.21), which shows a straight line with slope of forty-five degrees. Since the temporal evolution of the Fourier mode $k = 0$ is determined by the matrix $\mathbf{C}^{(0)}$, which is identical to the Jacobian matrix that governs the evolution of an isolated Chua's oscillator, the behavior of the ring in synchronized state will be the same as that of an isolated Chua's oscillator, that is, the typical double-scroll represented in Fig. 3.22.

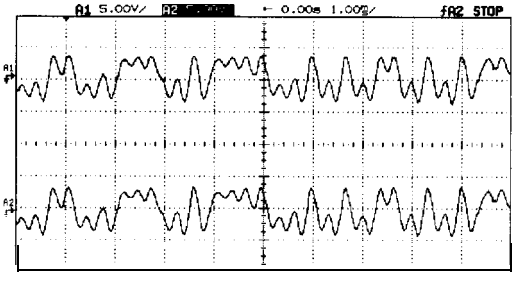

Figure 3.20: Synchronization among chaotic circuits obtained experimentally for a ring of five unidirectionally coupled Chua's circuits. The temporal evolution of the voltage at the capacitor C_1 has been represented for two circuits.

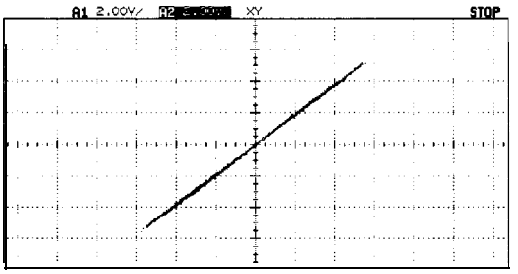

Figure 3.21: Representation of the voltage through capacitor C_1 corresponding to one circuit of a ring of five oscillators versus the same quantity for another circuit. This plot indicates synchronization among the circuits.

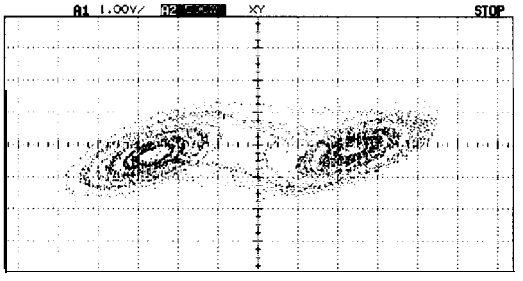

Figure 3.22: Representation of the voltage through capacitor C_1 versus the voltage through capacitor C_2 for a Chua's circuit of a ring of five synchronized oscillators. The typical double-scroll characteristic of an isolated chaotic circuit has been obtained.

Figure 3.23 represents a rotating wave obtained experimentally for a ring of six oscillators. In particular, the temporal evolution of the voltage at the capacitor C_1 for four contiguous circuits is shown in that figure. This allows to see more clearly the *fingerprint* of these waves: they are waves with an aperiodic modulated envelope, indicating the superposition of the modes $k = 0$ and $k = 1$. This envelope includes waves with an approximate phase relationship of $2\pi/N$ (characteristic of the mode 1), being N the number of oscillators (N = 6 in our case). Figure 3.24 contains a representation of the voltages across capacitor C_2 corresponding to two contiguous circuits in the same ring, where the typical straight line characteristic of synchronization appears broadened as a consequence of the phase shift. Figure 3.25 shows the voltage across capacitor C_1 versus the voltage across capacitor C_2, both corresponding to the same circuit. Notice that the resulting chaotic behavior is not the same as the one of an isolated chaotic Chua's oscillator.

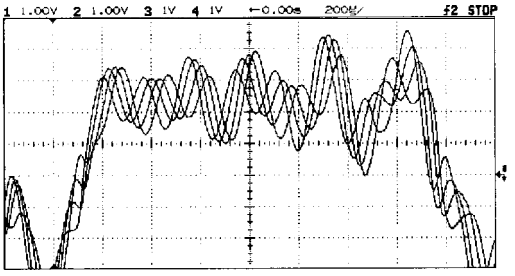

Figure 3.23: Chaotic rotating wave obtained experimentally for a ring of six unidirectionally coupled Chua's circuits. Representation of the time series of the voltage at the capacitor C_1 in four contiguous circuits.

[htb]

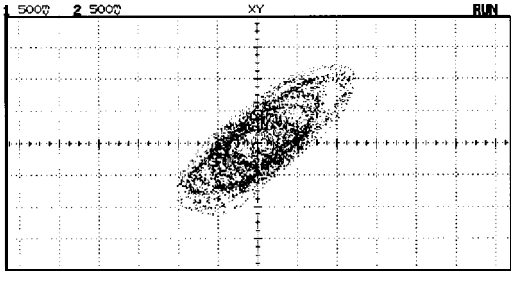

Figure 3.24: Representation of voltages at capacitors C_2 in two contiguous circuits, one as a function of the other, for a chaotic rotating wave obtained experimentally with six Chua's circuits.

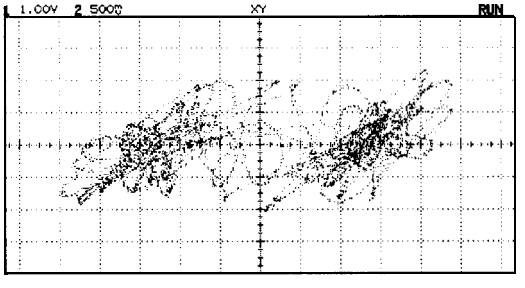

Figure 3.25: Phase plane of the two voltages at both capacitors of one circuit for a chaotic rotating wave obtained experimentally with six Chua's circuits.

3.4.3 Interaction between two Rings of Chua's Oscillators.

As mentioned in the numerical and experimental setup, two rings of N Chua's ocillators each one have also been considered [140]. These rings have been coupled in the way described by Eq. (3.5), that in compact form can be written as

$$\dot{\mathbf{x}}_j = \mathbf{G}_j(\mathbf{x}_0, \ldots, \mathbf{x}_{N-1}) \quad j = 0\ ,\ldots,\ \mathbf{N\text{-}1} \tag{3.38}$$

where $\mathbf{x}_j = (\mathbf{x}_j^0, \mathbf{x}_j^1) = (x_j^0, y_j^0, z_j^0, x_j^1, y_j^1, z_j^1)$ and the form of function $\mathbf{G}_j$ depends on the type of coupling: parallel or antiparallel.

As in the case of only one ring, a linear stability analysis of the system described above around the globally synchronized state, now s = $(x_s(t), y_s(t), z_s(t), x_s(t), y_s(t), z_s(t))$, has been carried out. This analysis starts by performing an expansion of Eq. (3.5) around this state and keeping only linear terms. One obtains a system of N coupled differential equations for every $\delta\mathbf{x}_j = (\delta\mathbf{x}_j^0, \delta\mathbf{x}_j^1) = (\delta x_j^0, \delta y_j^0, \delta z_j^0, \delta x_j^1, \delta y_j^1, \delta z_j^1)$ with a quite sparse structure. In particular, two different cases will be analyzed in this section: parallel and antiparallel coupling (see Fig. 3.26), focusing our attention on the interaction between the chaotic rotating waves introduced in the previous section.

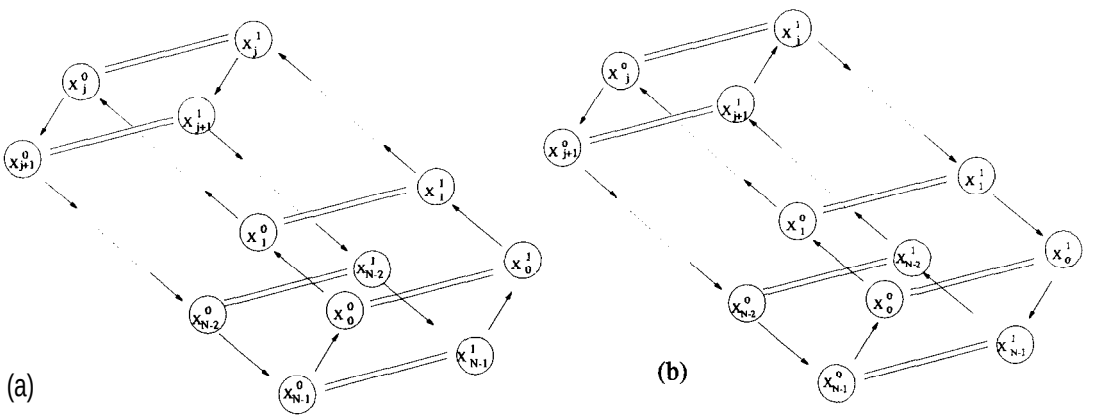

Figure 3.26: Scheme of parallel (a) and antiparallel (b) coupling.

Parallel Coupling.

In the case of parallel coupling the functions $\mathbf{G}_j$ that represent the dynamical evolution of the variable $\mathbf{x}_j$ are defined by

$$\begin{aligned}\mathbf{G}_j(\mathbf{x}_0,\ldots,\mathbf{x}_{N-1}) \;=\; & (\alpha[y_j^0 - x_j^0 - f(x_{j-1}^0)] + D(x_j^1 - x_j^0), x_j^0 - y_j^0 + z_j^0,\\ & -\beta y_j^0 - \gamma\, z_j^0, \alpha[y_j^1 - x_j^1 - f(x_{j-1}^1)] + D(x_j^0 - x_j^1),\\ & x_j^1 - y_j^1 + z_j^1, -\beta y_j^1 - \gamma z_j^1)\end{aligned} \tag{3.39}$$

where the index j is mod N. Since these functions are shift-invariant the evolution of the perturbations around the synchronized state can be written as in Eq. (3.34), where now the matrices are

$$\mathbf{H}_0 \;=\; \begin{pmatrix} -\alpha - D & \alpha & 0 & D & 0 & 0\\ 1 & -1 & 1 & 0 & 0 & 0\\ 0 & -\beta & -\gamma & 0 & 0 & 0\\ D & 0 & 0 & -a - D & \alpha & 0\\ 0 & 0 & 0 & 1 & -1 & 1\\ 0 & 0 & 0 & 0 & -\beta & -\gamma \end{pmatrix},$$

$$\mathbf{H}_1 \;=\; \begin{pmatrix} -\alpha f'(x_s) & 0 & 0 & 0 & 0 & 0\\ 0 & 0 & 0 & 0 & 0 & 0\\ 0 & 0 & 0 & 0 & 0 & 0\\ 0 & 0 & 0 & -\alpha f'(x_s) & 0 & 0\\ 0 & 0 & 0 & 0 & 0 & 0\\ 0 & 0 & 0 & 0 & 0 & 0 \end{pmatrix}, \tag{3.40}$$

$$\mathbf{H}_2 \;=\; \ldots = \mathbf{H}_{N-1} \;=\; \mathbf{0}_{6\times 6}.$$

Matrix $\mathbf{H}$ can be put in block-diagonal form by applying a DFT, as it was done for a single ring of Chua's cells. The resulting system is

$$\begin{pmatrix} \dot{\eta}^{(0)}\\ \dot{\eta}^{(1)}\\ \vdots\\ \dot{\eta}^{(N-1)} \end{pmatrix} = \begin{pmatrix} \mathbf{C}^{(0)} & \mathbf{0} & \cdots & \mathbf{0}\\ \mathbf{0} & \mathbf{C}^{(1)} & \cdots & \mathbf{0}\\ \vdots & \vdots & \ddots & \vdots\\ \mathbf{0} & \mathbf{0} & \cdots & \mathbf{C}^{(N-1)} \end{pmatrix} \cdot \begin{pmatrix} \eta^{(0)}\\ \eta^{(1)}\\ \vdots\\ \eta^{(N-1)} \end{pmatrix} \tag{3.41}$$

where $\eta^{(k)} = \sum_{j=0}^{N-1} \delta\mathbf{x}_j e^{\frac{2\pi i j k}{N}}$, are vectors of six components and matrices $\mathbf{C}^{(k)}$ are 6 x 6 dimensional, with the block circulant structure

$$\mathbf{C}^{(k)} = \begin{pmatrix} \mathbf{Q}_0^{(k)} & \mathbf{Q}_1^{(k)}\\ \mathbf{Q}_1^{(k)} & \mathbf{Q}_0^{(k)} \end{pmatrix}, \tag{3.42}$$

being

$$\mathbf{Q}_0^{(k)} = \begin{pmatrix} -\alpha[1 + f'(x_s)\, e_k] - D & \alpha & 0 \\ 1 & -1 & 1 \\ 0 & -\beta & -\gamma \end{pmatrix} \quad \text{and} \quad \mathbf{Q}_1^{(k)} = \begin{pmatrix} D & 0 & 0 \\ 0 & 0 & 0 \\ 0 & 0 & 0 \end{pmatrix}. \tag{3.43}$$

In this way, the initial problem has been brought to 6 x 6 block-diagonal form by applying a DFT. Besides, the components of each vector $\eta^{(k)}$ can also be divided in two different vectors: $\xi_0^{(k)}$ containing the three first components of $\eta^{(k)}$, and $\xi_1^{(k)}$ containing the three last ones

$$\xi_0^{(k)} = (\eta_1^{(k)}, \eta_2^{(k)}, \eta_3^{(k)}) \quad \text{and} \quad \xi_1^{(k)} = (\eta_4^{(k)}, \eta_5^{(k)}, \eta_6^{(k)}). \tag{3.44}$$

The dynamical evolution of each new vector can be represented by the following convolutional sum

$$\dot{\xi}_j^{(k)} = \sum_{i=O}^{1} \mathbf{Q}_{j-i}^{(k)}\, \xi_i^{(k)} \quad j = 0, 1. \tag{3.45}$$

Applying a DFT to the sequence $\{\mathbf{Q}_0^{(k)}, \mathbf{Q}_1^{(k)}\}$ and to the sequence $\{\xi_0^{(k)}, \xi_1^{(k)}\}$, the transformed variational equations can be written as

$$\dot{\nu}^{(k,m)} = \mathbf{D}^{(k,m)}\, \nu^{(k,m)} \tag{3.46}$$

where the structure of each 3 x 3 block is the following,

$$\mathbf{D}^{(k,m)} = \begin{pmatrix} -\alpha[1 + f'(x_s) e_k] + D\ (\mathrm{e}, -1) & \alpha & 0 \\ 1 & -1 & 1 \\ 0 & -\beta & -\gamma \end{pmatrix}, \tag{3.47}$$

with $e_k = \exp(i\, 2\pi\, k/N)$ and $e_m = \exp(i\, \pi\, m)$, being k = 0,. ..,$(N-1)$ and m = 0, 1 the indices of Fourier modes of the system, with N the number of oscillators of each ring. Note that the terms $\nu^{(k,m)}$ have been obtained after applying twice the Discrete Fourier Transform (with respect to the indices j = 0,. . . (N − 1) and $i = 0, 1$) to $\delta \mathbf{x}_j$, resulting in the following expression

$$\nu^{(k,m)} = \sum_{j=0}^{N-1} \delta \mathbf{x}_j^0 e^{\frac{2\pi i j k}{N}} + \left(\sum_{j=0}^{N-1} \delta \mathbf{x}_j^1 e^{\frac{2\pi i j k}{N}} \right) \quad e^{\pi i m} \tag{3.48}$$

The (k, m) = (0,0) Fourier mode represents the uniform global chaotic synchronized state of the coupled system and the stability of this state can be characterized by analyzing the transverse Lyapunov spectrum. Global (double-scroll) synchronization occurs only if all the Transverse Lyapunov Exponents (TLEs) are negative. It is

important to notice from Eq. (3.47) that the Jacobian matrices corresponding to the Fourier modes $(k, 0)$ are identical as the ones corresponding to the modes k of a single ring (see Section 3.4.2), while the Jacobian matrices corresponding to the modes $(k, 1)$ take into account the coupling between rings.

Figure 3.27 shows the highest TLEs associated with Fourier modes $(k, 0)$ and (k, 1) for two different values of the coupling coefficient *D:* the plot on the left for D = 2.3 and the plot on the right for D = 4. In both plots the upper curve represents the highest TLEs for the modes $(k, 0)$ while the lower curve represents the one corresponding to (k, 1).

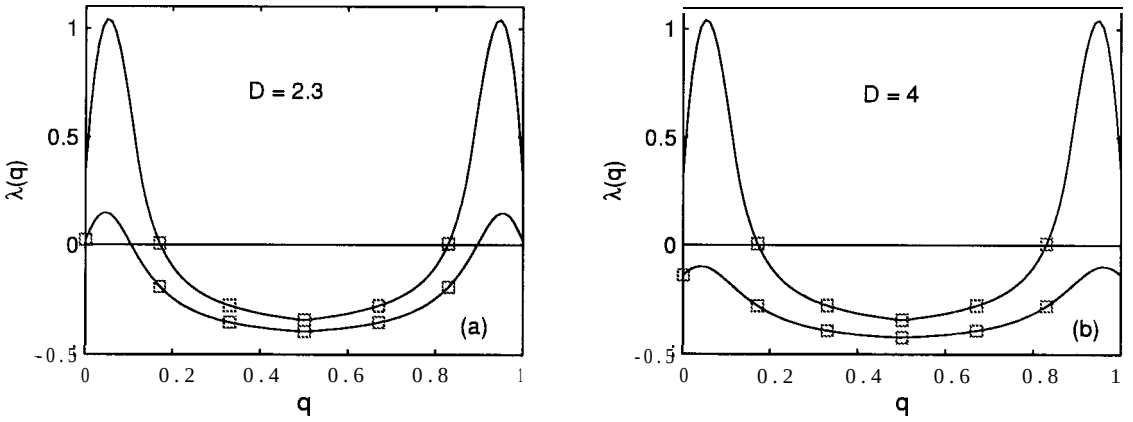

Figure 3.27: Representation of the highest Transverse Lyapunov Exponent, λ as a function of $q = k/N$ (being N the total number of Chua's circuits in each ring and $k = 0,. . . , N - 1$ the Fourier modes associated with the size of the ring) for two diffusively coupled rings with the same sense of driving (parallel coupling): (a) D = 2.3 and (b) D = 4. The upper curve in both plots represents the highest TLE for the modes $(k, \mathrm{m}) = (k, 0)$, which corresponds with the case of a single ring without coupling, while the lower curve represents the highest TLE for the modes $(k, \mathrm{m}) = (k,1)$, which depend on the coupling between the two rings. The squares represent the TLEs when considering N = 6.

Two facts can be appreciated from Fig. 3.27(a). On the one hand, the fact that for N = 6, the (1,0) mode is unstable, which corresponds to a chaotic rotating wave (recall Fig. 3.23), since, now, the circuits are not synchronized inside each ring. On the other hand, we can observe another instability in the mode (0, l), what indicates that for D = 2.3 there are not synchronization between rings. Thus, for N = 6 one must expect to observe two desynchronized chaotic rotating waves, each one in a different ring. Fig. 3.27(b) represents the TLEs for a greater value of the coupling coefficient D. We can observe that now all the TLEs associated to the Fourier modes

$(k, 1)$ are negative, which indicates synchronization between the two rings. Therefore, for N = 6 linear theory predicts synchronization between the two chaotic rotating waves. Notice that for this value of the coupling coefficient and a smaller number of elements in each ring, global (double-scroll) synchronization is expected, since all the TLEs are negative.

From Fig. 3.27 it is also apparent that mode (0,l) moves from positive to negative values as the coupling coefficient D grows. Thus, we can study the evolution of this mode as a function of $\boldsymbol{D}$ to find out when the transition from positive to negative values appears. Figure 3.28 shows that this happens approximately for $\boldsymbol{D} \approx 2.5$.

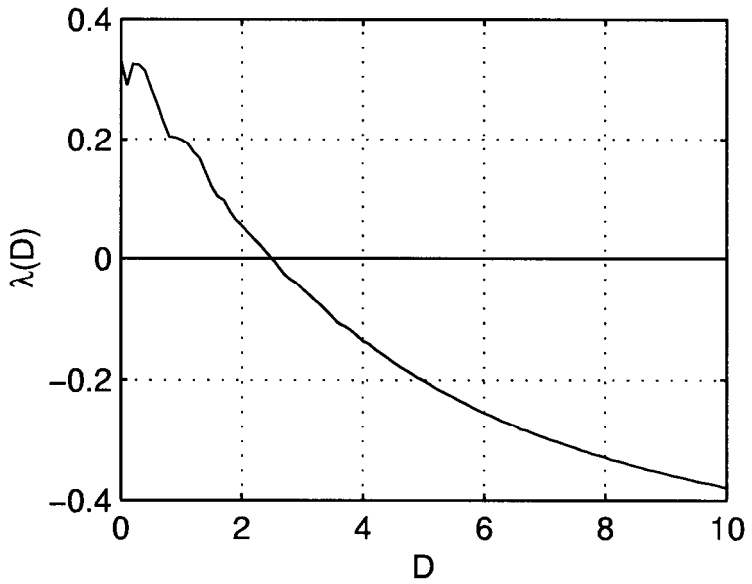

Figure 3.28: Representation of the highest TLE for the mode $(k, \mathrm{m}) = (0,\mathrm{l})$ versus the coupling coefficient D. The values of the parameters for each circuit in Eq. (3.5) are: $(\alpha, \beta, \gamma, a, b) = (10, 12.1, 0.22, -1.26, -0.79)$. Notice that $\lambda(D) = 0$ when $D \approx 2.5$.

Therefore, for weak coupling between rings (high values of R_c, low values of D), rotating waves do not see each other, and the observed behavior corresponds to non-interacting waves. Figure 3.29 shows these two desynchronized chaotic rotating waves, each one corresponding to a different ring. On the other hand, if the coupling is strong enough (low values of R_c, high values of $\boldsymbol{D}$) these two waves are synchronized, as shown in Fig. 3.30.

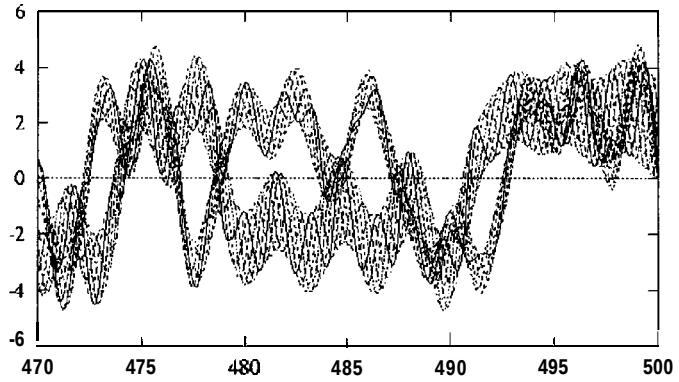

Figure 3.29: Representation of two non synchronized chaotic rotating waves, obtained for weak parallel coupling (D = 2) between two rings of Chua's oscillators. The values of the parameters for each circuit in Eq. (3.5) are: $(\alpha, \beta, \gamma, a, b)$ = (10,12-l, 0.22, – 1.26, -0.79).

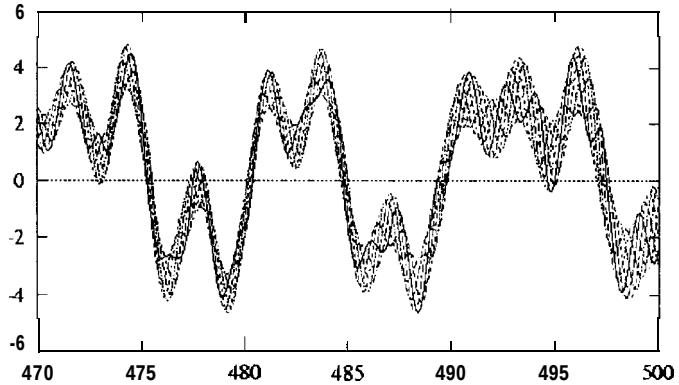

Figure 3.30: Synchronization between two chaotic rotating waves, obtained for strong parallel coupling (D = 6) between two rings of Chua's oscillators. The values of the parameters for each circuit in Eq. (3.5) are the same as in Fig. 3.29.

Antiparallel Coupling.

In the case of antiparallel coupling the functions $\mathbf{G}_j$ that represent the dynamical evolution of the variable $\mathbf{x}_j$ are defined by

$$\begin{aligned}\mathbf{G}_j(\mathbf{x}_0, \ldots, \mathbf{x}_{N-1}) = \; & (\alpha[y_j^0 - x_j^0 - f(x_{j-1}^0)] + D(x_j^1 - x_j^0), x_j^0 - y_j^0 + z_j^0, \\ & -\beta y_j^0 - \gamma z_j^0, \alpha[y_j^1 - x_j^1 - f(x_{j+1}^1)] + D(x_j^0 - x_j^1), \\ & x_j^1 - y_j^1 + z_j^1, -\beta y_j^1 - \gamma z_j^1) \end{aligned} \tag{3.49}$$

where the index j is mod N. Since these functions are shift-invariant, the evolution of the perturbations around the synchronized state can be written as in Eq. (3.34),

where now the matrices are

$$\mathbf{H}_0 = \begin{pmatrix} -\alpha - D & a & 0 & D & 0 & 0 \\ 1 & -1 & 1 & 0 & 0 & 0 \\ D & -\beta & -\gamma & -a & -D & \alpha & 0 \\ 0 & 0 & 0 & 1 & -1 & 1 \\ 0 & 0 & 0 & 0 & -\beta & -\gamma \end{pmatrix},$$

$$\mathbf{H}_1 = \begin{pmatrix} -\alpha f'(x_s) & 0 & 0 & 0 & 0 & 0 \\ 0 & 0 & 0 & 0 & 0 & 0 \\ 0 & 0 & 0 & 0 & 0 & 0 \\ 0 & 0 & 0 & 0 & 0 & 0 \\ 0 & 0 & 0 & 0 & 0 & 0 \\ 0 & 0 & 0 & 0 & 0 & 0 \end{pmatrix}, \quad \mathbf{H}_2 = \ldots = \mathbf{H}_{N-2} = \mathbf{0}_{6\times 6}$$

$$\mathbf{H}_{N-1} = \begin{pmatrix} 0 & 0 & 0 & 0 & 0 & 0 \\ 0 & 0 & 0 & 0 & 0 & 0 \\ 0 & 0 & 0 & 0 & 0 & 0 \\ 0 & 0 & 0 & -\alpha f'(x_s) & 0 & 0 \\ 0 & 0 & 0 & 0 & 0 & 0 \\ 0 & 0 & 0 & 0 & 0 & 0 \end{pmatrix} \tag{3.50}$$

The main difference with respect to the case of parallel coupling is that now it is not possible to bring the problem to a block-diagonal form, at least in an obvious way, to yield a 3 x 3 decoupled problem (that runs over $k = 0, \ldots, (N-1)$ and m = $0, 1$). In the present situation it is possible to apply once a DFT but the simplification that one can attain is, at most, to a 6 x 6 problem in which the two cells of different rings that are resistively coupled appear together. The structure of the 6 x 6 problem is, analogously to the case of parallel coupling, of the form

$$\dot{\eta}^{(k)} = \mathbf{C}^{(k)}\,\eta^{(k)} \tag{3.51}$$

where

$$\eta^{(k)} = \sum_{j=0}^{N-1} \delta \mathbf{x}_j e^{\frac{2\pi i j k}{N}} \tag{3.52}$$

and

$$\mathbf{C}^{(k)} = \begin{pmatrix} \mathbf{Q}_0^{(k)} & \mathbf{Q}_1^{(k)} \\ \mathbf{Q}_1^{(k)} & \mathbf{Q}_0^{(k)\dagger} \end{pmatrix}, \tag{3.53}$$

being $\mathbf{Q}_0^{(k)}$ and $\mathbf{Q}_1^{(k)}$ the same 3 x 3 matrices already described in the parallel case (see Eq. (3.43)), and $\mathbf{Q}_0^{(k)\dagger}$ the complex conjugate of $\mathbf{Q}_0^{(k)}$.

The characterization of the instability has been performed as a function of the coupling coefficient D (corresponding to the coupling resistance R,). Figure 3.31 shows the dependence on the coupling coefficient, D, of the highest Lyapunov exponent, $X(D)$, corresponding to the Fourier modes $k = 0,\ldots, N-1$ when N = 6. Actually, the curves corresponding to the transverse Fourier modes k = 4,5 are not plotted because they are the same as those corresponding to modes k = 2,1, respectively.

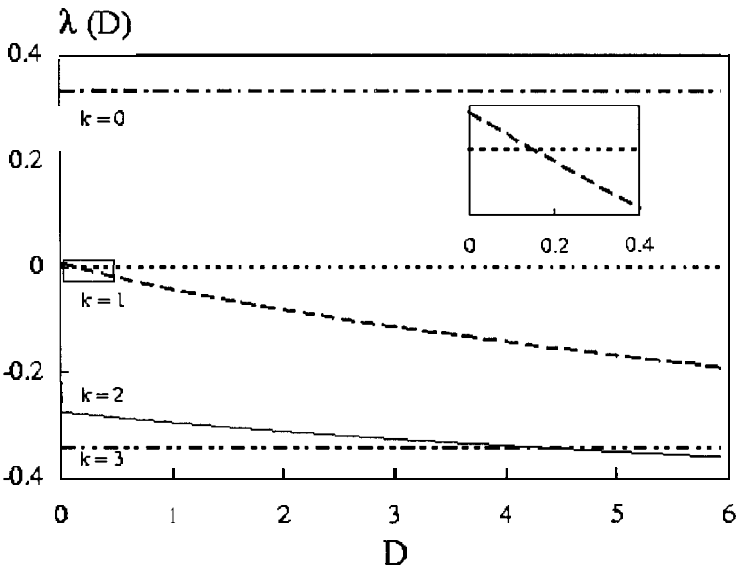

Figure 3.31: Dependence of the highest Lyapunov Exponent X(D), corresponding to the modes $k = 0,\ldots,3$ (for $N = 6$), on the coupling (diffusion) coefficient D between rings with opposite sense of driving. The inset shows the transition from positive to negative of the TLE corresponding to mode k = 1 for D = 0.17. Set of parameters as in Fig. 3.27.

Notice that for $D \geq 0.17$ all transverse Lyapunov exponents are negative and, therefore, the Fourier mode $k = 0$ is stable. Using the properties of the DFT [163], this means that $\delta\mathbf{x}_0 = \delta\mathbf{x}_1 = \ldots = \delta\mathbf{x}_{N-1} = \mathbf{c}(t)$, that is,

$$\begin{pmatrix} \delta\mathbf{x}_0^0 \\ \delta\mathbf{x}_0^1 \end{pmatrix} = \begin{pmatrix} \delta\mathbf{x}_1^0 \\ \delta\mathbf{x}_1^1 \end{pmatrix} = \cdots = \begin{pmatrix} \delta\mathbf{x}_{N-1}^0 \\ \delta\mathbf{x}_{N-1}^1 \end{pmatrix} = \begin{pmatrix} \mathbf{c}^0(t) \\ \mathbf{c}^1(t) \end{pmatrix}. \tag{3.54}$$

It is apparent from Eq. (3.54) that two possible situations exist:

- $\mathbf{c}^0(t) \neq \mathbf{c}^1(t)$: all the circuits in each ring are synchronized but there is no synchronization between rings.

- $\mathbf{c}^0(t) = \mathbf{c}^1(t)$: all the circuits in the whole system are synchonized.

The fact that the Fourier mode $k = 0$ is stable for $D \geq 0.17$, implies that the system will evolve either to the first or to the second of the situations mentioned above. Reaching one or the other will depend on the particular value of the coupling coefficient. To know when global synchronization between all oscillators can be achieved we can resort to the properties of the matrices $\mathbf{C}^{(k)}$. Although these matrices are not circulant for all possible values of k, it is important to realize that the matrix $\mathbf{C}^{(0)}$ shows a circulant structure, since $\mathbf{Q}_0^{(0)}$ and $\mathbf{Q}_0^{(0)\dagger}$ are identical. This allows to apply a second DFT to the sequence $\{\mathbf{Q}_0^{(0)}, \mathbf{Q}_1^{(0)}\}$ and to the sequence $\{\xi_0^{(0)}, \xi_1^{(0)}\}$ (defined as in the parallel case, see Eq. (3.44)), which leads to

$$\dot{\nu}^{(0,m)} = \mathbf{D}^{(0,m)}\, \nu^{(0,m)} \tag{3.55}$$

where m = 0,1 and

$$\mathbf{D}^{(0,m)} = \begin{pmatrix} -\alpha[1 + f'(x_s)] + D\,(e_m - 1) & \alpha & 0 \\ 1 & -1 & 1 \\ 0 & -\beta & -\gamma \end{pmatrix}. \tag{3.56}$$

These matrices are the same as the corresponding to the parallel coupling case, so the problem analysis at this point is also the same. In particular, the matrix $\mathbf{D}^{(0,0)}$ coincides with the Jacobian matrix of an isolated Chua's circuit. Therefore, when all the Lyapunov exponents associated to $k \geq 1$ and to the mode (0, m) = (0,1) are negative, all oscillators in the system will be synchronized exhibiting the typical double-scroll attractor. Recall that Fig. 3.28 showed the dependence of the highest Lyapunov exponent corresponding to the mode (0,1) on the value of the coupling coefficient D. There, a transition from positive to negative values of the Lyapunov exponent appeared when $D \approx 2.5$.

The above argument indicates that in the case of antiparallel coupling the range of possible behaviors is richer than in the case of parallel coupling, since we can distinguish three possible different situations depending on the value of the coupling coefficient *D:*

- For weak coupling, $D < 0.17$, there is no interaction between rings and each ring behaves as if it was isolated (see Fig. 3.32). Thus, for N = 6, we observe two desynchronized rotating waves, one in each ring.

- For intermediate coupling, $0.17 < D < 2.5$, synchronization is observed inside each ring but not between them. Figure 3.33 shows the evolution of the system for $\boldsymbol{D} = 2.4$, where all the circuits within each ring are synchronized. Both rings are quite correlated since the value of the coupling coefficient is very close to the range of strong coupling.

- For strong coupling, all the oscillators in the two rings become synchronized in double-scroll regime. Figure 3.34 represents the evolution of both rings for $\boldsymbol{D} = 2.6$.

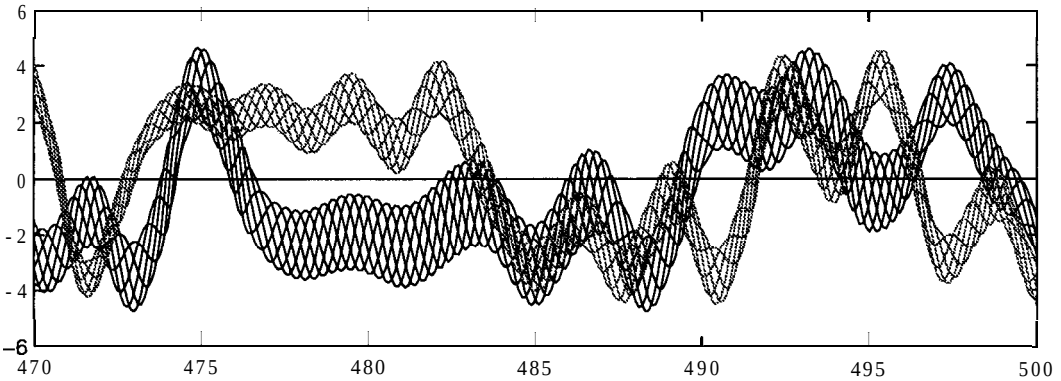

Figure 3.32: Representation of two non synchronized chaotic rotating waves, obtained for weak antiparallel coupling ($D = 0.1$) between two rings of Chua's oscillators. The values of the parameters for each circuit are: $(\alpha, \beta, \gamma, a, b)$ = (10,12.1,0.22, -1.26, -0.79).

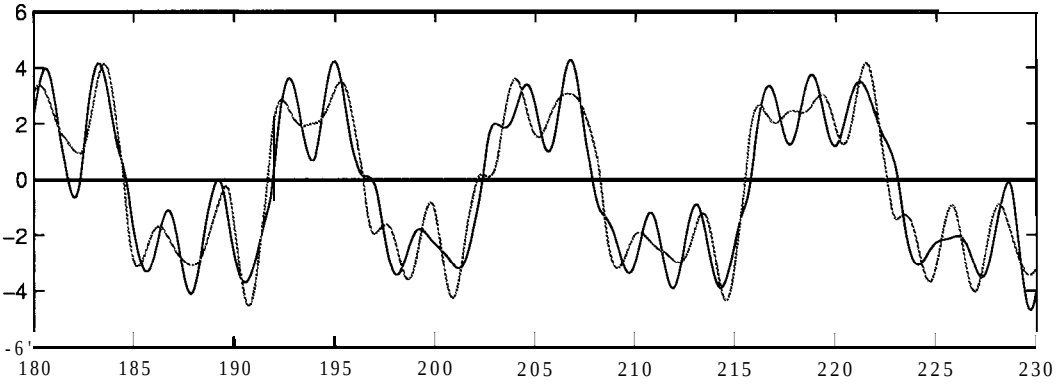

Figure 3.33: Representation of the temporal evolution of two rings of Chua's oscillators with intermediate antiparallel coupling ($D = 2.4$). The values of the parameters for each circuit are the same as in Fig. 3.32.

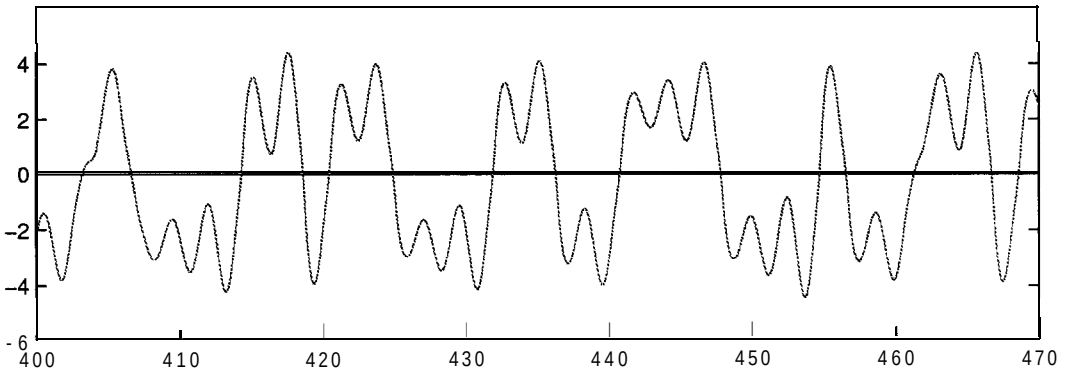

Figure 3.34: Representation of the temporal evolution of two rings of Chua's oscillators with strong antiparallel coupling (D = 2.6). The values of the parameters for each circuit are the same as in Fig. 3.32.

It is remarkable that transverse coupling is able to overcome the instability induced in a single ring by driving coupling, what has also been obtained with the experimental setup described in Section 3.2.2. Thus, Fig. 3.35 represents the phase portrait for a given circuit of the system, that is, the voltage at capacitor C_2 versus the voltage at capacitor C_1 when considering $R_c = 1\Omega$, showing the classical double-scroll chaotic attractor. Besides, Fig. 3.36 and Fig. 3.37 represent the voltages across capacitor C_2 corresponding to two contiguous circuits in the same ring and to two directly coupled circuits of different rings, respectively. Synchronized behavior of all circuits of the system can be deduced from such figures, in which the y = x characteristic behavior is observed, although with some thickness due to the fact that the circuits are not identical.

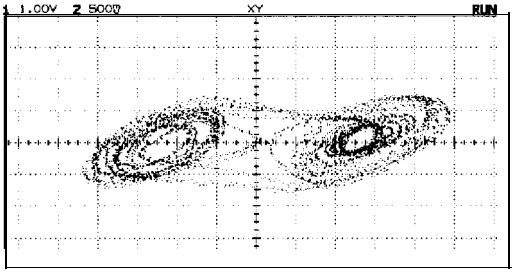

Figure 3.35: Phase plane of two voltages at both capacitors of one circuit of the experimental setup consisting of two antiparallel coupled rings, each one with 6 circuits, when considering $R_c = 1\Omega$. This circuit exhibits the classical Chua's double-scroll chaotic attractor.

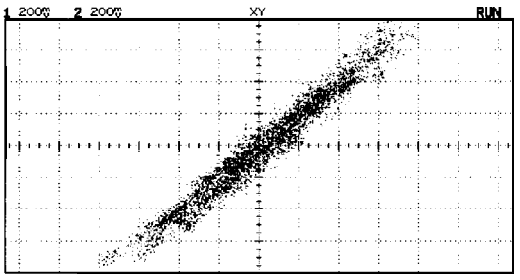

Figure 3.36: Representation of the voltages at capacitor C_2 for two contiguous circuits of a given ring for the same experimental setup as in Fig. 3.35. Synchronization among the circuits of the **same** ring is shown.

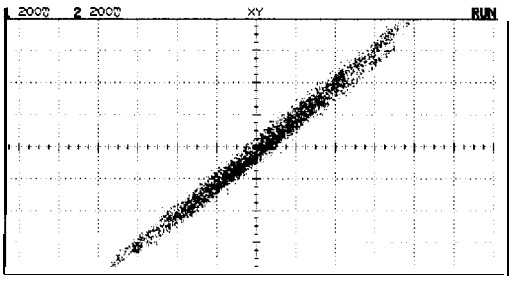

Figure 3.37: Representation of the voltages at capacitor C_2 for two diffusively coupled circuits, one from each ring, for the same experimental setup as in Fig. 3.35. Synchronization between directly coupled circuits of different rings is shown.

Another interesting effect has been obtained in the experimental setup for N = 6. In particular, for $R_c = 27\Omega$ each ring experiments some kind of on-off intermittency between the double-scroll and the chaotic rotating wave behavior. The fact that the uniform synchronized chaotic state in each ring is stable implies that the corresponding transverse Lyapunov spectrum must be negative [94]. However, even when the largest transverse exponent is negative (although close to zero) interesting phenomena may occur [177], as during short periods of time it may become positive (this exponent is guaranteed to be negative only in the asymptotic limit). In particular, the behavior that we get in our system is very close to an on-off intermittency [95], that in our case manifests in that the double-scroll attractor appears to be alive and breath. The system is subject to perturbations, that, notwithstanding, are not able to induce a transition to a different behavior. This

type of situation can be observed in Fig. 3.38 and Fig. 3.39. Notice the coexistence in time of both kinds of attractors, namely the doublescroll and the rotating wave shown in Fig. 3.35 and Fig. 3.25. The most striking aspect of this behavior is that typical lifetimes of each of the two transient states may be up to a few minutes, what is quite uncommon in this type of electronic analog circuits, with usual characteristic times of the order of the milliseconds. However, the transition itself is very fast. Moreover, the blurring in the characteristic y = x line shown in Fig. 3.36 implies that the double-scroll synchronized state is contaminated by perturbations, that resemble the characteristic Lissajoux-type figure of a chaotic rotating wave.

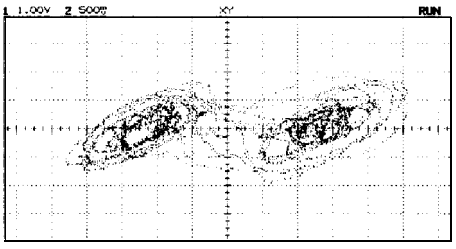

Figure 3.38: Phase plane of two voltages at both capacitors of one circuit showing the transition from a double-scroll chaotic attractor to a chaotic rotating wave. This experimental image has been obtained for antiparallel coupling when considering 6 circuits in each ring and with $R_c = 27\Omega$. Notice that this captured image is a genuine effect and not a technical feature of the oscilloscope (see the label RUN in the right-top of the panel).

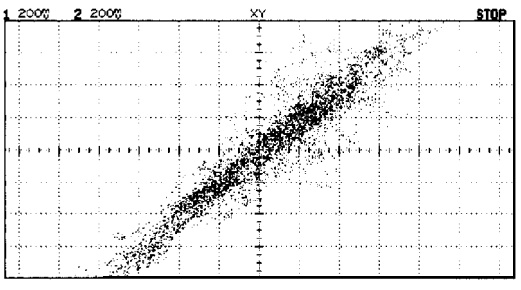

Figure 3.39: Representation of the voltages at the capacitor C_2 for two contiguous circuits of a given ring for the same experimental setup as in Fig. 3.38. A blur of the characteristic $y = x$ line is shown. This implies that the double-scroll synchronized state inside the ring is contaminated by the chaotic rotating wave state.

This implies that the double-scroll synchronized state inside the ring is contaminated

Comparison between Parallel and Antiparallel Coupling.

In the previous sections we have carried out an study of the behavior of coupled rings of cells with chaotic behavior. There is a lot of interest in this type of systems in neurobiology, as well as in technological applications like robotics. In particular, in the so-called CPGs (Central Pattern Generators), that are basically rings of neurons capable of autonomous rhythmic activity in response to a suitable stimulus. However, the direct physiological evidence of these structures is quite scarce and, thus, one may expect that these CPGs are coupled and intertwined in complicated arrangements that may affect to their dynamical behavior. In the previous sections, we analyze the simplest situation involving the interaction of these CPG-like structures, namely, the case in which two of such rings interact. We consider the case in which the local dynamics of the cells is chaotic.

As it has been shown, this fact ensures that the uniform synchronized state of the rings cannot be stable for an arbitrary number of cells and/or coupling coefficients. An instability in this state must appear for some values of the parameters. Such instabilities lead to spatio-temporal (discrete) structures that travel over the assembly of cells. Transverse coupling between the rings guarantees interaction between the structures that appear within each ring. Coupling within each ring is unidirectional in our study, but there are two possibilities in the way of coupling the two rings, depending on the sense of driving within each one: parallel and antiparallel. The result of this study is that the observed behavior in these two cases is different, particularly in the region of intermediate and strong coupling.

Thus, in the case of parallel coupling there are two definite behaviors: if coupling is weak one has two desynchronized chaotic rotating waves, while if coupling is strong these two waves are synchronized between the two rings. Instead, in the case of antiparallel coupling the situation is richer: for weak coupling one has (logically) the same behavior, i.e. two desynchronized rings. For intermediate coupling, all the cells inside each ring become synchronized but there is no synchronization between rings. And, for strong coupling all the cells in the two rings are synchronized, being their behavior like that of an isolated cell: a double scroll. Thus, transverse coupling is able to overcome the instability induced in a single ring by driving coupling.

3.5 Conclusions.

This chapter has been devoted to the study of the stability of the global synchronized state in open linear arrays and rings of identical chaotic oscillators. Numerical simulations have been carried out with assemblies of Lorenz oscillators and Chua's oscillators, whereas experiments have been done in a board of Chua's oscillators. In all cases unidirectional coupling between circuits is set by the driving method of Giiemez and Matias, in such a way that synchronization can be achieved when considering two oscillators.

Synchronization of chaotic oscillators arranged in an open linear array has been studied first. It has been found both experimentally and numerically that the oscillators synchronize in a consecutive way as a synchronization wave with constant velocity spreads through the array. We have also supplied a theoretical analysis that explains the linear relationship between the time required for all oscillators to synchronize and the number of elements in the array. It has been shown that the velocity of the synchronization wave depends linearly on the highest of the Lyapunov exponents corresponding to transverse perturbations to the synchronization manifold of two consecutive oscillators.

The appearance of synchronization in circular geometries (or rings) of chaotic oscillators has also been studied. Numerical simulations and experimental results show that synchronization cannot be achieved for an arbitrary number of elements in the ring, but there exists an upper bound in the size of the ring above which an instability in the global synchronized state arises. This upper bound can be theoretically obtained by means of a linear stability analysis around the uniform synchronized state. It has been shown that, beyond this instability, some stable spatio-temporal structures (periodic and chaotic rotating waves) can arise from a symmetric Hopf bifurcation, such that neighboring oscillators exhibit a phase lag of approximately l/N of a period (being N the number of oscillators in the ring), characteristic of the first Fourier mode transverse to the synchronization manifold that becomes unstable.

Finally, we have investigated the interaction between chaotic rotating wave structures when two rings are diffusively coupled cell-toocell. Depending on the sense of driving within each ring, two different configurations have been analyzed: parallel

and antiparallel coupling. In the case of parallel coupling two definite behaviors have been obtained: when coupling is weak two desynchronized chaotic rotating waves are observed, each one in a different ring, and when coupling is strong these two waves become synchronized. Instead, in the case of antiparallel coupling the situation is richer: for weak coupling the same behavior is obtained, namely, two desynchronized rotating waves. For intermediate coupling, the rotating wave structure vanishes and all oscillators inside each ring become synchronized but there is no synchronization between different rings. And, for strong coupling all the oscillators synchronize exhibiting the behavior of an isolated chaotic oscillator: a double-scroll.

Chapter 4

Chaos in Communications.

4.1 Why Chaos in Communications?.

The appearance in the year of 1990 of two seminal papers [174, 166] involving fundamentals of chaotic systems, generated a tremendous amount of interest and work with subsequent applications in synchronization [174] and control [166] of chaos. In particular, the peculiar features of chaotic systems well explored in Ref. [174] (synchronization capability) and in Ref. [166] (sensitivity to initial condition), opened up a whole new field for using chaotic signals as information carriers [45, 46, 88, 210, 179, 110, 22]. It is currently accepted that chaotic systems provide a rich mechanism for signal design and generation, with promising potential applications to communications and signal processing. Since chaotic signals are typically broadband, noiselike and difficult to predict they can be used in various contexts for masking information-bearing waveforms. They can also be used as modulating waveforms in spread spectrum systems, like Code Division Multiple Access (CDMA) that is becoming very popular in many fields of telecommunication.

Two fundamental characteristics of chaos in physical systems are the complexity of the dynamics and the sensitivity of the time evolution to small perturbations. The sensitivity of chaos to small perturbations has been seen for a long time as merely a barrier to prediction, and not as a useful property. Major developments in the area of controlling chaos using small perturbations have proved otherwise: the sensitivity to small perturbations exhibited by chaotic systems allows to control them using

electrical signals with a power far below the one produced by the chaotic system itself. Thus, the complexity of chaos and its sensitivity to small perturbations can be combined harmoniously by using the sensitivity to *control* (and take advantage of) the complexity. As *a* consequence, it is currently recognized by many engineers that the fact that chaos provides complex behavior from simple systems can be exploited to obtain technological advantages over conventional means for information transmission [88].

4.2 **Chaos in Communications.**

Several approaches have been proposed for communications using chaotic systems. Most of these methods are based on the principle of chaotic masking, where the message signal is added to a much more powerful chaotic carrier generated by the transmitting system. Then, it is recovered at the receiver by regenerating the carrier through synchronization and substracting it out of the received signal [45, 46, 236]. As examples, we can mention the communication schemes proposed by Oppenheim *et al.* [164], Kocarev *et al.* [109], Parlitz *et al.* [170], Cuomo and Oppenheim [45] and Halle *et al.* [85], where the transmitter works as the driving system, the receiver works as the response system and a subvector $\mathbf{x}_p = (x_1, x_2, \ldots, x_p)$ of the state vector x is transmitted causing the receiver to synchronize with the transmitter. This is shown in Fig. 4.1. In practice, it would be desirable to have p, the number of components of $\mathbf{x}_p$, as small as possible, so less of the state needs to be transmitted.

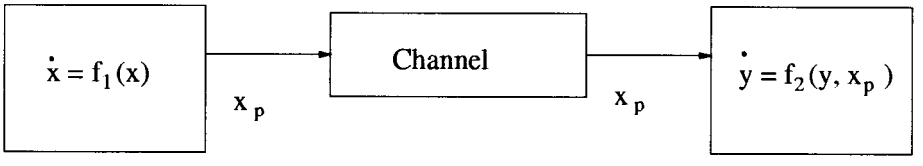

Figure 4.1: Communication system based on synchronizing master-slave configuration.

Many chaotic systems [13, 25, 217, 39, 161, 158] can be used to generate a communication system in a master-slave configuration using solely x_1 as the transmitted signal. There are many possible variations but let us consider, as an example, a transmitted signal of the form *s(t) = xl(t) + m(t),* where $m(t)$ is the information-bearing signal and xi(t) is the chaotic carrier. For masking, it is assumed that the power level of m(t) is significantly lower than that of $x_1(t)$. Thus, if the

receiver has synchronized with $s(t)$ as the drive, then $y_1(t) \approx x_1(t)$ and, consequently, m(t) can be recovered as $\hat{m}(t)$ = s(t) $- y_1(t)$ [45, 46, 109] (see Fig. 4.2).

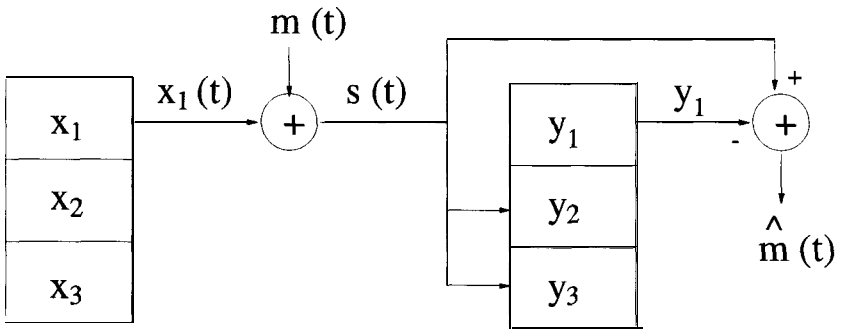

Figure 4.2: **Chaotic signal masking system.**

This type of communications schemes is based on Pecora-Carroll synchronization. The receiver's main elements are the cascaded slave subsystems that are necessary to recover the information signal added to the chaotic carrier. However, in the context of chaotic masking, the idea of adding a chaotic signal to an information signal [45, 46, 109, 131] is known to suffer from certain disadvantages. The main drawback is the requirement that the information signal power level be, at least, 30 dB below the power level of the chaotic carrier. The consequence is that it is difficult to ensure a correct detection when the noise power at the receiver is the same as, or higher than, the information signal power. Since this signal is assumed to be fairly weak (otherwise, there would be no masking) this troublesome situation is likely to be usual in practice.

A more general approach is to use the message signal as a driver for the transmitting system, so that the message becomes a dynamical perturbation rather than an additive one [l10, 171]. Now the information is injected into the dynamical system constituting the transmitter and, thus, the transmitter is not autonomous anymore, but driven by the information signal.

Another approach based on chaotic synchronization is to use the message signal to modulate the parameters of the transmitting system [46, 56, 240]. The main idea is to modulate a control parameter associated with the transmitter or driver using a digital information-bearing waveform and transmit the resulting chaotic signal. At the receiver, the coefficient modulation will produce a synchronization error that is the difference between the received drive signal and the receiver's regenerated drive

signal. Measuring this difference, an error-signal, $e_1(t)$, is obtained, the amplitude of which depends on the modulation. Therefore, it is possible to detect the parameter modulation in the transmitter by observing the fluctuations in $e_1(t)$.

This modulation/detecction process is illustrated in Fig. 4.3. Any coefficient of the transmitter is modulated by the information-bearing waveform, m(t). This information is propagated through the channel with the chaotic signal $x_1^{(m)}$ (t). The noisy received signal r(t) = $x_1^{(m)}(t)$ + n(t) serves as the driving input to the receiver. There, the modulation is detected by forming the difference between the received noisy drive signal and the reconstructed drive signal, $e_1(t) = r(t) - y_1(t)$. Let us suppose the information signal is a binary valued bit stream, with a "1" representing a coefficient mistmatch and a "0" representing no coefficient mismatch. If we assume that the signal-to-noise ratio (SNR) of r(t) is large, the error signal $e_1(t)$ will exhibit a relatively large average power (due to the parameter mismatch) during the time period that a "1" is transmitted, whereas it will nearly vanish during the transmission of a "0", because perfect synchronization is achieved. Figure 4.4 illustrates the relationship between the binary information waveform and the squared error signal, $e_1^2(t)$. It is immediate to detect the information bits by low pass filtering $e_1^2(t)$ and sampling the resulting signal (a "smooth" version of m(t)) at adequate time instants.

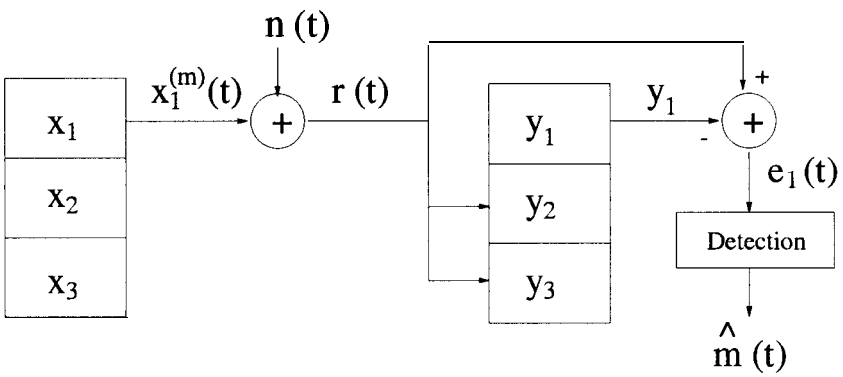

Figure 4.3: Chaotic communication system using parameter modulation.

Other approaches to use chaos for the purpose of communication include controlling techniques to encode binary information by means of small perturbations to the system trajectory [88,89,90,91]. The fact of controlling the system using direct trajectory perturbations is slightly less involved than with parameter perturbations. These controlling techniques have been applied to different chaotic oscillators, such as the Rossler [90, 91], Chua [91, 88] and Lorenz [89, 90] systems. Since this is the starting point for the ideas presented in the following chapters, it is interesting to

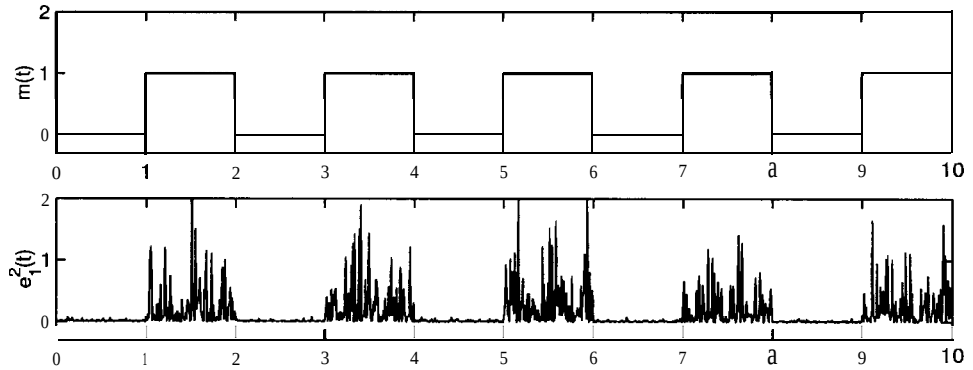

Figure 4.4: Digital information waveform, m(t), and power of the synchronization error, $e_1^2(t)$, in a chaotic communication system using parameter modulation.

get some insight into the work carried out by Hayes and Grebogi [89, 90] to encode binary information in the Lorenz attractor.

4.2.1 Encoding Technique by Hayes and Grebogi.

A chaotic oscillator, like the Lorenz system [126] for instance, can be controlled with small trajectory perturbations that will make its trajectory follow a desired path [89, 90]. The perturbations are small enough not to introduce significant changes in the topological properties of the system, and still able to make the $x(t)$ component follow a prescribed sequence of ups and downs where each up corresponds to "1" and each down corresponds to "0". The analog x(t) signal becomes a natural carrier of digital information where any desired message can be encoded. A digital signal can thus be produced directly at the transmission stage, with no need for subsequent amplification. Because chaotic behavior occurs in simple systems, and because of the extremely low power requirement of the control mechanism, the high-power device can be simple and efficient, and all the control and guidance electronics can remain at the microelectronic level. So far, it has been shown that applying simultaneously small perturbations to two variables of the Lorenz system it is possible to guide its trajectory to encode the desired binary information [89, 90].

For standard parameter values, σ = 10, R = 28 and $b = 8/3$, the Lorenz system produces a chaotic attractor in a three-dimensional state space. The state point (x, y, z) executes an apparently random dance, circling one lobe a few times, then

jumping to the other for a few cycles, then back. The binary information is carried by the sequence of cycles on the two lobes. It is possible to label one lobe of the attractor with the symbol 0 and the other one with the symbol 1. Then, every time the system cycles on the 0 lobe, it generates a 0, and similarly for the 1 lobe. Therefore, the sequence of cycles on the two lobes can be easily translated into a sequence of bits. When the system is running freely, the sequence of lobe cycles approximates a coin toss. When the $x(t)$ scalar signal is observed, the binary digits appear as a sequence of positive and negative spikes, the positive spikes representing the $1s$ and the negative spikes the $0s$. In this sense, it is straightforward to understand the signal $x(t)$ as a carrier of digital symbols.

To explain this behavior in detail [90, 89] two surfaces of section given by the half-planes $y = \pm\sqrt{b(R-1)}$ and $|x| \geq \sqrt{b(R-1)}$ have been considered. The points $(x, y, z) = (\pm\sqrt{b(R-1)}, \pm\sqrt{b(R-1)}, R-1)$ are the unstable fixed points, or foci of the outward spiraling trajectories on either lobe. A projection of the Lorenz attractor onto the $x-y$ plane is shown in Fig. 4.5 where the two half-planes are represented by two straight lines, labeled 0 and 1, respectively. These are the two branches of a Poincare surface. In the x projection of the full state point, it can be seen that the oscillations around the 0 and 1 attractor lobes correspond to negative and positive maxima, or spikes, respectively (see Fig. 4.6). If this x projection x(t) is chosen as the transmitted signal, then the message could be extracted by simply observing the sequence of spikes in the waveform. Thus, the Lorenz system offers probably the simplest example of how symbolic dynamics can be used to transmit a message.

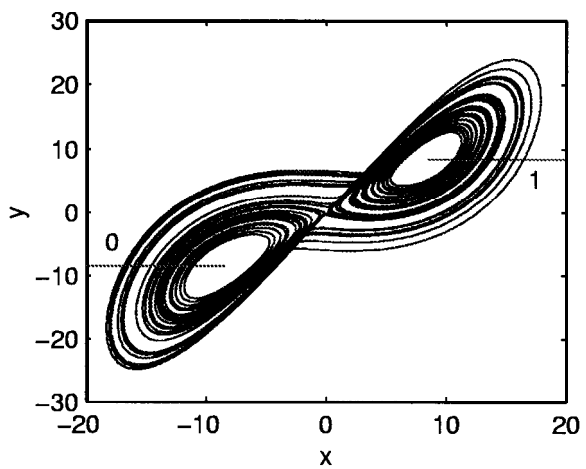

Figure 4.5: Lorenz state trajectory projected onto the x-y plane. The two branches of the Poincaré surface appear as half-lines and are labeled with binary symbols 0 and 1.

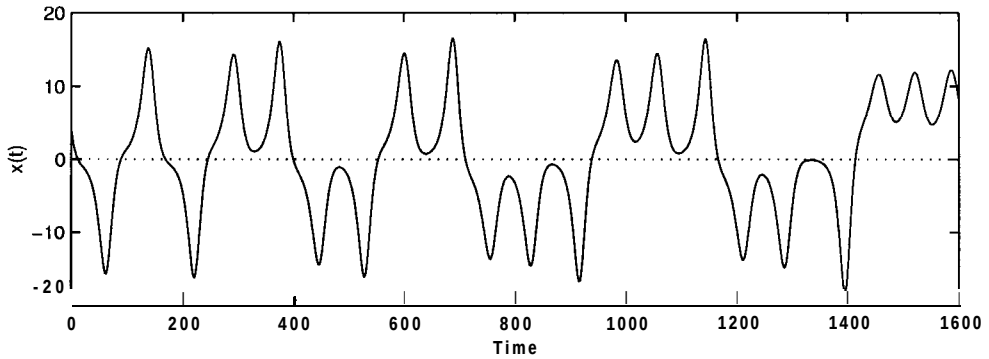

Figure 4.6: Temporal evolution of the variable x of the Lorenz system.

There exists a correspondence between the point where the state coordinate (x, y, z) crosses one of the Poincare surfaces and the n-bit symbol sequence, $b_1 b_2 \ldots b_n$, associated to the subsequent evolution of the system. Because the Lorenz equations represent a flow that is highly dissipative and therefore strongly contracting along the stable direction, the intersection of the attractor with each surface forms an essentially one-dimensional arc (see Fig. 4.7 and Fig. 4.8). For this reason, the future symbol evolution is determined well by a proper choice of a single magnitude. If we define the two Poincare coordinates $\xi = |x| - \sqrt{b(R-1)}$ and ζ = z – (R – 1) as a normalization of the coordinates x and z, respectively, at the moment when the Poincare surfaces are crossed, the distance along the one-dimensional arc between (ξ, ζ) and the fixpoint at the center of the respective lobe can be written as $\chi = \xi \cos\theta + \zeta \sin\theta$, where θ is the angle that the line segment makes with the x – y plane. This magnitude χ contains all useful information about the state coordinate at the crossing point. Because absolute values are used in defining χ, called generalized Poincare coordinate, such magnitude can be used for both lobes of the attractor.

To determine how state-space crossing-points on the surfaces of section, represented by the generalized Poincare coordinate χ, are related to the subsequent bit sequences generated after the crossing it is possible to resort to the *binary fraction*

$$r = \sum_{i=1}^{n} b_i 2^{-i} \tag{4.1}$$

associated to that sequence. The main contribution in [89, 90] is to show that the binary fraction is actually a function of (ξ, ζ), i.e., there exists a coding function $c(\chi)$ such that $c(\chi)$ = r = $\sum_{i=1}^{n} b_i 2^{-i}$. Furthermore, this function is invertible and knowing $c^{-1}(r) = \chi$, the *inverse coding function,* it is straightforward to encode any

symbol sequencer in the system trajectory by properly changing the values of ξ and ζ associated to χ (notice that the angle θ is previously known). Thus, in order to transmit a long sequence of bits, it is necessary to perturb the coordinates (ξ,ζ) at every crossing point with the surfaces of section.

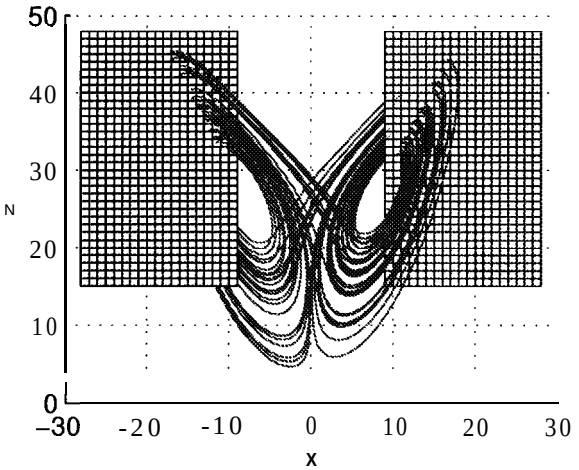

Figure 4.7: Projection onto the x-z plane of the chaotic Lorenz attractor crossed by the Poincaré surfaces defined by y = $+\sqrt{b(R-1)}$ and $|x| \geq \sqrt{b(R-1)}$ (left side) and by y = $-\sqrt{b(R-1)}$ and $|x| \geq \sqrt{b(R-1)}$ (right side). Notice that the intersection of the attractor with each surface forms an essentially one-dimensional arc.

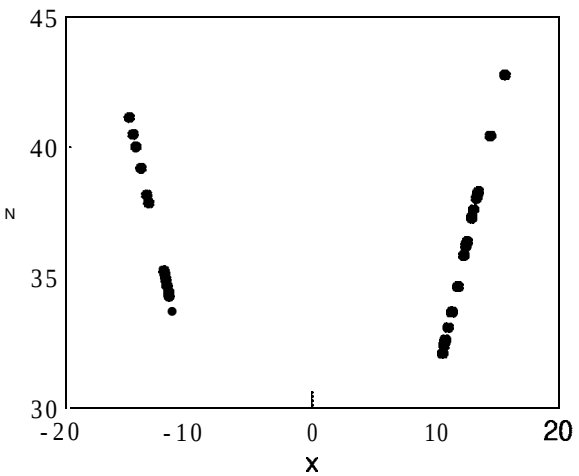

Figure 4.8: One-dimensional arcs on the Poincaré surfaces of section. Left side represents the $x-z$ variables on the surface y = $+\sqrt{b(R-1)}$ and $|x| \geq \sqrt{b(R-1)}$ and right side represents the same for the surface y = $-\sqrt{b(R-1)}$ and $|x| \geq \sqrt{b(R-1)}$.

'Except for those sequences that may be *forbbiden* by the Lorenz dynamics.

Chapter 5

Information Encoding in Chaotic Systems.

5.1 Introduction.

In the previous chapter, we have reviewed some of the most outstanding applications of chaos to the field of communications. Now, we focus on the idea of controlling the chaotic oscillator through small perturbations to the system trajectory [88,89,90,91]. It has been shown how these control techniques can be used to encode information in the oscillator trajectory, but not much attention has been paid to the relationship of the resulting encoding device with current Digital Communication Systems (DCS). Section 5.2 is devoted to establish this relationship.

Next, Section 5.3 introduces a simple control technique that allows to encode any desired sequence of information bits in the trajectory of the Lorez system. The initial idea is basically the same exploited by Hayes and Grebogi in [90, 89], already described in Section 4.2.1, but a new result has been achieved that leads to a more simple control algorithm. This algorithm also has the benefit of preserving most of the properties of the chaotic signal. Namely, the information carrying waveform remains deterministic up to a certain extent. From the point of view of communications, this determinism provides some redundancy that can be exploited in two different ways: to improve the transmission reliability and to increase the transmission capacity.

Section 5.4 is devoted to reliability improvement. One of the more harmful forms of interference in a communications channel is impulse noise (see Appendix B.2), that is, huge noise spikes that completely hide the transmitted signal, rendering it impossible for a conventional demodulator to detect the transmitted bits. Hence, in this chapter we introduce two methods that take advantage of the knowledge of the chaotic system at the encoder (here the Lorenz) to reconstruct the signal in this extremely noisy intervals, that will be modeled for convenience as *dropouts,* i.e., complete absence of signal.

To conclude, Section 5.5 describes an alternative application of the results in dropout reconstruction to implement an efficient *time division multiplexing* system: relying on the dropout reconstruction methods several information sources can share a communication channel by transmitting in turns only small bursts of their encoded chaotic signals and let the intended receiver to reconstruct the entire waveform. Thus, the overall capacity of the communication link is increased.

5.2 Block Diagram of a Chaotic Digital System.

In this section, we will describe how control-based encoding techniques, like the one proposed by Hayes and Grebogi [90, 89] or the one described later in this chapter can fit into a conventional Digital Communication System (DCS) (see Appendix B for a brief introduction to digital communications). For a communication engineer, such encoding techniques can be seen as a new type of digital modulations with some advantages arising from the properties of chaotic behavior. It must be remarked that our goal is not to replace the succesfull current DCS scheme, but to convey the idea that chaotic signals exhibit interesting features that can really make a difference and bring some improvement to communication systems.

Figure 5.1 illustrates the elements of a conventional DCS where the *digital modulator* and the *digital demodulator* have been replaced by blocks labeled waveform encoder and waveform *decoder,* respectively. These names are chosen to emphasize that the function of these elements is to translate from an information binary sequence to a waveform (continuous time and amplitude signal) carrying this information and viceversa, but the functionality is the same. This system will be referred as chaotic DCS.

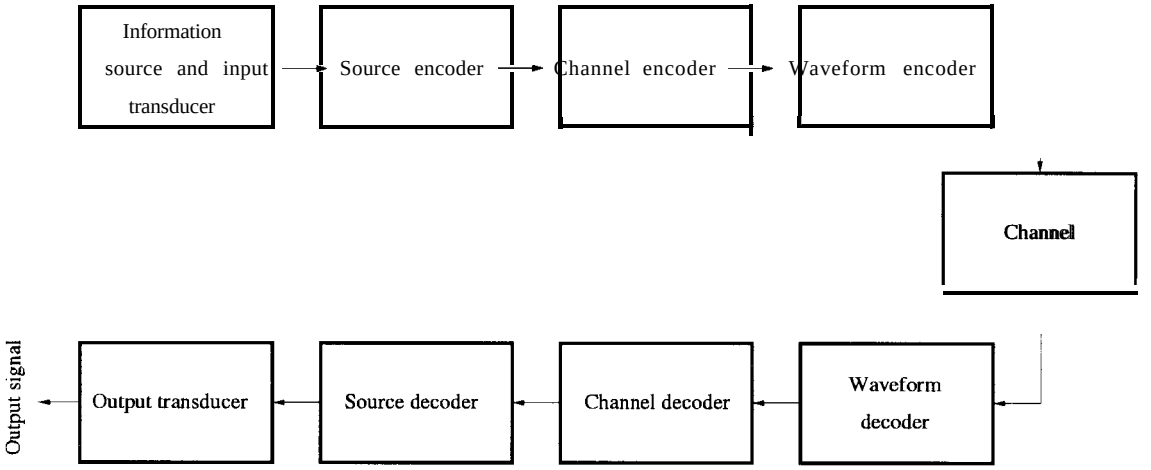

Figure 5.1: Block diagram of a chaotic digital communication system.

The waveform encoder consists of a chaotic oscillator and a controller, as shown in Fig. 5.2. The latter is fed with the binary information sequence and, starting from a previous knowledge of the chaotic system, forces the oscillator to follow a certain trajectory, encoding in this way the desired binary sequence into an output waveform. This waveform is sent through a channel and then the waveform decoder recovers, starting from this waveform, the transmitted sequence of symbols. This recovery can be made by direct observation of the received signal or by using it to drive a local oscillator and observing its trajectory.

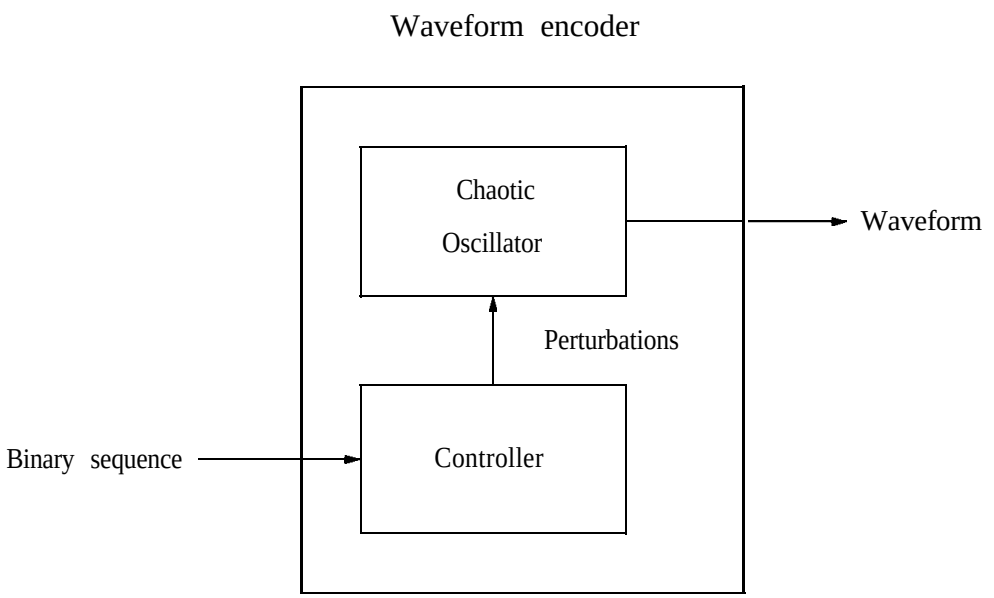

Figure 5.2: Structure of the waveform encoder.

Notice that the controller in Fig. 5.2 can operate as described in 4.2.1 or in some other publications (see, for example, [88, 91]). In the next section, we will introduce a new encoding method that departs from the same principles but results in a more simple control algorithm.

5.3 Encoding Technique.

It has been demonstrated that chaotic systems can be manipulated via arbitrarily small perturbations on the system trajectory to generate controlled chaotic orbits whose symbolic representation corresponds to the encoding of a desired message [88, 89, 90, 91]. Several chaotic systems have been used to this end, but we will focus our attention in the Lorenz system (see Fig. 5.3 for a x-z projection of the chaotic attractor) because a rather straightforward connection can be established between the system trajectory and a binary information sequence. Hayes and Grebogi already exploited this feature in [89, 90]. These references have been reviewed in Section 4.2.1 together with some other useful properties of this system.

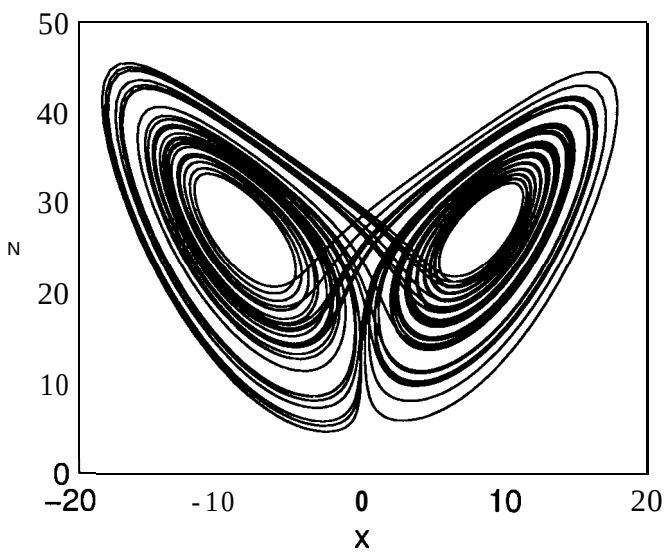

Figure 5.3: Lorenz attractor projected onto the x-z plane.

Recall that for standard parameter values, σ = 10, R = 28 and b = 8/3, the Lorenz system produces a chaotic attractor in a three-dimensional state space. The state point (x, y, z) executes an apparently random dance, circling one lobe a few

times, then jumping to the other for a few cycles, then back. It is possible to label one lobe of the attractor with the symbol 0 and the other one with the symbol 1. Then, every time the system cycles on the 0 lobe, it generates a 0 and similarly for the 1 lobe. Therefore, the sequence of cycles on the two lobes can be easily translated into a sequence of bits. When the system is running freely, the sequence of lobe cycles approximates a binary symmetric information source, i.e. a source of binary symbols that emits O's and l's with equal probability and independently of its history, like a coin toss. When the $x(t)$ scalar signal is observed, the binary digits appear as a sequence of positive and negative spikes, the positive spikes representing the l's and the negative spikes the $0's$. In this sense, it is straightforward to understand the signal $x(t)$ as a carrier of digital symbols.

As it was said in Section 4.2.1, it is possible to control the future sequence of bits encoded in the variable x by applying small perturbations to the trajectory of the system at each crossing with the Poincaré surfaces of section, defined by $y = \pm\sqrt{b(R-1)}$ and $|x| \geq \sqrt{b(R-1)}$ (see Fig. 4.5 in the previous chapter). Because the Lorenz equations represent a flow that is highly dissipative and, therefore, strongly contracting along the stable direction, the intersection of the attractor with each surface forms an essentially one-dimensional arc, as shown in Fig. 4.7 and Fig. 4.8. For this reason, the future symbol evolution is well determined by a proper choice of a single magnitude. Hayes and Grebogi [89, 90] have chosen as such magnitude the distance along the one-dimensional arc on the plane x $-z$ from the fixed point at the center of the respective lobe to the crossing point on the surface of the respective section. This choice implies the perturbation of two coordinates of the state point, x and z. However, we will show here that the system trajectory can also be accurately controlled when the system coordinate z at the crossing points is chosen as the magnitude to be perturbed. The verification of this fact readily leads to a more simple information encoding method.

To understand why perturbing the variable z is enough to determine the sequence of crossings followed by the system trajectory, let us resort to the inverse coding *function, z(r),* which gives the required value of the coordinate z at each crossing with the surfaces as a function of the binary fraction. Recall from the previous chapter that the *binary fraction, r,* is a real number

$$r = \sum_{i=1}^{n} b_i 2^{-i} < 1 \tag{5.1}$$

calculated from the bits $b_1 b_2 \ldots b_n$ associated to the system trajectory crossings with the Poincare surfaces. Bit b_1 corresponds to the current crossing, b_2 corresponds to the next crossing and so on up to the n-th bit.

Figure 5.4 plots the inverse coding function $z(r)$. Note that the resulting curve is symmetric with respect to the straight line r = 0.5 because of the symmetry of the coordinate z on both lobes of the attractor (see Fig. 5.3).

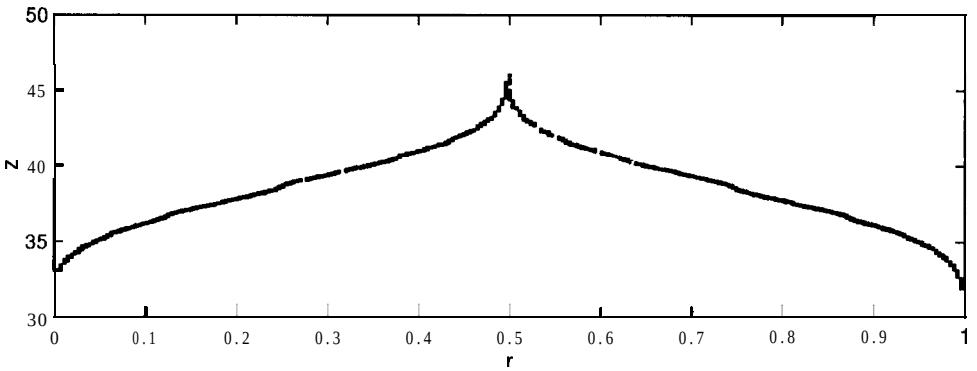

Figure 5.4: Inverse coding function, $z(r)$.

In the inverse coding function, $z(r)$, the same value of the coordinate z is associated to two complementary sequences, as for example, the sequences 01101110 and 10010001. If we restrict to the left-half (alternatively to the right-half) of the figure then, since the function $z(r)$ is monotonically increasing (alternatively monotonically decreasing), there exists a one-to-one correspondence between the sequence and the value of z (the sequence is completely determined by a value of z and vice versa). The apparent problem of two sequences associated to the same value of z is not actually a problem. The symmetric character of the function $z(r)$ is a consequence of the symmetry of the Lorenz system. For $z = z_0$, there are two different state points: either (x_0, y_0, z_0) at the "0" lobe, or (x_0', y_0', z_0) at the "1" lobe. Since the intersection of the Lorenz attractor with each Poincare surface is a one-dimensional arc, each value of z corresponds to only one value of x for a given Poincare surface. Therefore, when $x_0 < 0$ (alternatively $x_0 > 0$) the system is at the "0" lobe (alternatively "1" lobe) and only sequences starting with "0" (alternatively "1") can be generated. Thus, the ambiguity of having two complementary sequences associated to the same value of z is completely removed.

In order to know the perturbation we need to apply at each crossing, it is necessary

to know the behavior of the free running Lorenz system. So, we let the system run for a long period of time and store the value of the coordinate z at each crossing together with the subsequent n-bit sequence. The first bit in the sequence represents the current crossing, the next bit represents the next crossing, and the last bit of the sequence represents what happens n $-$ 1 oscillations after this crossing. Now, let z_1 and z_2 be the value of the coordinate z at two consecutive crossings with any of these surfaces and let $b_1 b_2 \ldots b_n$ be the corresponding n-bit sequence associated to the crossing at z_1. Then, the n-bit sequence associated to the crossing at z_2 is the same sequence associated to the former crossing, z_1, but left-shifted one place and with a new bit at the right most position, that is, $b_2 b_3 \ldots b_{n+1}$, *as* shown in Table 5.1.

z_1	10011010
z_2	00110100
z_3	01101000
z_4	11010001
.	.
.	.
.	.

Table 5.1: 8-bit sequences and associated z-crosspoints. As the Lorenz system runs, the succesive crosspoints of the variable z with the Poincaré surface (z_i) are recorded, together with the subsequent symbolic bit sequence. The sequence corresponding to the $(i+1)$th crosspoint results from left-shifting one bit the ith sequence, with a new bit entering on the right-most position.

When the system runs freely, it can be observed that close values of the coordinate z produce the same n-bit sequence. Therefore, the different sequences of n bits are represented by different windows of close values of the variable z, and it is possible to associate to each of these sequences the average value of the coordinate z in these windows, as shown in Table 5.2. The value of z_a in that table, for instance, would be calculated as $z_a = \frac{1}{M}\sum_{i=1}^{M} z_i$, where all different (but close) z_i generate the sequence 00000001.

In this way, we have obtained a relationship between the n-bit sequences and the required values of the variable z. If the n-bit sequences are represented by their binary fractions, this relationship is the inverse coding function $z(r)$ we have already represented in Fig. 5.4.

Now that the free running Lorenz system has been studied, we proceed

00000001	z_a
00000010	z_b
00000011	z_c
.	.
.	.
.	.

Table 5.2: 8-bit sequences and associated averaged z-crosspoints. Since different (but close) z-crosspoints may correspond to the same symbolic sequence, it is reasonable to associate this sequence to the average of such crosspoints.

to explain in detail the control technique. Let `011100010. .` be the desired transmitted sequence of bits, that is, the input of the waveform encoder, and let 010110011000111000111 be the sequence of bits generated by the free running system during some time for a certain initial condition of the state coordinate (x, y, z), as illustrated in Fig. 5.5(a). The goal of the waveform encoder is to produce a waveform that encodes the desired sequence of bits representing the message. Table 5.3 shows the values of the coordinate z for six consecutive crossings with the surfaces of section when the system runs freely.

z_1 = 40.0001	01011001
z_2 = 39.3510	10110011
z_3 = 40.9571	01100110
z_4 = 37.7601	11001100
z_5 = 41.0665	10011000
z_6 = 37.6657	00110001

Table 5.3: Six consecutive z-crosspoints and their corresponding 8-bit sequences in a free running Lorenz system.

Suppose that the control starts at the sixth crossing. The sequence associated to z_6 = 37.6657 is 00110001, as seen in Table 5.3. However, a small perturbation of $z_6, \Delta z_6$, yields a new value of z at the crossing, $\hat{z}_6 = z_6 + \Delta z_6$ = 37.5801, with a new associated sequence 00110000. We only need to apply a small perturbation to the variable $z, \Delta z_6$ = `-0.0856,` to force the system to produce the first desired bit (a 0 bit) seven oscillations after the present one, as seen in Fig. 5.5(b), where the first vertical line indicates the point where this perturbation is applied, and the second one the instant where the effect of this perturbation is noticed. The second desired bit is encoded changing the value of the z coordinate at the next crossing,

z_7, by the corresponding $\hat{z}_7$ (looked up from Table 5.2) with the associated sequence 011000101. Repeating this process at every crossing, the desired bit sequence is encoded, as shown in Fig. 5.5(b) and Table 5.4.

z_1	01011001
z_2	10110011
z_3	01100110
z_4	11001100
z_5	10011000
$\hat{z}_6$	00110000
$\hat{z}_7$	01100001
$\hat{z}_8$	11000011
$\hat{z}_9$	10000111
$\hat{z}_{10}$	00001110
$\hat{z}_{11}$	00011100
$\hat{z}_{12}$	00111000
$\hat{z}_{13}$	01110001
$\hat{z}_{14}$	11100010

Table 5.4: Behavior of the perturbed Lorenz system. Starting at $i = 6$, the value of the variable z at each succesive crossing with a Poincaré surface is corrected in order to select the new bit entering on the right most position of the associated symbolic bit sequence. Thus, the bits printed in bold-face have been selected by the controller to encode some desired message.

Notice that very small perturbations are sufficient to control the system because the effect on the trajectory is not to be felt until a given number of oscillations, n- 2, have been completed[1]. This number will depend on the number of bits considered in the encoding process: the more bits are used the smaller the perturbations are applied. Besides, controlling the chaotic oscillators through small perturbations provides two important advantages:

- the control device can remain at the microelectronic level because of the extremely low power requirement, and
- the perturbed system keeps the properties of the original chaotic system, such as a certain degree of determinism. From a communication point of view,

[1]It must be remarked that the system is actually perturbed at each crossing with a surface of section, but the perturbation at the kth crossing is to determine the bit produced by the system in the $(k + n - 1)$th crossing.

this determinism provides some redundancy that can be exploited to improve the transmission performance in different ways. This issue will be further investigated in Section 5.4 and Section 5.5.

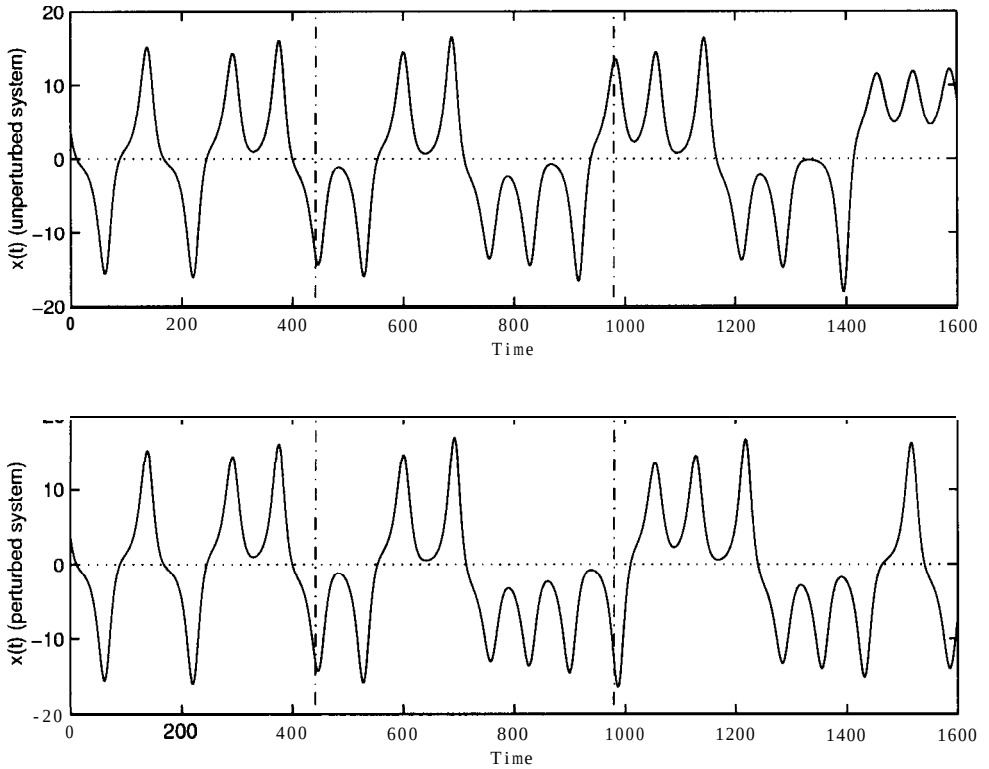

Figure 5.5: (a) Temporal evolution of the variable x for the non-perturbed Lorenz system. (b) Temporal evolution of the variable x for the perturbed Lorenz system.

5.3.1 Validation of the Control Procedure.

Computer simulations have been carried out in order to illustrate the performance of a chaotic DCS that employs the proposed encoding scheme. It has been assumed that the transmitter sends frames of 105 bits through a channel with additive, zero-mean, white Gaussian noise and the aim of the waveform decoder is to detect these 105 bits without the help of any channel code, so only the chaotic encoding is evaluated. The figure of merit is the *frame* error probability, i.e., the probability of having at least one bit error in a frame, that has been estimated for several values of the Signal *to Noise Ratio* (SNR). The SNR is calculated as

$$SNR = 10\log_{10}\left(\frac{P_{signal}}{P_{noise}}\right) \quad (dB) \tag{5.2}$$

where P_{signal} is the average power of the transmitted signal and P_{noise} is the power of the Gaussian noise (i.e., its variance, since zero mean is assumed).

There may exist several choices for the design of the waveform decoder. Figure 5.6 shows a block diagram of the one chosen for the experiment.

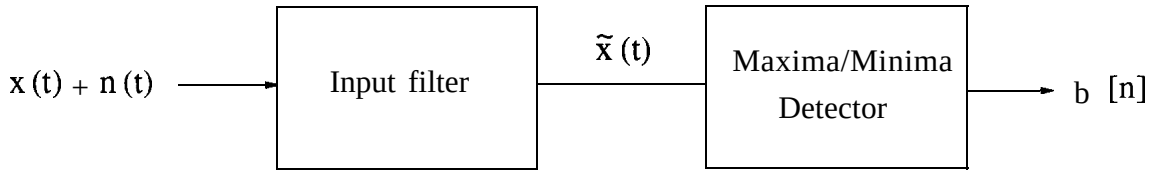

Figure 5.6: Block diagram of the proposed waveform decoder.

The goal is to find the positive local maxima (associated to bits 1) and negative local minima (associated to bits 0) in the received signal. This may be a rather difficult task in the received noisy signal, a;(t) + n(t), being n(t) the white Gaussian noise, so a linear system that performs both low pass filtering (achieving some noise reduction) and enhancement of the positive maxima and negative minima has been implemented in order to ease bit detection. Figure 5.7 depicts the impulse response of this filter, corresponding to the analytical expression

$$h(t) = \frac{11}{\sigma \sqrt{2\pi}} \exp \frac{-0.5\ t^2}{\sigma^2}. \qquad (5.3)$$

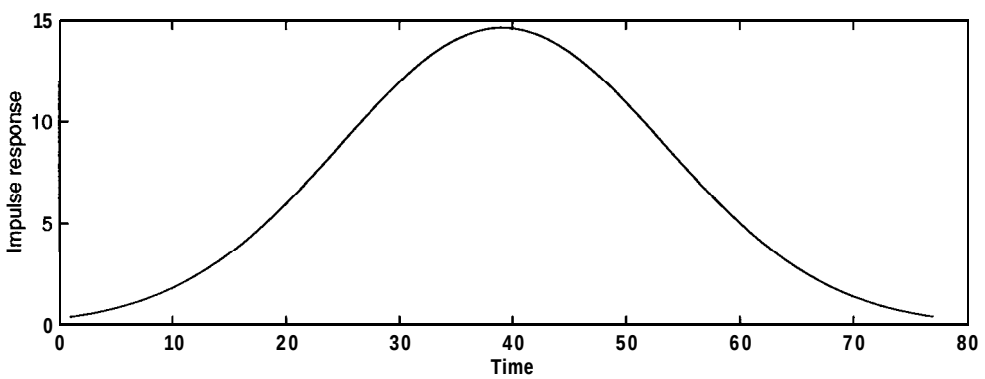

Figure 5.7: Impulse response of the input filter (5.3).

Note that $h(t)$ spreads over a time support interval that is approximately the same as in one oscillation of the Lorenz variable $x(t)$ and its amplitude has been tuned to be close to the amplitude of the peaks in this signal $x(t)$. In fact, the input filter thus defined intends to play the role of a *matched* filter [186] in a conventional

DCS. Figure 5.8 compares the noisy input signal (upper plot) and the (normalized) filtered waveform (lower plot) for an SNR of 1 dB.

Next, the filtered signal, Z(t), goes through a nonlinear device that identifies the most outstanding positive local maxima and negative local minima in the signal, so the most likely (in some sense) transmitted bits, b[n], are detected. These bits are depicted in Fig. 5.8 as square points.

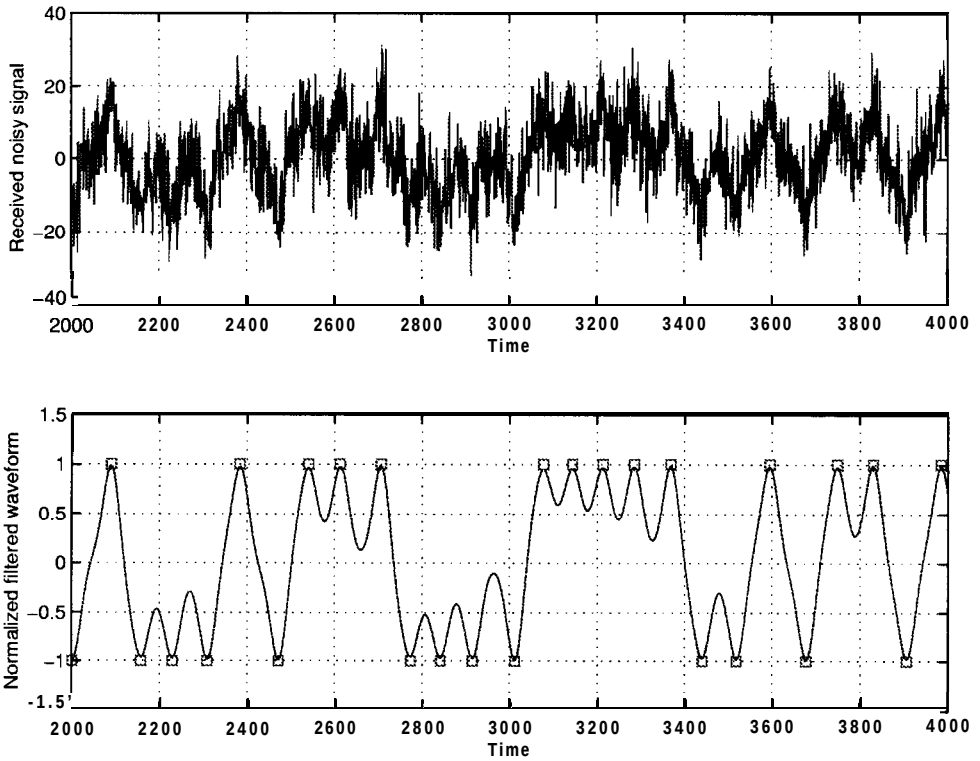

Figure 5.8: Representation of the received noisy signal (upper plot) and the normalized filtered waveform (lower plot), where the square points represent the detected bits.

Finally, Fig. 5.9 shows the quantitative results of the experiment. It can be seen that for an SNR of 2 dB the probability of a *frame* error (i.e., at least a bit error within a frame of 105 bits) is already as low as 10^{-3}. Since the values of the SNR assumed for conventional DCSs are typically higher (around 10 dB for wireless systems and higher for wired ones) it can be concluded that a practical implementation of the proposed system is possible[2].

[2]Note, however, that the experiment does not take into account several forms of distortion, different from Gaussian noise, that appear in a real communication channel.

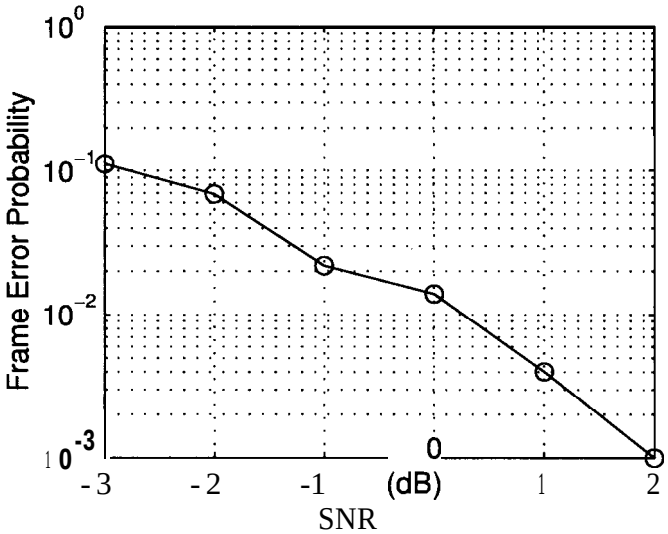

Figure 5.9: Frame error probability for different values of the SNR when frames of 105 bits are transmitted.

5.4 **Dropout Reconstruction.**

Most types of channel interference have reasonably predictable and constant magnitudes, so it is possible to find engineering solutions to cope with them in conventional DCSs (see Appendix B.2 for usual problems in transmission media). However, the primary source of errors in digital data communication is the impulse noise: an unpredictable noncontinuous signal consisting of irregular pulses or noise spikes of short duration and relatively high amplitude. This sort of impairment is very harmful for digital communications because the received signal is severely distorted and relatively long sequences of bits cannot be detected reliably. Hence, we are interested in showing the help that chaotic behavior can provide in such situations. It will be shown that these impairments can be succesfully dealt with resorting to the properties of chaotic behavior, particularly its determinism, that are preserved by the encoding technique discussed in the previous section.

Figure 5.10(a) illustrates the destructive effects of impulse noise on the signal received at the waveform decoder. It is apparent from the plot that having an interval of signal distorted by impulse noise is practically equivalent to having no signal at all, because no information for the bit detection process is available from the received signal. Therefore, it is possible to model these useless intervals as *dropouts,* i.e.,

complete absence of signal, as shown in Fig.5.10(b). The goal of this section is to present two different methods that take advantage of the determinism of the chaotic signal to reconstruct the lost parts of the waveform.

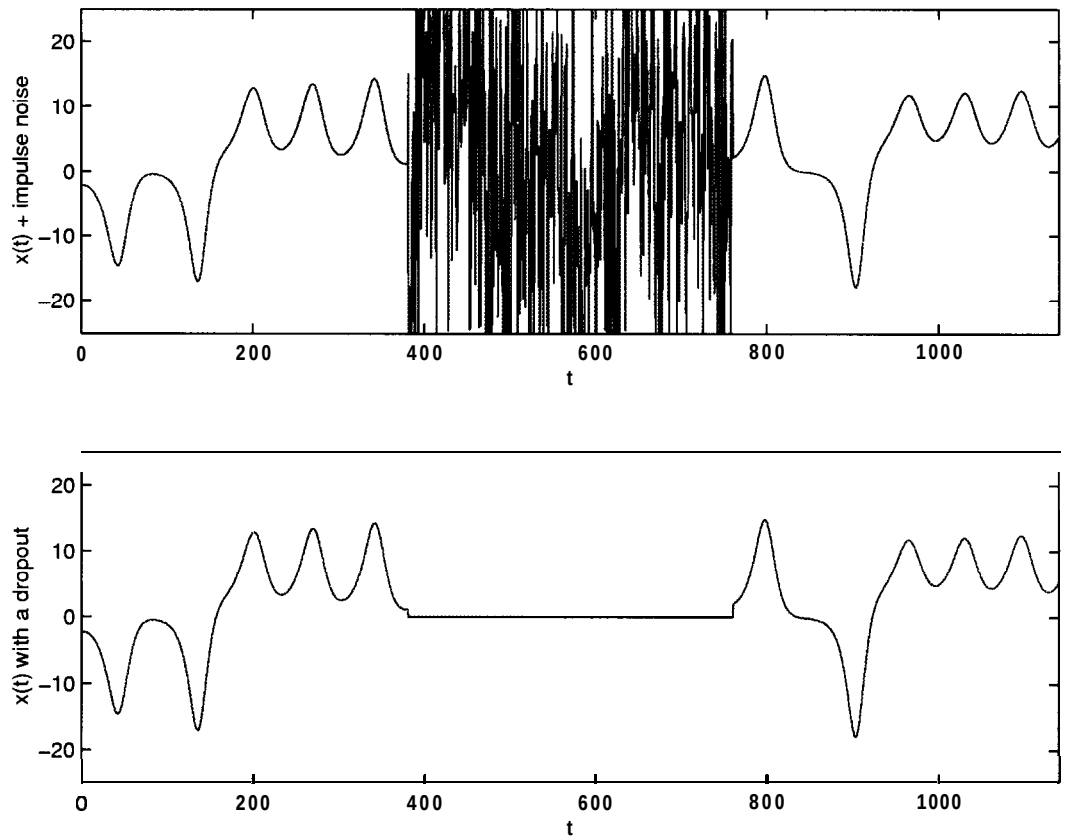

Figure 5.10: (a) Signal distorted by impulse noise. (b) Impulse noise modeled as a dropout.

Since the perturbed system preserves a certain degree of determinism and the Lyapunov time[3] of the Lorenz oscillator is big enough, it is possible to resort to the non perturbed system in order to reconstruct the signal transmitted originally in the time interval of the dropout. The maximum number of oscillations that can be reconstructed in a dropout (and, therefore, the maximum number of bits that can be recovered) is given by the number of bits used in the encoding process. Remember that the use of n bits in the encoding technique means that the oscillation $n - 1$ after the instant when a perturbation is applied may encode a different bit with respect to the natural evolution of the non perturbed Lorenz system from that instant. That is: the first oscillation represents the first bit (and the point where the perturbation

[3]The Lyapunov time is a measure of how much two almost identical trajectories diverge as time goes.

is applied), the next n – 2 oscillations produce exactly the same bits as in the non perturbed system and the nth oscillation represents the bit encoded with the perturbation applied n – 1 oscillations before. As a consequence, it is clear that the number of oscillations that makes sense to recover using n-encoding is n – 2.

Before proceeding any further let us point out that the device or devices implementing dropout detection and reconstruction can be considered as a subsystem within the waveform decoder. As depicted in Fig. 5.11, the new block fits naturally as an stage previous to those of matched filtering and bit detection, already explained in Section 5.3. Note that the ultimate goal of dropout reconstruction is to feed these subsequent operations with as much information as possible to improve bit detection accuracy and reliability.

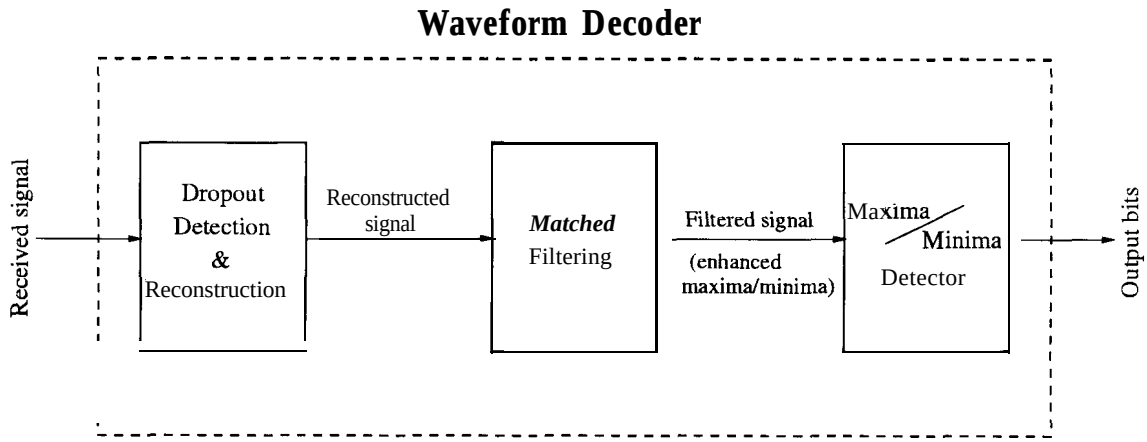

Figure 5.11: Block diagram of a waveform decoder that performs dropout reconstruction.

5.4.1 First Reconstruction Method (FRM).

Assume that the knowledge of the non perturbed Lorenz system is available in the form of some sort of storage where the time evolution of the variable x of the system has been recorded for a long period of time. This stored variable is termed $\overline{x}$. When a dropout is detected in the receiver (time t_0), the following steps are taken [139]:

- M samples of the input signal right before the dropout are recorded, to obtain the observation vector

$$V_0 = (x(t_0 - \delta), x(t_0 - \delta - T), \ldots, x(t_0 - \delta - (M-1)T)), \qquad (5.4)$$

where δ is a very small quantity of time to indicate that the first sample is taken very close to the begining of the dropout and T is the time distance between samples. Note that the samples are taken in reverse time order.

- Search the vector of samples

$$\overline{V_0} = (\overline{x}(t_0'), \overline{x}(t_0' - T), \ldots, \overline{x}(t_0' - (M - 1)T)) \tag{5.5}$$

from the stored variable, $\overline{x}$, corresponding to the non perturbed Lorenz system, that matches more tightly the observation vector, i.e., such that the Mean Square Error (MSE) defined by,

$$MSE = \frac{1}{M} \sum_{m=0}^{M-1} (\overline{x}(t_0' - mT) - x(t_0 - \delta - mT))^2 \tag{5.6}$$

is minimized.

- The dropout is reconstructed as

$$\begin{aligned} x(t_0) &= \overline{x}(t_0' + \delta) \\ x(t_0 + L) &= \overline{x}(t_0' + \delta + L) \end{aligned} \tag{5.7}$$

where L represents the size of the dropout.

Figure 5.12 illustrates the behavior of this recovery method. The upper plot shows the transmitted signal with the encoded message obtained after applying the proper perturbations. In the lower plot we can see the received signal (solid line) with several dropouts and how they are recovered (dashed line). It is evident that the reconstructed signal tracks the original one tightly. It must be remarked that the accuracy of the proposed method depends on the length of the signal dropouts, not on their frequency. Indeed, there exists a maximum dropout length for an adequate recovery, which depends on the perturbation amount: the smaller perturbations applied the longer dropouts can be recovered.

Notice that this reconstruction method can also be applied when the stored signal used for reconstruction comes from a perturbed system, instead of a free-running one. This could be useful when there exist some forbidden sequences in the free-running system. This is the case, for example, with the Rössler system [90,91]. Since there are

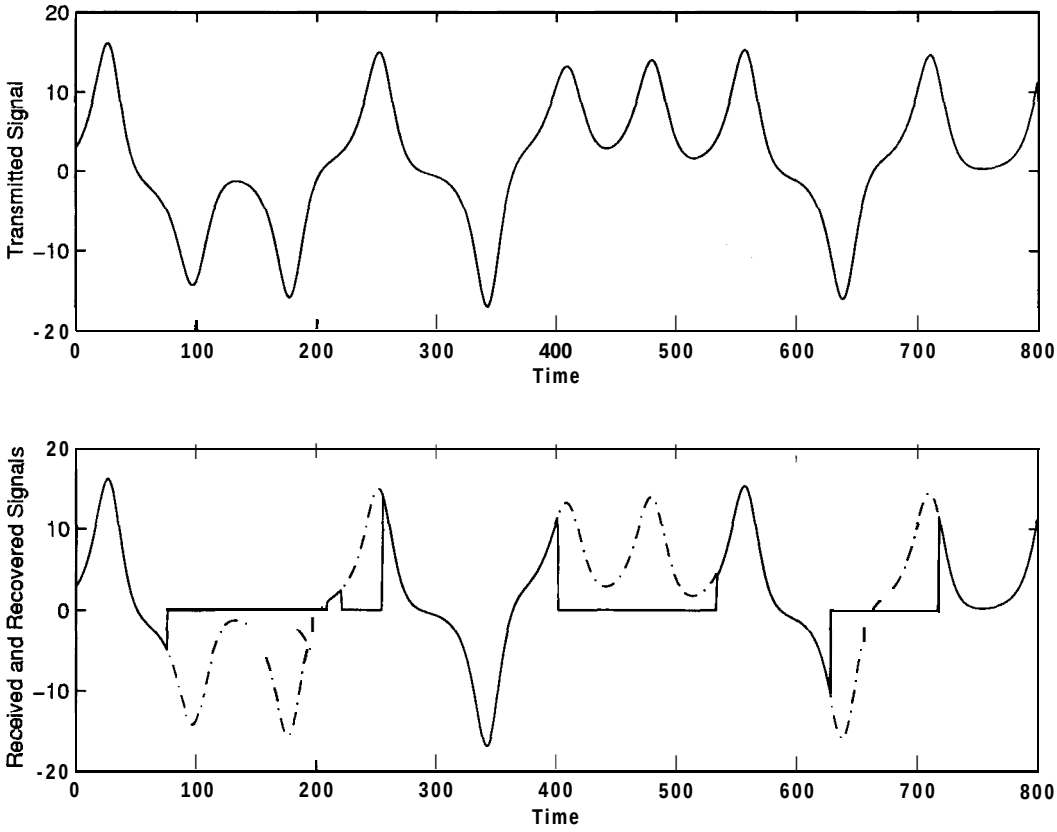

Figure 5.12: Variable x(t) of the Lorenz system representing an encoded message. (a) Transmitted signal; (b) received (solid line) and recovered (dashed line) signals.

sequences never produced by the free-funning oscillator it is neccesary to impose some grammar constraints (in the context of communication, *channel constraints) so* that the sequence of bits to be encoded is one that the system can generate[4]. However, this usually restricts even more the number of different generated sequences. For dropout reconstruction only the perturbed subset is useful since, although more sequences can be generated by the attractor, only this subset will be used in the transmission. So, it is clearly more efficient to build the signal storage from the perturbed system instead of the free-running one. One of the reasons why we have chosen the Lorenz system as the chaotic oscillator used to encode the message at the transmitter instead of other chaotic systems is that for 8-bit encoding there are no forbidden sequences, that is, if

[4]This means that if we have to encode a message consisting of a sequence $b_1, \ldots b_n$ that the Rössler cannot produce, then we need to apply some invertible function $F(b_1, \ldots, b_n) = \hat{b}_1, \ldots, \hat{b}_m, \quad n < m$ *such* that the resulting m-bit sequence is not forbidden by the system dynamics. This m-bit sequence is the one actually encoded into the system trajectory. At the receiver, the original message is recovered as $b_1, \ldots b_n = F^{-1}(\hat{b}_1, \ldots \hat{b}_m)$. For example, if two consecutive O's cannot be generated by the attractor, a possible grammar constraint could be $0 \rightarrow 01, \quad 1 \rightarrow 11$.

we let the system evolve long enough all $2^{n \leq 8}$ possible n-bit sequences are generated. This is an important advantage because there is no need to impose constraints to the sequence of transmitted bits. Thus, there is no loss in transmission capacity and both the transmitter and the receiver are more simple.

5.4.2 Second Reconstruction Method (SRM).

The problems of the previous method are the necessity of having some sort of storage for the free Lorenz system and the time spent in searching through this storage. To avoid them, a second method is proposed. To apply this second method it is necessary just the knowledge of three consecutive samples of the variable x. **As** the signal reaches the receiver, we record its value $x(t_0)$ right before the gap, as well as the values $x(t_0 - h)$ and $x(t_0 - 2h)$, where ***h*** is some small time interval. These three consecutive samples of the variable x are then employed to numerically evaluate $[y(t_0 - 2h), z(t_0 - 2h)]$ that correspond to the sample $x(t_0 - 2h)$, recorded at the receiver. Then, $[x(t_0 - 2h), y(t_0 - 2h), z(t_0 - 2h)]$ are used as initial conditions in the Lorenz equations to yield the evolution of the x component of the system during the dropout.

Let us describe the process in detail. The initial conditions before the dropout can be found solving the following equation,

$$f\begin{pmatrix} y(t_0-2h) \\ z(t_0-2h) \end{pmatrix} = \begin{pmatrix} p_x \circ g_{RK4}(x(t_0-2h), y(t_0-2h), z(t_0-2h)) \\ P_X \circ g_{RK4} \circ g_{RK4}(x(t_0-2h), y(t_0-2h), z(t_0-2h)) \end{pmatrix} - \\ - \begin{pmatrix} x(t_0-h) \\ x(t_0) \end{pmatrix} = \begin{pmatrix} 0 \\ 0 \end{pmatrix} \quad (5.8)$$

where $g_{RK4}(x(t), y(t), z(t)) = (x(t+h), y(t+h), z(t+h))$ represents one iteration forward of the fourth order Runge-Kutta algorithm with time step ***h***, $p_x(x(t), y(t), z(t)) = x(t)$ is the projection of the three dimensional vector onto the first component and the symbol $\circ$ denotes function composition.

To solve (5.8) we can resort to the well known Newton method. This is a numerical method used to find an aproximated root of $f(x) = 0$ given an initial approximation $\mathbf{x}_0$ and using the recursion

$$\mathbf{x}_n = \mathbf{x}_{n-1} - |\mathbf{Df}(\mathbf{x}_n)|^{-1}\mathbf{f}(\mathbf{x}_n) \quad \mathbf{n} = 1, 2, \ldots, \quad (5.9)$$

where $\mathbf{x}_n$ represents the succesive approximations to the actual root (in our case, the vector $\mathbf{x}_n$ represents succesive approximations to the coordinates $y(t_0 - 2h)$ and $z(t_0 - 2h)$), and $\mathbf{Df}\ (\mathbf{x}_n)$ is the Jacobian of the function **f(x)** with respect to the vector x. Then, the only problem to find the root of Eq. (5.8) is to find an initial aproximated root, i.e., $\hat{y}(t_0 - 2h), \hat{z}(t_0 - 2h)$, to start the recursion[5]. It is possible to obtain this approximated root starting from the knowledge of $[x(t_0 - 2h), x(t_0 - h), x(t_0)]$ just going backward in time with the Euler method[6]. In particular, it is only necessary to evaluate the first of the following equations at $t = t_0, t_0 - h$ and the second one at $t = t_0 - h$.

$$\begin{aligned} x(t) &= x(t - h) + h\sigma(y(t - h) - x(t - h)) \\ y(t) &= y(t - h) + h(Rx(t - h) - y(t - h) - x(t - h)z(t - h)) \end{aligned} \tag{5.10}$$

The values of $[\hat{y}(t_0 - 2h), \hat{z}(t_0 - 2h)]$ obtained in this way are,

$$\begin{aligned} \hat{y}(t_0 - 2h) &= x(t_0 - 2h) + \tfrac{1}{h\sigma}(x(t_0 - h) - x(t_0 - 2h)) \\ \hat{z}(t_0 - 2h) &= \tfrac{\frac{1}{h}(\hat{y}(t_0-2h)-\hat{y}(t_0-h))+\hat{y}(t_0-2h)-Rx(t_0-2h)}{x(t_0-2h)} \end{aligned} \tag{5.11}$$

where

$$\hat{y}(t_0 - h) = x(t_0 - h) + \tfrac{1}{h\sigma}(x(t_0) - x(t_0 - h)). \tag{5.12}$$

Once the aproximated root, $[\hat{y}(t_0 - 2h), \hat{z}(t_0 - 2h)]$, is obtained, we apply the Newton recursion (5.9) in order to find the initial conditions $[x(t_0 - 2h), y(t_0 - 2h), z(t_0 - 2h)]$. Obtaining an accurate enough approximation may require several iterations of the algorithm. This number of iterations can be either previously fixed or not. In the latter case, the algorithm must be iterated until the error is less than a certain value, ε. Finally, the fourth order Runge-Kutta algorithm is used to reconstruct the dropout starting from $[x(t_0 - 2h), y(t_0 - 2h), z(t_0 - 2h)]$.

The capability of this method is illustrated in Fig. 5.13, where it can be seen that with very few samples of the signal it is possible to reconstruct it completely. This maximum number of well reconstructed oscillations will depend on the number of bits used in the encoding process, that is, of the n-bit encoding.

---

[5]This approximation will play the role of $\mathbf{x}_0$.

[6]This method could have been used to numerically integrate the Lorenz system as well, but the Runge Kutta of fourth order method is more precise.

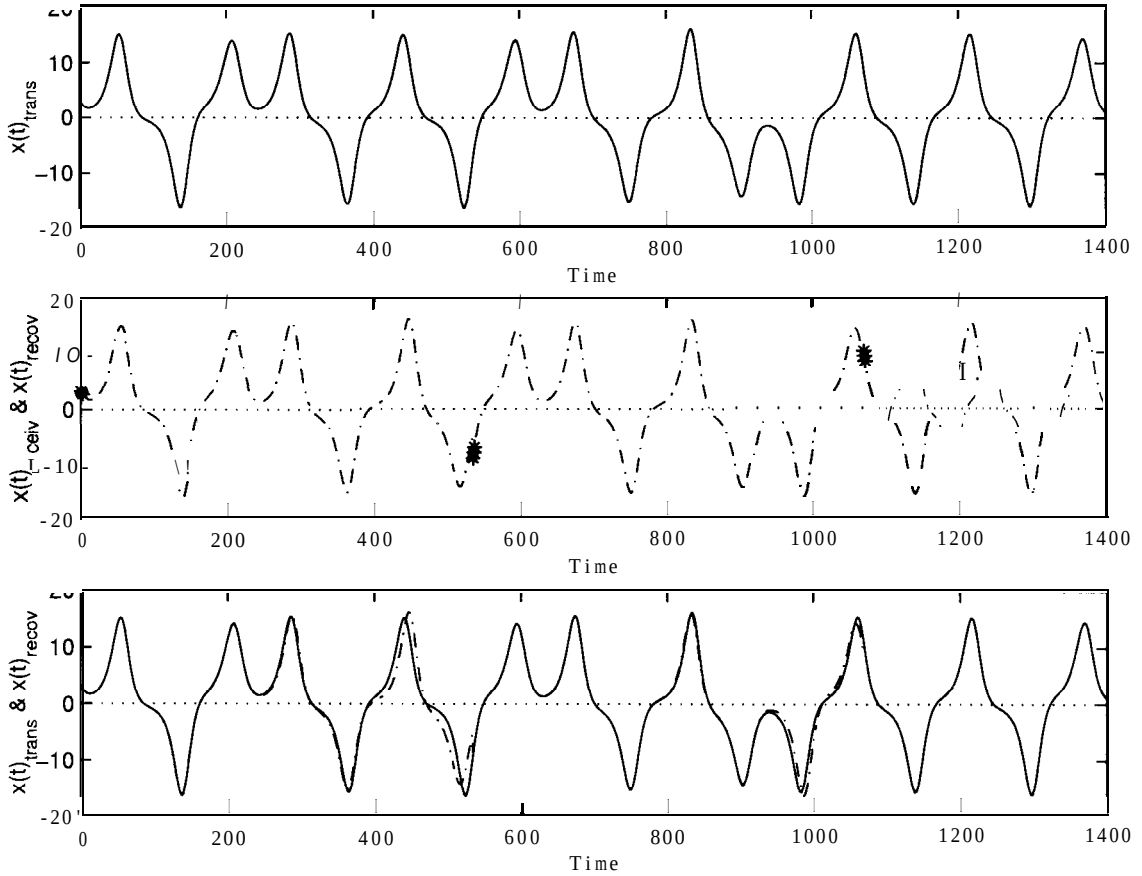

Figure 5.13: Reconstruction of the variable $x(t)$ using the second reconstruction method (a) Transmitted signal $x(t)$ with an encoded message; (b) received signal $x(t)$('$*$') and signal recovered (dashed line) just starting from the received signal. (c) Overlapping of the transmitted (solid line) and recovered (dashed line) signals.

5.4.3 Performance of the Reconstruction Methods.

The goal of this section is to evaluate the performance of the two reconstruction methods and, to do so, some figure of merit that quantifies this performance must be devised. Let us consider a dropout that spreads over N cycles of the received signal, that is, a dropout that causes N bits to be lost. Both the FRM and the SRM try to recover these N bits by means of the reconstruction of the received signal from the uncontrolled Lorenz system. This is possible because the system is practically deterministic, except for the little non determinism produced by the small perturbations, and the Lyapunov time of the system is big enough. However, some small numerical error either in the FRM or the SRM may cause the recovered signal

to diverge from the transmitted one due to the high sensitivity of chaos. At that moment, an erroneous bit is recovered and all subsequent bits in the dropout are be recovered randomly.

This argument leads to a performance index consisting of the probability of making the first bit recovery error in the i-th reconstructed cycle, i = 1,. . . , N. This performance index will be referred as First Error Probability (FEP) of the i-th bit and all simulations in this section are devoted to computing the FEP of the bits in a dropout with both the FRM and SRM. When an 8-bit encoding is considered, the maximum number of reconstructed oscillations (what implies the maximum number of recovered bits) in each dropout will be equal to six. Dropouts of six oscillations have been simulated and we have evaluated the probability of having the first error in the first oscillation of the reconstructed dropout, the probability of having the first error in the second oscillation of the reconstructed dropout and so on. This FEP will be computed in two different scenarios: with and without Gaussian noise.

Let us consider first that the channel effects on the transmitted signal are negligible except for the dropouts themselves, so the reconstruction methods can work on noiseless samples. Figure 5.14 plots the FEP for both the FRM and the SRM. For the FRM, the number of components of the observation vector (see Eq. (5.4)), i.e., *M*, has been taken equal to three. In both cases, a noiseless received signal with 32400 dropouts of 6 oscillations have been simulated. It is apparent that the SRM exhibits a better performance for the six bits in the dropout. Actually, the results obtained with the SRM can be qualified as excellent, since the overall probability of making at least one error is as low as 0.0487. The results obtained with the FRM are not so remarkable, although doubtlessly good. This is because in practice the FRM operates on a finite register of stored waveforms, whenever the possible realizations of the received signal are infinite. Since the SRM does not suffer this limitation, it outperforms the FRM.

However, there are not many practical applications where the typical SNR is sufficiently high as to justify the assumption of receiving a noiseless signal. Therefore, we have repeated the former simulations for the FRM when the received signal is contaminated with additive, zero-mean, white Gaussian noise for different values of the SNR. The number of samples, *M*, has been taken equal to 30 (vs. 3 in the noiseless case). This number has been increased to improve the robustness of this

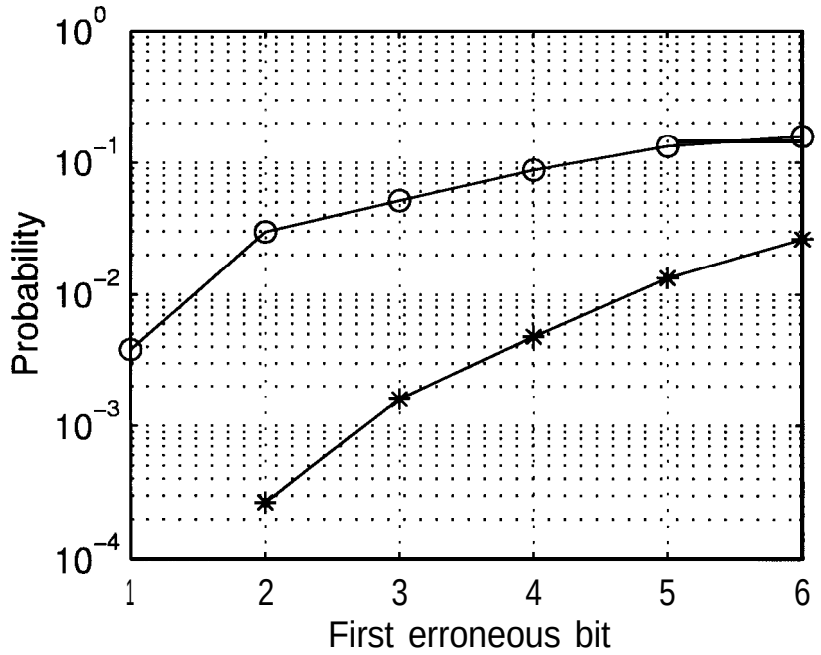

Figure 5.14: First Error Probability for the FRM ('o') and SRM ('*').

method in noisy channels, as can be seen by resorting to the noise statistics. Let us define the vector of A4 samples from the received signal as

$$V_0 = (x(t_0 - \delta) + n_0, x(t_0 - \delta - T) + n_1, \ldots, x(t_0 - \delta - (M-1)T) + n_{(M-1)})$$

where $x(t_0 - \delta - mT)$, m = 0,. ..,M – 1 represents the components of the transmitted signal and n_m, m = 0, ...,M – 1 represents the noise of each sample. If the number of samples, M, is too small it may occur that a vector

$$\overline{V_0} = (\overline{x}(t_0'), \overline{x}(t_0' - T), \ldots, \overline{x}(t_0' - (M - 1)T))$$

from the stored signal matches V_0 quite well due to the randomness of the noise but it is not actually a good choice to reconstruct the dropout because there is little resemblance between $\overline{V}_0$ and the samples from the transmitted signal,

$$V_0^{clean} = (x(t_0 - \delta), x(t_0 - \delta - T), \ldots, x(t_0 - \delta - (M-1)T)).$$

To guarantee that an small error with respect to the transmitted noiseless signal is also achieved when there is an small error between the noisy samples, V_0, and the stored ones, $\overline{V}_0$, it is necessary to increase the value of M. Recall from Section 5.4.1 that the FRM tries to minimize the mean square error between V_0 and $\overline{V}_0$, that can

be written as

$$MSE_{noisy} = \frac{1}{M}\sum_{m=0}^{M-1}(\overline{x}(t_0' - mT) - x(t_0 - \delta - mT) - n_m)^2. \qquad (5.13)$$

If the value of A4 is not high enough, a minimization of the mean square error does not involve a minimization of

$$\frac{1}{M}\sum_{m=0}^{M-1}(\overline{x}(t_0' - mT) - x(t_0 - \delta - mT))^2,$$

that is what one actually is looking for. However, for a sufficiently high value of M a minimization of the mean square error implies a minimization of such expression. It is simple to show that when the signal components, $x(t_0 - \delta - mT)$, match exactly the stored samples, $\overline{x}(t_0' - mT)$, then

$$MSE_{noisy} = \frac{1}{M}\sum_{m=0}^{M-1} n_m^2 \qquad (5.14)$$

that approximates the noise power, $E[n^2] = \sigma^2$ ($E[\cdot]$ denotes mathematical expectation), for sufficiently high M. However, when $x(t_0 - \delta - mT) \neq \overline{x}(t_0' - mT)$ it can be proved[7] that, when M is high enough, the mean square error turns out to be

$$MSE_{noisy} = \sigma^2 + C \qquad (5.15)$$

where C is a positive constant proportional to

$$\frac{1}{M}\sum_{m=0}^{M-1}(\overline{x}(t_0' - mT) - x(t_0 - \delta - mT))^2.$$

Hence, if M is high enough, the MSE_{noisy} will be approximately σ^2 when adequate samples are found in the storage, whereas the constant C will increase the value of the MSE_{noisy} when there exist some mismatch. As a consequence, a minimization of the mean square error implies a minimization of the difference between V_0^{clean} and $\overline{V_0}$. Thus, the FRM can be safely applied as in the noiseless case with the only difference that the MSE_{noisy} cannot go below the threshold of the noise power σ^2.

Figure 5.15 illustrates the performance of the FRM when considering SNR values of 20, 25 and 30 dB, and M has been taken equal to 30. As in the noiseless case, a received signal containinig 32400 dropouts of 6 cycles has been simulated. It can be

[7] The proof is easily carried out if we let the differences $\overline{x}(t_0' - mT) - x(t_0 - \delta - mT)$, $m = 1, \ldots, M$ be samples of a random variable statistically independent of the noise.

seen that, as the SNR decreases, most of the FEP mass is shifted to the beginning of the dropout This means that for low SNR the first reconstruction error is more likely to happen in the first bits, thus reducing the method reliability because all bits after the first error are recovered randomly. However, the figure also shows that for an SNR of 25 dB or above, the method performance becomes reasonably good, in the sense that it attains relatively low values of the FEP (below 10^{-1} for the first 3 bits when SNR = 30 dB), and sound because most of the FEP mass concentrates on the Past bits in the dropout so the recovery errors, if any, can be expected to affect only these bits.

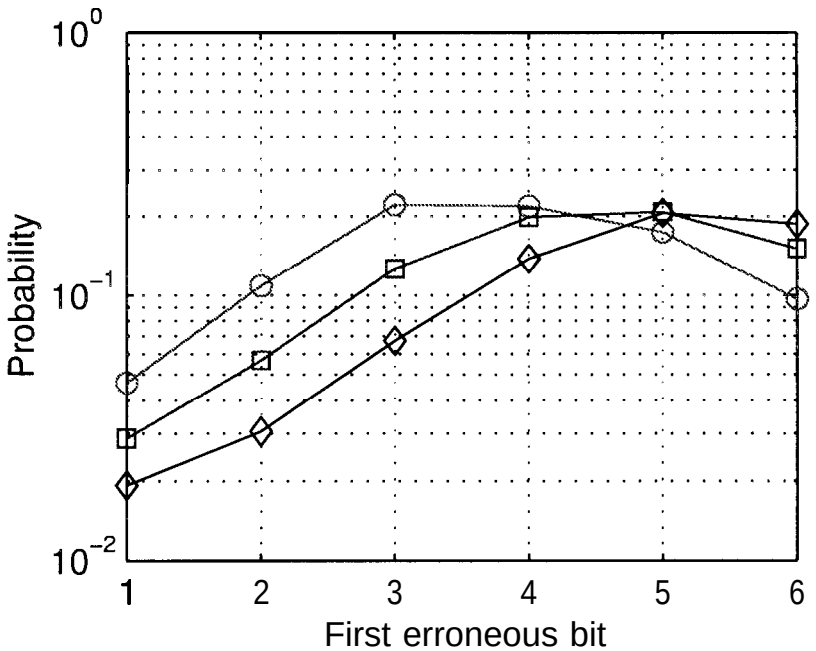

Figure 5.15: First Error Probability for the FRM when the SNR is 20 dB ('o'), 25 dB ('squares') and 30 dB ('diamonds').

Note that we are not presenting simulation results concerning the performance of the SRM in the noisy channel. The reason is that this method is very sensitive to the effect of noise in the samples used to compute the reconstructed signal. Actually, we have observed that the performance obtained by the FRM method with SNR=30 dB is not achieved by the SRM until the SNR rises to about 70 dB. A possible solution to improve these results could be to perform some sort of filtering (prior to the application of the SRM) on the received signal that removes noise while leaving the chaotic signal fairly undistorted. One such filtering could be the one proposed in [191].

5.5 Multiplexing of Chaotic Signals.

In the previous section two methods have been presented that allow to reconstruct large signal dropouts in the received chaotic signal starting from just a few samples of the signal right before the dropout. We have seen that this is advantageous to combat some very harmful impairments in digital communications such as impulse noise. Alternatively, if the communication channel is not a hostile one (no noise spikes, no severe multipath propagation, . ..) it is straightforward to think of using these reconstruction techniques to increase the system transmission capacity by multiplexing several information signals within the same communication link.

Multiplexing refers to a variety of techniques used to make more efficient use of a transmission facility (see Appendix C). In many cases, the capacity of a transmission facility exceeds the requirements for the transfer of data between two devices. That capacity can be shared among multiple transmitters by multiplexing a number of signals onto the same medium. In this case, the actual transmission path is referred to as a *circuit* or *link,* and the portion of capacity dedicated to each pair of transmitter/receiver is referred to as a channel.

One method for creating multiple channels within a link is to subdivide a reference time interval of duration T_f, called the frame *duration,* into, say, N nonoverlapping subintervals called *slots,* each of duration T_f/N. Then each user who wishes to transmit information is assigned to a particular time slot within each frame. This multiplexing method is called *time-division multiplexing* (TDM) (see Appendix C) and it is frequently used in data and digital voice transmission (mobile telephone systems, satellite communications, computer networks, . ..).

Let us see an example that will illustrate how it is immediate to design a TDM transmission system relying either on the FRM or on the SRM analyzed above. Consider a digital transmission system with a maximum allowed frame duration of 450 μs (T_f = 450 μs). Assume the available hardware offers a sampling frequency of f_s = 1 MHz (sampling period of 1 μs). If each oscillation of the Lorenz signal spreads over 75 samples (approximately), then the chaotic DCS discussed in Section 5.2 can provide up to $450/75$ = 6 bits per frame, i.e., $6/(450*10^{-6}) \approx$ 13330 bits per second (bps) = 13.33 $kbps$. However, and assuming no dropouts are present, the link capacity may be used more cleverly. Specifically, we can transmit small bursts

of several different encoded signals (as shown in Fig. 5.16) and use the FRM (in case the channel noise is significant) to reconstruct all signals and, thus, recover all transmitted bits.

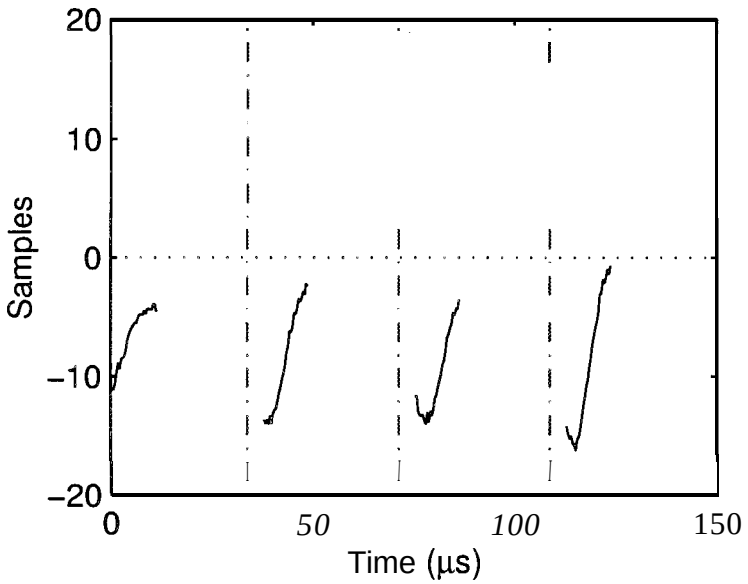

Figure 5.16: First, second, third and fourth time slots within a multiplexed frame. Each slot contains a burst from a different 8-bit encoded signal that is passed to the corresponding receiver by a demultiplexer device. Then, the receiver applies either the FRM or the SRM to reconstruct the whole encoded signal and recover the bits. The SNR has been taken equal to 30 dB.

To follow with the same example, and assuming M = 30 samples are enough to apply the FRM then 450/30 = 15 bursts from different signals can be transmitted during the frame duration T_f. Let us assume that, due to time dispersive channel effects [186] or hardware constraints, only 13 bursts can actually be transmitted in one frame. Assume also that the original signals are 8-bit encoded but, due to bit error rate requirements, each burst is used to obtain only four reconstructed bits, i.e., R = 4 bits (see Fig. 5.17). Then, the overall transmission bit rate is (4 x 13)/(450 * 10^{-6}) = 115560 *bps*, i.e., 115.56 *kbps*. Therefore, the system capacity has been increased by a gain factor of 8.6. Generalizing this example, it can be easily calculated that the gain factor is

$$G = \frac{75R}{M} \tag{5.16}$$

where R is the number of bits reconstructed from each signal burst formed by M samples (here M also accounts for the samples *wasted* in avoiding time dispersion).

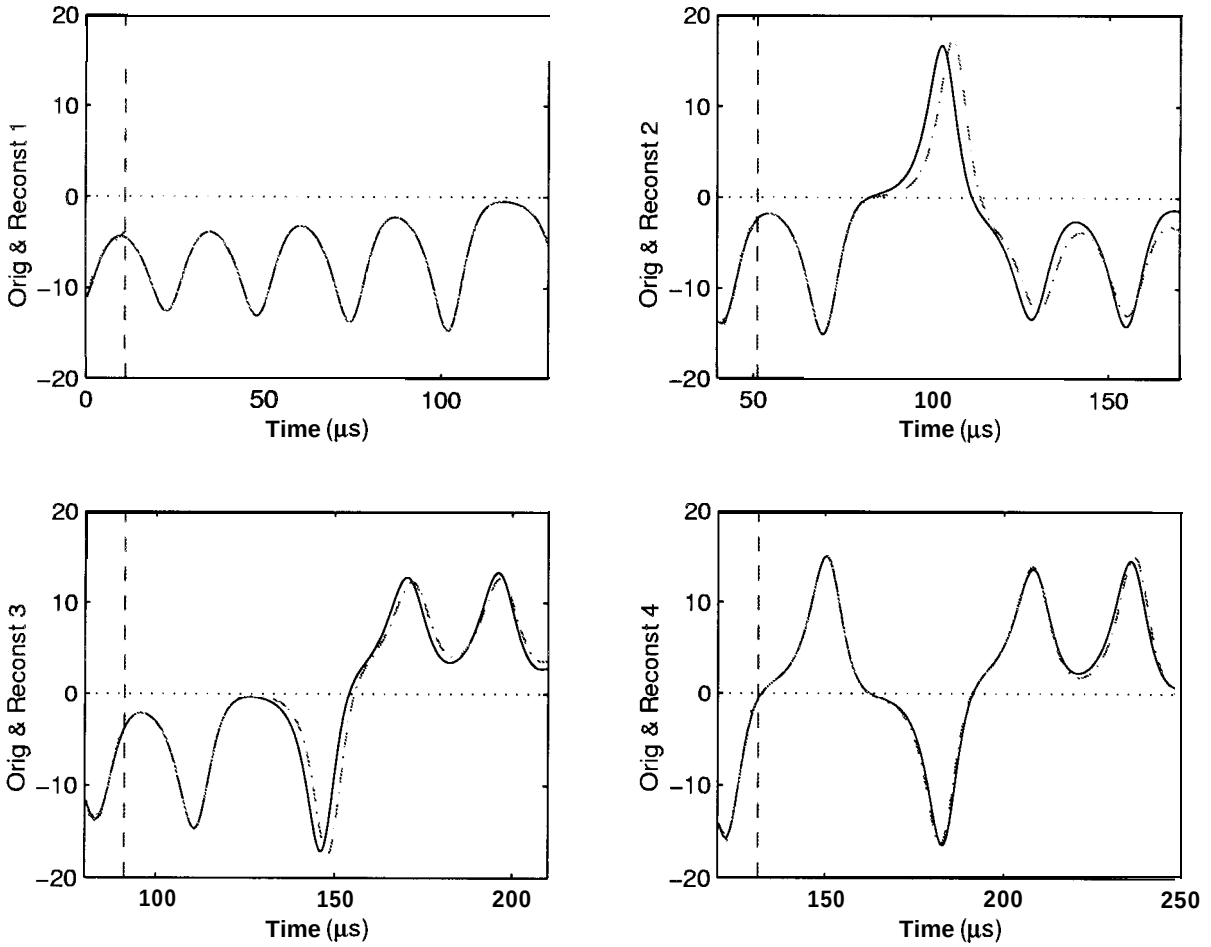

Figure 5.17: Reconstructed signals (dash-dotted line) versus original transmitted signal (solid line) corresponding to ***4*** signal bursts of ***M = 30*** samples. The SNR has been taken equal to 30 dB. The dashed vertical lines separates the received noisy signal used for reconstruction from the reconstructed signal.

To summarize, Fig. 5.18 depicts the functional diagram of a multiplexed chaotic DCS where N channels are accomodated within the communications link. Each transmitter is made up of a source encoder, a channel encoder and a waveform encoder (plotted in Fig. 5.2) which generates a different encoded chaotic waveform. The block labeled *multiplexer* scans these chaotic waveforms periodically in a round robin fashion. After a whole round, the multiplexer has brought together N signal bursts, one from every transmitter, and concatenates them to form a composite signal called frame. This frame is transmitted through the communication link and is received at the *demultiplexer*. The task of this block is to take this frame, divide it into N signal bursts and send the i-th burst to the i-th receiver. Each receiver is made up of a

waveform decoder, a channel decoder and a source decoder. The waveform decoder is the one already shown in Fig. 5.11 where now the block label dropout detection and reconstruction will be better called just *i-th signal reconstruction,* since it will apply either the FRM or the SRM to reconstruct the original i-th encoded signal and recover the desired bits.

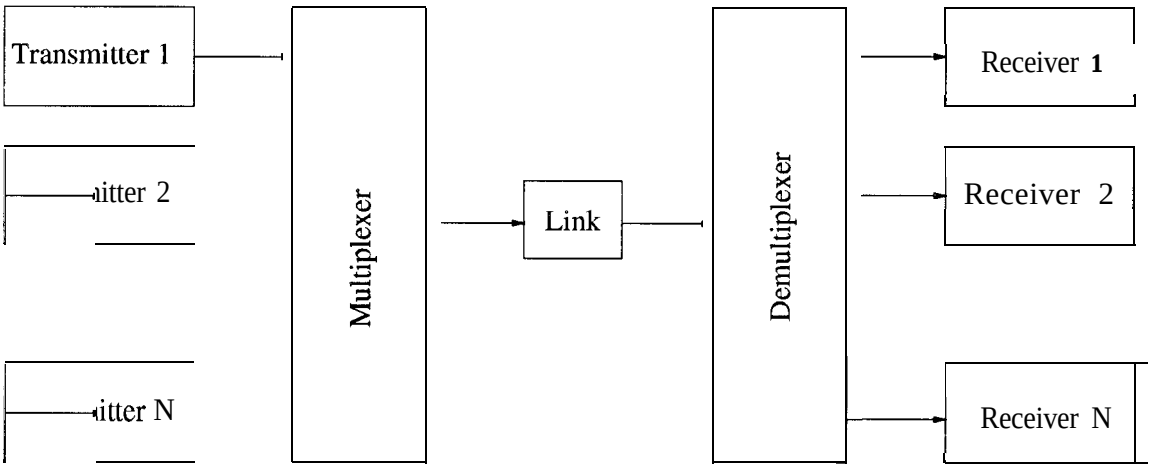

Figure 5.18: Functional diagram of a synchronous TDM system with N channels.

The scheme in Fig. 5.18 actually corresponds to a synchronous TDM system [186], but it is our belief that if the distortion is not as severe as to prevent the application of any reconstruction method, the channel may be more efficiently used than with conventional transmission.

5.6 **Conclusions.**

This chapter has been devoted to the use of chaotic signals as carriers of information in a digital communication system (DCS). It has been introduced a new control technique that allows to encode any desired sequence of information bits in just one variable of the chaotic Lorenz system by applying small perturbations to the system trajectory. The method departs from the same principles as the one proposed by Hayes and Grebogi in [90, 89] but it exhibits the novel feature of controling the system trajectory by perturbing only the variable z, wehereas previous approaches proposed to carry out this control by perturbing a compound magnitude that involved variables x and z. Therefore, the encoding technique herein introduced may lead to a more simple implementation in practice: only variable z has to be perturbed and

only one variable (the variable x) has to be transmitted through the communication channel

Since the power of the perturbations employed to encode the information bits is very small, the perturbed Lorenz system keeps most of the properties of the uncontrolled one, including a certain degree of determinism. From the point of view of communications, this determinism provides some redundancy that can be exploited either to improve the transmission reliability or to increase the information rate. Both improvements are based on the realization that relatively long intervals of a chaotic signal carrying digital information can be recovered from just a few samples. Two methods to achieve this reconstruction have been introduced. The first reconstruction method (FRM) relies on the availability of an storage containing samples from the signal produced by the free running Lorenz system, whereas the second reconstruction method (SRM) resorts to the integration of the system equations. The latter has proved to be more precise in an ideal channel without noise, but the former is more robust when the received signal is contaminated with Gaussian noise.

Both the FRM and the SRM have been applied to the problem of recovering series of bits lost due to the effect of impulse noise on the received signal. This is the primary source of errors in a conventional DCS but the results presented in this chapter show how its effect can be significantly alleviated when the proposed encoding technique and reconstruction methods are employed together.

Alternatively, when impulse noise or other sources of unpredictable distortion are not a concern, the same procedures can be used to design an efficient time division multiplexing communication system. Since only a few samples of the chaotic signal are necessary to reconstruct a long interval that contains several bits, there is no need to transmit the whole waveform. Thus, several transmitters may share the communication link by tranmitting short bursts of their encoded chaotic signal in turns. The intended receiver only has to choose the burst from the corresponding transmitter and apply either the FRM or the SRM to reconstruct the whole waveform and extract the encoded bits. If N transmitters can share the link, then the overall information rate is multiplied by N.

Chapter 6

Conclusions and Outlooks.

The aim of this work has been the study of synchronization and control of chaotic systems with some potential applications to biology and the field of communications.

The first part has been devoted to the study of the stability of the global synchronized state in open linear arrays and rings of identical chaotic oscillators. Numerical simulations have been carried out with assemblies of Lorenz oscillators and Chua's oscillators, whereas experiments have been done in a board of Chua's oscillators. In all cases unidirectional coupling between circuits is set by the driving method of Güemez and Matías, in such a way that synchronization can be achieved when considering two oscillators. The results obtained are the following:

1. Synchronization of chaotic oscillators arranged in an open linear array has been found both experimentally and numerically. The oscillators synchronize in a consecutive way as a synchronization wave with constant velocity spreads through the array. A theoretical analysis that explains the linear relationship between the time required for all oscillators to synchronize and the number of elements in the array has also been supplied. It has been shown that the velocity of the synchronization wave depends linearly on the highest of the Lyapunov exponents corresponding to transverse perturbations to the synchronization manifold of two consecutive oscillators.

2. The appearance of synchronization in circular geometries (or rings) of chaotic oscillators has also been studied. Numerical simulations and experimental

results show that synchronization cannot be achieved for an arbitrary number of elements in the ring, but there exists an upper bound in the size of the ring above which an instability in the global synchronized state arises This upper bound can be theoretically obtained by means of a linear stability analysis around the uniform synchronized state. It has been shown that, beyond this instability, some stable spatio-temporal structures (periodic and chaotic rotating waves) can arise from a symmetric Hopf bifurcation, such that neighboring oscillators exhibit a phase lag of approximately $1/N$ of a period (being N the number of oscillators in the ring), characteristic of the first Fourier mode transverse to the synchronization manifold that becomes unstable.

3. The interaction between chaotic rotating wave structures when two rings are diffusively coupled cell-to-cell has been investigated. Depending on the sense of driving within each ring, two different configurations have been analyzed: parallel and antiparallel coupling. In the case of parallel coupling two definite behaviors have been obtained: when coupling is weak two desynchronized chaotic rotating waves are observed, each one in a different ring, and when coupling is strong these two waves become synchronized. Instead, in the case of antiparallel coupling the situation is richer: for weak coupling the same behavior is obtained, namely, two desynchronized rotating waves. For intermediate coupling, the rotating wave structure vanishes and all oscillators inside each ring become synchronized but there is no synchronization between different rings. And, for strong coupling all the oscillators synchronize exhibiting the behavior of an isolated chaotic oscillator: a double-scroll.

The second part has been devoted to the use of chaotic signals as carriers of information in a digital communication system (DCS). The results obtained are the following:

1. We have introduced a new control technique that allows to encode any desired sequence of information bits in just one variable of the chaotic Lorenz system by applying small perturbations to the system trajectory. The method departs from the same principles as the one proposed by Hayes and Grebogi in [90, 89] but it exhibits the novel feature of controling the system trajectory by perturbing only the variable z, wehereas previous approaches proposed to carry out this control by perturbing a compound magnitude that involved variables x

and z. Therefore, the encoding technique herein introduced may lead to a more simple implementation in practice: only variable z has to be perturbed and only one variable (the variable x) has to be transmitted through the communication channel.

2. Since the power of the perturbations employed to encode the information bits is very small, the perturbed Lorenz system keeps most of the properties of the uncontrolled one, including a certain degree of determinism. From the point of view of communications, this determinism provides some redundancy that can be exploited either to improve the transmission reliability or to increase the information rate. Both improvements are based on the realization that relatively long intervals of a chaotic signal carrying digital information can be recovered from just a few samples. Two methods to achieve this reconstruction have been introduced. The first reconstruction method (FRM) relies on the availability of an storage containing samples from the signal produced by the free running Lorenz system, whereas the second reconstruction method (SRM) resorts to the integration of the system equations. The latter has proved to be more precise in an ideal channel without noise, but the former is more robust when the received signal is contaminated with Gaussian noise.

3. Both the FRM and the SRM have been applied to the problem of recovering series of bits lost due to the effect of impulse noise on the received signal. This is the primary source of errors in a conventional DCS and the results presented in this work show how its effect can be significantly alleviated when the proposed encoding technique and reconstruction methods are employed together.

4. Finally, when impulse noise or other sources of unpredictable distortion are not a concern, the same procedures can be used to design an efficient time division multiplexing communication system. Since only a few samples of the chaotic signal are necessary to reconstruct a long interval that contains several bits, there is no need to transmit the whole waveform. Thus, several transmitters may share the communication link by tranmitting short bursts of their encoded chaotic signal in turns. The intended receiver only has to choose the burst from the corresponding transmitter and apply either the FRM or the SRM to reconstruct the whole waveform and extract the encoded bits. If N transmitters can share the link, then the overall information rate is multiplied by N.

Regarding the future possible extensions of the first part of this work, the following lines may be considered:

- Analyzing the effect of different driving and diffusive connections in assemblies of chaotic systems in order to extend the results presented in this work to more complex situations.
- Trying to take advantage of the useful tools that group theory can provide in order to predict the possible structures that can arise in complex systems. We expect that the appearance of these structures can be explained in terms of the group of symmetries that characterize the problem.

With respect to the second part, interesting extensions could be:

- To increase the information rate of the chaotic signal obtained from the perturbed Lorenz oscillator in such a way that several bits can be encoded in each oscillation.
- To extend the second method of reconstructing chaotic signals to improve its robustness in noisy channels.
- To consider the variable z of the Lorenz system to be transmitted by the communication channel instead of the variable x since the message is visible in the signal x but not in z. In this case, the message would be masked in the chaotic transmitted signal.

Appendix A

Chua's Circuit.

The Chua's circuit is a rather simple electronic circuit that became popular for the study of chaos during the 1980's [147, 36, 37, 39, 134], although arrays of Chua's circuits have also been used to model reactiondiffusion systems and autowave propagation [153, 215, 180, 181, 136, 137, 154, 51, 155, 52, 53, 54, 55]. The Chua's circuit allows almost all of the dynamical behavior seen in computer simulations to be implemented in an electronics lab and viewed on an oscilloscope. As designed and popularized by L.O. Chua, an electronic engineering professor at the University of California at Berkeley, and the Japanese scientist T. Matsumoto, it is an RLC circuit that contains four linear elements (two capacitors with capacitances C_1 and C_2, one linear resistor with resistance l/G, and one inductor with inductance L) and a nonlinear resistor, N_R, called Chua's diode [44]. This diode is responsible for the great richness of dynamical behavior that the circuit can describe.

A schematic of this circuit is shown in Fig. A.1 where V_1 and V_2 represent the voltages associated to the capacitors C_1 and C_2.

The Chua's circuit can be modeled by a system of three differential equations. The explicit form of the equations is given below

$$\begin{aligned} C_1\frac{dV_1}{dt} &= G(V_2 - V_1) - g(V_1) \\ C_2\frac{dV_2}{dt} &= G(V_1 - V_2) + I_L \\ L\frac{dI_L}{dt} &= -V_2 - I_L r_0 \end{aligned} \tag{A.1}$$

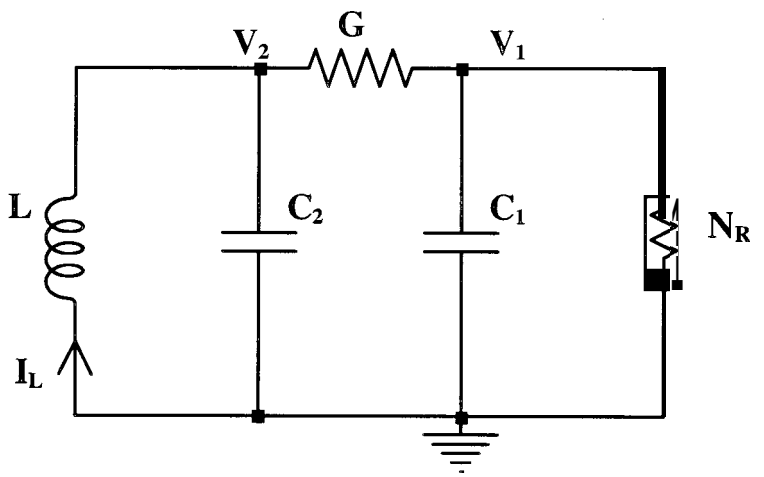

Figure A.l: Schematic of a Chua's circuit.

Here r_0 is the internal resistance of the physical inductor and $g(V_1)$ denotes the intensity that circulates through the nonlinear element N_R. This intensity can be represented by the following three-segment piecewiseelinear function

$$g(V_1) = \left\{ G_b V_1 + \frac{1}{2}(G_a - G_b)[|V_1 + B_p| - |V_1 - B_p|] \right\} \tag{A.2}$$

where the slopes of the inner and outer regions are G_a and G_b, respectively, and B_p and $-B_p$ denote breakpoints (see Fig. A.2).

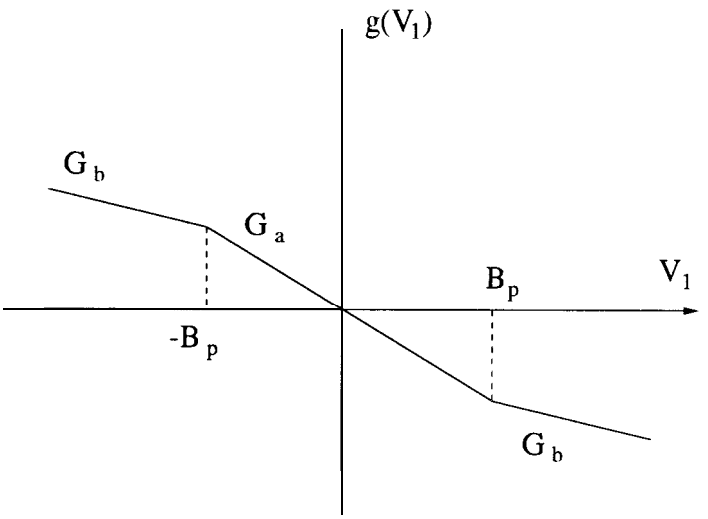

Figure A.2: Three-segment piecewise-linear function that represents the intensity that circulates through the nonlinear element N_R as a function of the voltage V_1.

Most of the analytical studies of the circuit have focussed on a dimensionless form of the equations, represented by

$$\begin{aligned} \frac{dx}{da} &= \alpha(y - x - f(x)) \\ \frac{dy}{d\tau} &= x - y + z \\ \frac{dz}{d\tau} &= -\beta y - \gamma z \ . \end{aligned} \tag{A.3}$$

where

$$x = \frac{V_1}{B_p}, \quad y = \frac{V_2}{B_p}, \quad z = \frac{I_L}{B_p G}, \quad \tau = \frac{tG}{C_2},$$

and $f(x)$ is the dimensionless form of the characteristics $g(V_1)$:

$$f(x) = \left\{ bx + \frac{1}{2}(a - b)[|x+1| - |x-1|] \right\} \tag{A.4}$$

The dimensionless parameters are defined as follows:

$$\alpha = \frac{C_2}{C_1}, \quad \beta = \frac{C_2}{L G^2}, \quad \gamma = \frac{C_2 r_0}{L G}, \quad a = \frac{G_a}{G}, \quad b = \frac{G_b}{G}$$

A.1 Modified Chua's Circuit.

A modification on the Chua's oscillator has been introduced (see [203, 205]) in order to allow a driving coupling through the nonlinear element, in such a way that the Chua's diode can receive an external input from another Chua's oscillator. Thus, the Chua's diode is replaced by a voltage controlled current source (VCCS), namely N_R'. This modified Chua's circuit is represented in Fig. A.3, where a new input can be introduced in the nonlinear element through node 3. The non-modified Chua's circuit can be recovered just by connecting node 3 with node 1. Therefore, the modified Chua's circuit allow to simulate more complex connections.

A schematic of this modified nonlinear element is shown in Fig. A.4, where the nodes 1, 2 and 3 corresponds to the analogous nodes shown in Fig. A.3.

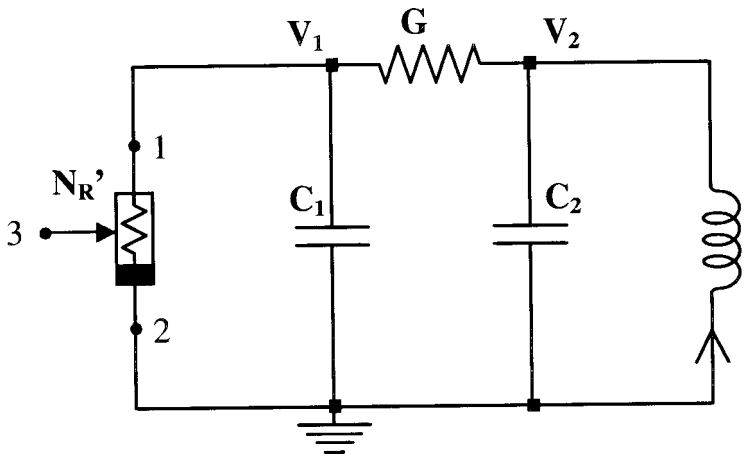

Figure A.3: Schematic of a modified Chua's circuit.

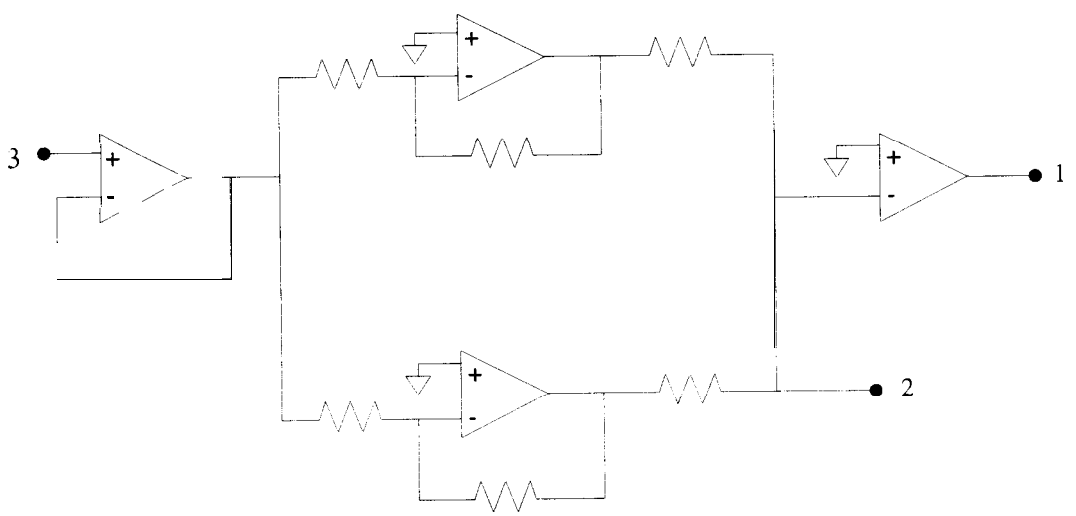

Figure A.4: Schematic of a modified Chua's diode.

Appendix B

Digital Communication Systems.

The subject of digital communications involves the transmission of information in digital form from a source that generates the information to one or more destinations. The principal feature of a digital communication system (DCS) is that, during a finite time interval, it sends a waveform from a finite set of possible waveforms whereas, in an analog communication system, the transmitted waveform is chosen from an infinite variety of waveform shapes with theoretically infinite resolution [186]. In a DCS, the objective at the receiver is not to reproduce a transmitted waveform with precision; but to determine from a noise-perturbed signal which waveform from the finite set of waveforms had been sent by the transmitter. Thus, in a DCS the important measure of system performance is the probability of incorrectly detecting the transmitted waveform (or, simply, the probability of error, P_E) [186]. This is in contrast to an analog communication system, where the figure of merit should be a fidelity criterion, such as the signal-to-noise ratio (SNR), percent distortion or the expected mean square error (MSE) between the transmitted and received waveforms.

DCSs are more robust than analog systems because signals can be regenerated at regular intervals in the transmission line and, in this way, noise and other disturbances are not accumulated. This is due to the nature of the transmission process. Analog transmission is a means of transmitting analog signals without regard to their content. This signal will become weaker (attenuate) after a certain distance. To achieve longer distances, the analog transmission system includes amplifiers that boost the energy in the signal. Unfortunately, the amplifier also boosts the noise components. With amplifiers cascaded to achieve long distances, the signal becomes more and

more distorted. Digital transmission, in contrast, is concerned with the content of the signal. A digital signal can be transmitted only a limited distance before attenuation endangers the integrity of the information it contains. To achieve greater distances, repeaters are used. A repeater receives the digital signal, recovers the original waveform and retransmits a new signal. Thus the attenuation is overcome and the distortion is not accumulated [218].

B.1 Block Diagram of a Conventional Digital Communication System.

Figure B.l illustrates the functional diagram and the basic elements of a digital communication system. The source output may be either an analog signal or a digital signal that is discrete in time and has a finite number of output characters. In a DCS, the messages produced by the source are converted into a sequence of binary digits. Ideally, the source output (messages) should be represented by as few binary digits as possible. In other words, an efficient representation of the source output that results in little or no redundancy is pursued. The process of efficiently converting the output of either an analog or digital source into a sequence of binary digits is called source encoding or data *compression*. Examples of source encoding are techniques such as pulse code modulation (PCM) [214] or moving pictures expert group (MPEG) [159, 211].

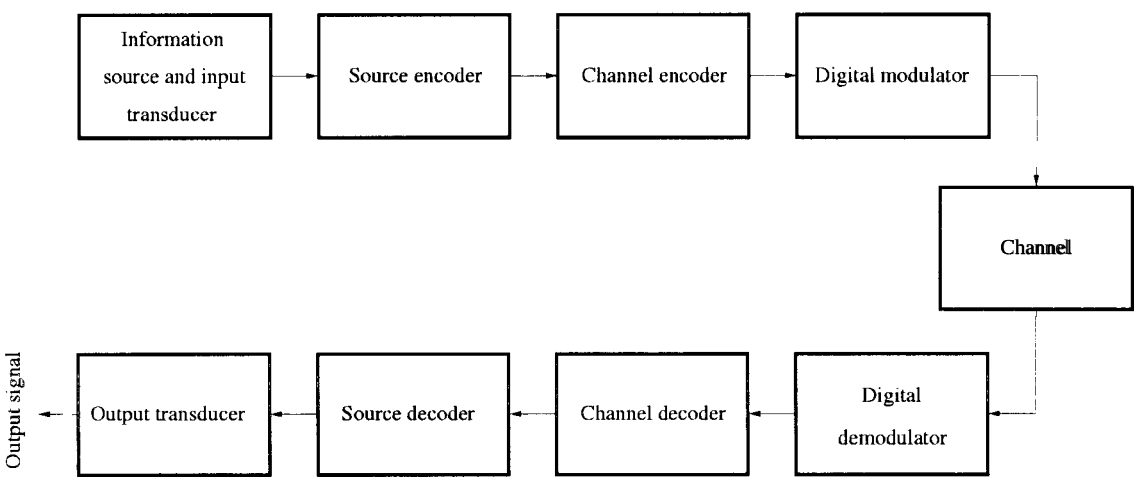

Figure B.1: Block diagram of a conventional digital communication system.

The sequence of binary digits from the source encoder, which is called information sequence, is passed to the *channel* encoder. The purpose of the channel encoder is to introduce, in a controlled manner, some redundancy in the binary information sequence that can be used at the receiver to overcome the effects of noise and interference encountered in the transmission of the signal through the channel. Thus, the added redundancy serves to increase the reliability of the received data [188]. In effect, redundancy in the information sequence aids the receiver in decoding the desired information sequence. A trivial form of encoding of the binary information sequence is simply to repeat each binary digit m times, where m is some positive integer. More sophisticated encoding involves taking k information bits at a time and mapping each k-bit sequence into a unique n-bit sequence, called a code word. The amount of redundancy introduced by encoding the data in this manner is measured by the ratio *n/k.* The reciprocal of this ratio, namely *k/n,* is called the code rate.

The binary sequence at the output of the channel encoder is passed to the *digital modulator,* which is the interface to the communications channel. Nearly all of the communication channels encountered in practice are capable of transmitting electrical signals (waveforms). So, the main purpose of the digital modulator is to map the binary information sequence into signal waveforms. To elaborate on this point, let us suppose that the coded information sequence is to be transmitted one bit at a time at some uniform rate *R* bits/s. The digital modulator may simply map the binary digit 0 into a waveform $s_0(t)$ and the binary digit 1 into a waveform $s_1(t)$. In this way, each bit from the channel encoder is transmitted separately. This is called *binary modulation*. Alternatively, the modulator may transmit *b* coded information bits at a time by using A4 = 2^b distinct waveforms $s_i(t), i = 0, 1, \ldots, M-1$, one waveform for each of the 2^b possible b-bit sequences. This is called *M-ary modulation* $(M > 2)$. When the channel bit rate *R* is fixed a new b-bit sequence enters the modulator every *b/R* seconds. So, the amount of time available to transmit one of the M waveforms corresponding to a b-bit sequence is *b* times the time period in a system that uses binary modulation.

The *communication channel* is the physical medium that is used to send the signal from the transmitter to the receiver. This medium can be guided (copper wires, optical fiber or coaxial cables) or unguided (the atmosphere or free space). In the latter case the communication system is said to be wireless. Good examples of wireless transmission are current mobile digital telephone systems like GSM [149].

Whatever the physical medium used for transmission of the information, the essential feature is that the transmitted signal is corrupted in a random manner by a variety of phenomena, such as additive *thermal noise* generated by electronic devices, man-made noise (e.g., automobile ignition noise), and atmospheric noise (e.g., electrical lightning discharges during thunderstorms).

At the receiving end of a digital communications system the digital *demodulator* processes the channel-corrupted transmitted waveform and reduces the waveforms to a sequence of numbers that represent estimates of the transmitted data symbols (binary or M-ary). This sequence of numbers is passed to the channel decoder, which attempts to reconstruct the original information sequence from knowledge of the code used by the channel encoder and the redundancy contained in the received data.

A measure of how well the demodulator and the decoder perform is the frequency with which errors occur in the decoded sequence. More precisely, the average probability of a bit-error at the output of the decoder is a measure of the performance of the demodulator-decoder combination. In general, the probability of error is a function of the code characteristics, the types of waveforms used to transmit the information over the channel, the transmitted power, the channel characteristics (i.e., the amount of noise, the nature of the interference, etc.), and the method of demodulation and decoding.

As a final step, when an analog output is desired, the source decoder accepts the output sequence from the channel decoder and, from knowledge of the source encoding method used, attempts to reconstruct the original signal. However, due to the demodulation/decoding errors and the lack of precission in the analog to digital (A/D) and digital to analog (D/A) conversions, the obtained signal is just an approximation to the original source output. The difference or some function of the difference between the original signal and the reconstructed signal is a measure of the distortion introduced by the DCS.

B.2 Possible Problems in a Transmission Medium.

Fundamentally every communication system requires three elements, a sending or transmitting station, a receiving station, and a transmission medium or *channel* to

connect the two together.

The most elementary channel is simply a pair of wires such as in telegraph or telephone systems. Other common channels are the earth's atmosphere, vacuum space, or combinations of the two as in a satellite link.

With any communications system, it must be recognized that the signal that is received will differ from the signal that is transmitted due to various transmission impairments. For analog signals, these impairments introduce various random modifications that degrade the signal quality. For digital signals, bit errors are introduced: A binary 1 is transformed into a binary 0 and vice versa. The most significant impairments are: attenuation and attenuation distortion, delay distortion and noise.

B.2.1 Attenuation.

The strength of a signal falls off with distance over any transmission medium. For guided media, this reduction in strength, or attenuation, is generally logarithmic and thus is typically expressed as a constant number of decibels per unit distance. For unguided media, attenuation is a more complex function of distance and the makeup of the atmosphere. Attenuation introduces three considerations for the transmission engineer. First, a received signal must have sufficient strength so that the electronic circuitry in the receiver can detect and interpret the signal. Second, the signal must maintain a level sufficiently higher than noise to be received without error. Third, attenuation is an increasing function of frequency.

The first and second problems are dealt with by attention to signal strength and the use of amplifiers or repeaters. For a point-to-point link, the signal strength of the transmitter must be strong enough to be received intelligibly, but not so strong as to overload the circuitry of the transmitter, which would cause a distorted signal to be generated. Beyond a certain distance, the attenuation is unacceptably great, and repeaters or amplifiers are used to boost the signal from time to time. These problems are more complex for multipoint lines where the distance from transmitter to receiver is variable.

The third problem is particularly noticeable for analog signals. Because the

attenuation varies as a function of frequency, the received signal is distorted, reducing intelligibility. To overcome this problem, techniques are available for equalizing attenuation across a band of frequencies. This is commonly done for voice-grade telephone lines by using loading coils that change the electrical properties of the line; the result is to smooth out attenuation effects. Another approach is to use amplifiers that amplify high frequencies more than lower frequencies.

Attenuation distortion is much less of a problem with digital signals since the strength of a digital signal falls off rapidly with frequency and most of the content is concentrated near the fundamental frequency or bit rate of the signal.

B.2.2 **Delay Distortion.**

Delay distortion is a phenomenon peculiar to guided transmission media. The distortion is caused by the fact that the velocity of propagation of a signal through a guided medium varies with frequency. For a bandlimited signal, the velocity tends to be highest near the center frequency and fall off toward the two edges of the band. Thus various frequency components of a signal will arrive at the receiver at different times.

This effect is referred to as delay distortion, since the received signal is distorted due to variable delay in its components. Delay distortion is particularly critical for digital data. Consider that a sequence of bits is being transmitted, using either analog or digital signals. Because of delay distortion, some of the signal components of one bit position will spill over into other bit positions, causing *intersymbol interference* [186], which is a major limitation to maximum bit rate over a transmission control.

Equalizing techniques can also be used for delay distortion [186].

B.2.3 Noise.

For any data transmission event, the received signal will consist of the transmitted signal, modified by the various distortions imposed by the transmission system, plus additional unwanted signals that are inserted somewhere between trasmission and

reception. The latter, undesired signals are referred to as noise. It is noise that is the major limiting factor in communications system performance.

Noise may be divided into four categories [62]: Thermal noise, Intermodulation noise, Crosstalk and Impulse noise.

Thermal Noise is due to thermal agitation of electrons in a conductor. It is present in all electronic devices and transmission media and is a function of temperature. Thermal noise is uniformly distributed across the frequency spectrum and hence is often referred to as white noise. Thermal noise cannot be eliminated and therefore places an upper bound on communications system performance.

When signals at different frequencies share the same transmission medium, the result may be *intermodulation noise.* The effect of intermodulation noise is to produce signals at a frequency that is the sum or difference of the two original frequencies or multiples of those frequencies. For example, the mixing of signals at frequencies f_1 and f_2 might produce energy at the frequency $f_1 + f_2$. This derived signal could interfere with an intended signal at the frequency $f_1 + f_2$.

Intermodulation noise is produced when there is some *nonlinearity* in the transmitter, receiver, or intervening transmission system. Normally, these components behave as linear systems; that is, the output is equal to the input times a constant. In a nonlinear system, the output is a more complex function of the input. Such nonlinearity can be caused by component malfunction or the use of excessive signal strength. It is under these circumstances that the sum and difference terms occur.

Crosstalk has been experienced by anyone who, while using the telephone, has been able to hear another conversation; it is unwnated coupling between signal paths. It can occur by electrical coupling between nearby twisted pair or, rarely, coax cable lines carrying multiple signals. Crosstalk can also occur when unwanted signals are picked up by microwave antennas; although highly directional, microwave energy does spread during propagation. Typically, crosstalk is of the same order of magnitude as, or less than, thermal noise.

All of the types of noise discussed so far have reasonably predictable and reasonably constant magnitudes. Thus it is possible to engineer a transmission

system to cope with them. Impulse noise, however, is noncontinuous, consisting of irregular pulses or noise spikes of short duration and of relatively high amplitude. It is generated from a variety of causes, including external electromagnetic disturbances, such as lightning, and faults and flaws in the communications system.

Impulse noise is generally only a minor annoyance for analog data. For example, voice transmission may be corrupted by short clicks and crackles with no loss of intelligibility. IIowever, impulse noise is the primary source of error in digital data communication. For example, a sharp spike of energy of 0.001 s duration would not destroy any voice data, but would wash out about 5 bits of data being transmitted at 4800 bps.

Appendix C

Multiplexing.

Multiplexing refers to a variety of techniques used to make more efficient use of transmission facility. In many cases, the capacity of a transmission facility exceeds the requirements for the transfer of data between two devices. That capacity can be shared among multiple transmitters by multiplexing a number of signals onto the same medium. In this case, the actual transmission path is referred to as a circuit or link, and the portion of capacity dedicated to each pair of transmitter/receivers is referred to as a channel.

Transmission facilities are, by and large, expensive. It is often the case that two communicating stations will not utilize the full capacity of a data link. For efficiency, it should be possible to share that capacity. The generic term for such sharing is multiplexing.

It is instructive to distinguish among several types of multiuser communication systems. One type is a multiple access system in which a large number of users share a common communication channel to transmit information to a receiver. Such a system is depicted in Fig. C.1. The common channel may be the up-link in a satellite communication system, or a cable to which are connected a set of terminals that access a central computer, or some frequency band in the radio spectrum that is used by multiple users to communicate with a radio receiver. For example, in a mobile cellular communication system, the users are the mobile trasmitters in any particular cell of the system and the receiver resides in the base station of the particular cell.

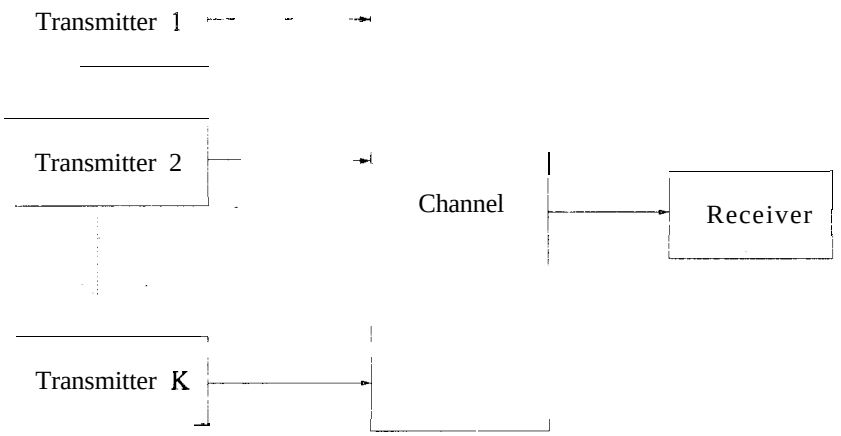

Figure C.l: A multiple access system.

A second type of multiuser communication system is a broadcast network in which a single transmitter sends information to multiple receivers as depicted in Fig. C.2. Examples of broadcast systems include the common radio and TV broadcast systems, as well as the down-links in a satellite system.

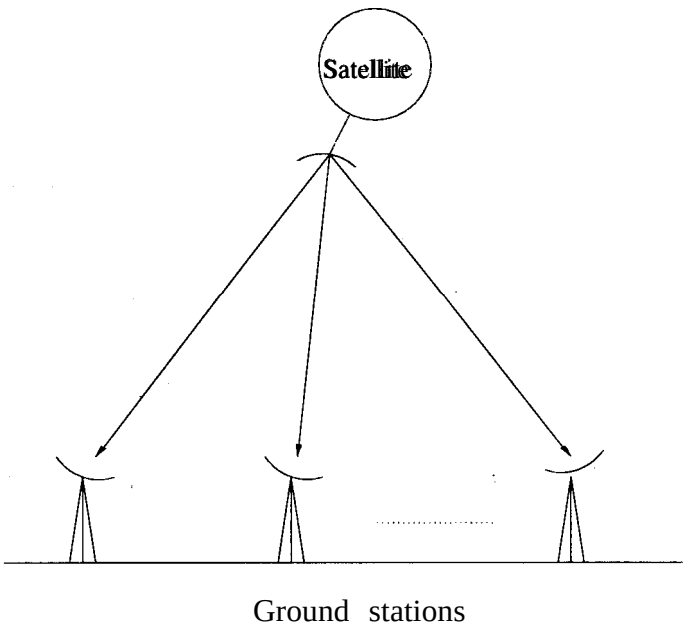

Figure C.2: A broadcast network.

The multiple access and broadcast networks are probably the most common multiuser communication systems. A third type of multiuser system is a store-and-forward network, as depicted in Fig. C.3.

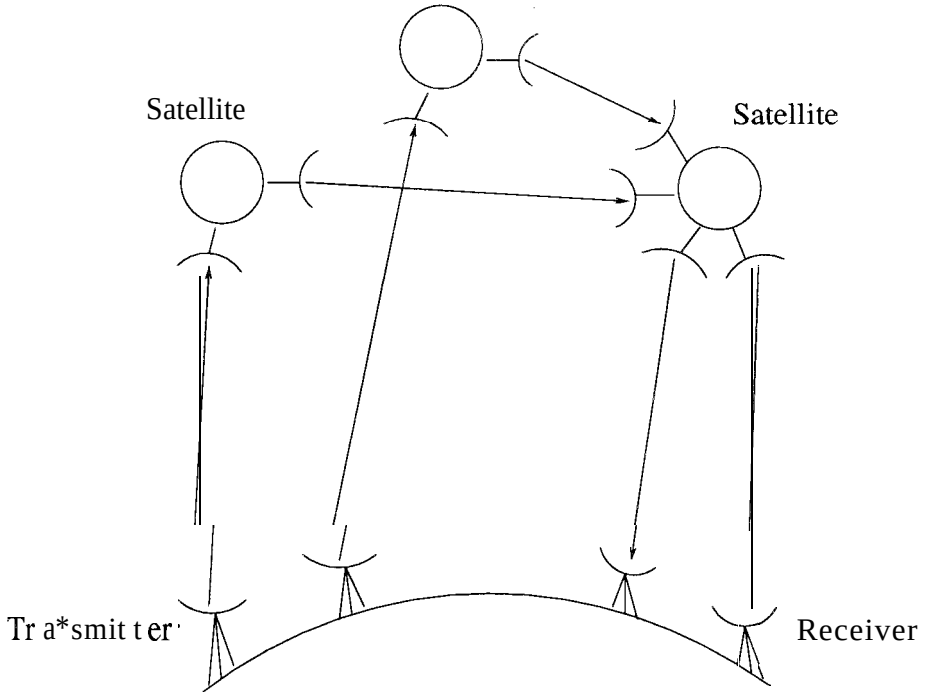

Figure C.3: A store-and-forward communication network with satellite relays.

Yet a fourth type is the two-way communication system shown in Fig. C.4.

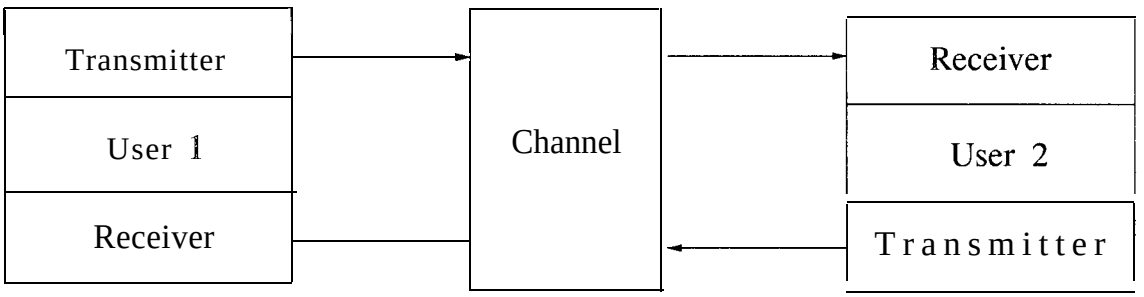

Figure C.4: A two-way communication channel.

In general, there are several different ways in which multiple users can send information through the communication channel to the receiver. One simple method is to subdivide the available channel bandwidth into a number, say N, of frequency nonoverlapping subchannels, as shown in Fig. C.5, and to assign a subchannel to each user upon request by the users. This method is generally called frequency-division multiple access (FDMA), and is commonly used in wireline channels to accommodate multiple users for voice and data transmission.

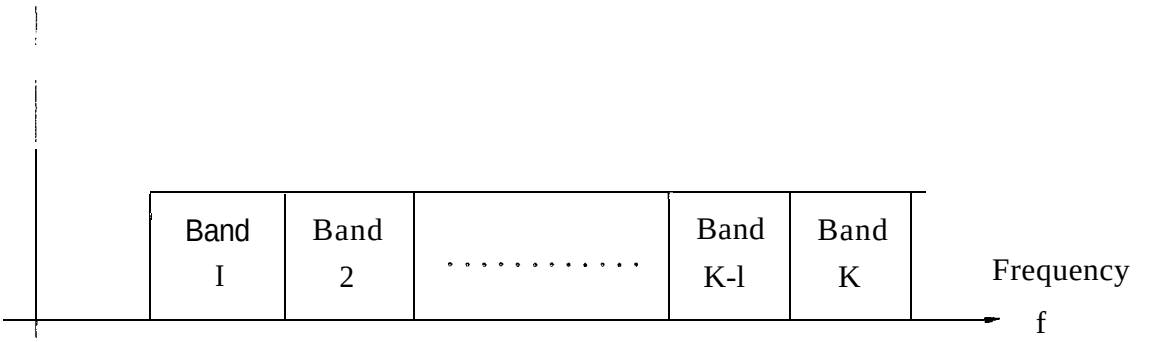

Figure C.5: Subdivisions of the channel into nonoverlapping frequency bands.

Another method for creating multiple subchannels for multiple access is to subdivide the duration T_f, called the frame *duration,* into, say, N nonoverlapping subintervals, each of duration T_f/N. Then each user who wishes to transmit information is assigned to a particular time slot within each frame. This multiple access method is called *time-division* multiple access (TDMA) and it is frequently used in data and digital voice transmission.

Glossary.

- Attractor: The bounded region or set of points of phase space (with zero volume) towards which orbits/trajectories originating from nearby points (basins) are attracted during long-time evolution in the case of dissipative systems. Point attractors (such as stable focus, centre, stable node), limit cycles, torus and chaotic (strange) attractors all are examples.

- Bifurcation: Sudden/abrupt significant changes in the set of fixed or periodic points or other sets of dynamic interest at critical control parameters values when the parameter is varied.

  Let us suppose the following system of differential equations

  $$\dot{x} + f(x, \lambda) = 0, \tag{C.1}$$

  where $x \in \Re^n, \lambda \in \Re$ is a bifurcation parameter, and $f : \Re^n \times \Re \to \Re^n$ is a smooth (C^∞) mapping defined near $(0, 0)$. We also assume that there is a trivial solution, so that $f(0, \lambda) \equiv 0$.

  Generally there are two types of bifurcation:

  (a) Steady-state bifurcation, when an eigenvalue of $(df)_{0,\lambda}$ passes through 0.

  (b) *Hopf bifurcation*, when a pair of conjugate complex eigenvalues of $(df)_{0,\lambda}$ crosses the imaginary axis with nonzero speed at $\pm\omega i$, w $\neq 0$.

  Generically these eigenvalues are simple. In case (a) subject to suitable nondegeneracy conditions, there will be a branch of steady-state solutions bifurcating from the origin. In case (b) a branch of periodic solution, of period near $2\pi/\omega$, will bifurcate.

- Chaos: Complicated and aperiodic motions which are highly sensitively dependent upon initial conditions in deterministic nonlinear systems.

Correspondingly, in the phase space two nearby chaotic trajectories diverge exponentially, though still confined to a bounded domain (in the case of dissipative systems).

- **Diffeomorphism:** A C^k–diffeomorphism $f : M \to N$ is a mapping f which is one-to-one, onto, and has the property that both f and f^{-1} are k-times differentiable.

- **Dynamical system:** Any set of equations giving the time evolution of the state of a system from a knowledge of its previous history. Examples are Maxwell's equations, the Navier-Stokes equations, and Newton's equations for the motion of a particle with suitably specified forces. A common setting is a system of k first-order autonomous ordinary differential equations

$$\dot{\mathbf{x}} = \mathbf{F}(\mathbf{x}), \tag{C-2}$$

where x = $(x^{(1)}, x^{(2)}, \ldots, x^{(k)})$ denotes *k* state components, considered as a vector in k-dimensional phase space, $\mathbf{F(x)} = (F^{(1)}\,\mathbf{(x)}, F^{(2)}(\mathbf{x}), \ldots, F^{(k)}\,\mathbf{(x))}$ is a k-dimensional vector function of x, and $\dot{\mathbf{x}}$ denotes the time derivative $d\mathbf{x}/dt$.

- **Eigenvector:** An eigenvector v of an n x n matrix **A** is a nonzero vector which satisfies $\mathbf{A}v = \lambda v$ for some $\lambda \in$ C. λ is the *eigenvalue* of v.

- **Global:** This term is applied to properties which cannot be analyzed in arbitrarily small neighborhoods of a single point.

- **Local:** A property is local if it can be analyzed in an arbitrarily small neighborhood of a given point.

- **Lyapunov exponents:** Numbers providing a quantitative average measure of the divergence of nearby trajectories in phase space. All negative exponents represent regular and periodic orbits, while at least one positive exponent signals the presence of chaotic motion.

  In particular, for a k-dimensional system of first-order ordinary differential equations

$$\dot{\mathbf{x}} = \mathbf{F}(\mathbf{x}), \tag{C.3}$$

if we consider the infinitesimally displaced orbit x(t) + 6x(t) and the tangent vector y(t) = $\delta\mathbf{x}(t)/\delta\mathbf{x}(0)$, in terms of which we have

$$\dot{\mathbf{y}} = \mathbf{DF}(\mathbf{x}(t))\mathbf{y}. \tag{C.4}$$

Thus, the Lyapunov exponents are then given by

$$h(\mathbf{x}(0), \mathbf{y}(0)) = \lim_{t \to \infty} \frac{1}{t} \ln \mathbf{y}(t). \tag{C.5}$$

- **Manifold:** An n-dimensional manifold M **c** $\Re^N$ is a set for which each $x \in \mathcal{M}$ has a neighborhood U for which there is a smooth invertible mapping (diffeomorphism) $\phi: \Re^n \to U (n \leq N)$.

- **Neighborhood:** A neighborhood of a point x is a set U which contains x in its interior.

- **Phase diagram:** A plot of the different types of dynamical behavior as a function of two or more control parameters.

- **Phase space/Phase portrait: The abstract** space of the dynamical variables is the phase space in which the state point moves along the phase trajectory constituting the phase portrait.

- **Submanifold:** A submanifold M of a manifold $\mathcal{N}$ is a subset of $\mathcal{N}$ which is a manifold.

Bibliography

[1] H.D.I. Abarbanel, *Analysis of Observed Chaotic Data*, (Institute for Nonlinear Science, Springer, 1995).

[2] H.D.I. Abarbanel, *Analysis of Observed Chaotic Time Series*, (Institute for Nonlinear Science, Springer, 1996a).

[3] H.D.I. Abarbanel, R. Huerta, M.I. Rabinovich, N.F. Rulkov, P.F. Rowat & A. Selverston, Neural Computat. 8, 1567 (1996b).

[4] H.D.I. Abarbanel, M.I. Rabinovich, A. Selverston, M.V. Bazhenov, R. Huerta, M.M. Sushchik & L.L. Rubchinskii, Physics-Uspekhi, 39, 337 (1996c).

[5] V.S. Afraimovich, N.N. Verichev & M.I. Rabinovich, Izvetiya Vusov, Radifizika 28, 1050 (1985).

[6] V.S. Afraimovich, N.N. Verichev & M.I. Rabinovich, Radiophys. Quantum Electron. 29, 795 (1986).

[7] V. Afraimovich & H.M. Rodrigues, preprint CDSN94-202, Center for Dynamical Systems and Nonlinear Studies, 39 (Georgia Institute of Technology, 1994).

[8] K. Aihara, G. Matsumoto & M. Ichikawa, Phys. Lett. A 111, 251 (1985).

[9] J.C. Alexander, SIAM J. Appl. Math 46, 199 (1986).

[10] R.E. Amritkar & N. Gupte, Phys. Rev. A 44, 3403 (1991).

[11] V.S. Anishchenko, I.S. Aranson, D.E. Postnov & M.I. Rabinovich, Sov. Phys. Dokl. 31, 169 (1991).

[12] V.S. Anishchenko, T.E. Vadivasova, D.E. Postnov & M.A. Safonova, Int. J. Bifurc. Chaos 2, 633 (1992).

[13] A. Arneodo, P. Coullet & C. Tresser, Commun. Math. Phys. 79, 573 (1981).

[14] P. Ashwin, J. Buescu & I. Stewart, Phys. Lett. A 193, 126 (1994).

[15] P. Badola, V.R. Kumar & B.D. Bulkarni, Phys. Lett. A 155, 365 (1991).

[16] K. Bar-Eli, Physica D 14, 242 (1985).

[17] B.L. Bardakjian & S.K. Sarna, IEEE Trans. Biomed. Eng. 27, 193 (1980).

[18] V.N. Belykh, N.N. Verichev, L. Kocarev & L.C. Chua, J. of Circuits Syst. and Comp. 3 (1993).

[19] M. di Bernardo, Int. J. Bifurc. Chaos 6, 557 (1996).

[20] 1.1. Blekhman, P.S. Landa & M.G. Rosenblum, Appl. Mech. Rev. 48, 733 (1995).

[21] T. Bohr, G. Grinstein, Y. He & C. Jayaprakash, Phys. Rev. Lett 58, 2155 (1987).

[22] E Bollt, Y.-C. Lai & C. Grebogi, Phys. Rev. Lett. 79, 3787 (1997).

[23] E Bolt & M. Dolnik, Phys. Rev. E 55, 6406 (1997).

[24] C Bracikowski & R. Roy, Chaos 1, 49 (1991).

[25] R.W. Brockett, On *conditions leading to chaos in feedback systems,* in Proceedings of the IEEE Conference on Decission and Control, 932-936 (1982).

[26] R. Brown, N.F. Rul'kov & N.B. Tufillaro, Phys. Rev. E 50, 4488 (1994).

[27] R. Brown, Phys. Rev. Lett. 81, 4835 (1998).

[28] G. Buzsaki, R. Llinas, R. Singer & A. Berthoz *Temporal* Coding in *the Brain: Research and Perspectives in Neurosciences,* (Berlin, Springer-Verlag, 1994).

[29] C.C. Canavier, J.W. Clark & J.H. Byrne, Biophys. J. 57, 1245 (1990).

[30] T.L. Carroll & L.M. Pecora, IEEE Trans. Circuits Syst. 38, 453 (1991).

[31] T.L. Carroll & L.M. Pecora, Int. J. Bifurc. Chaos 2, 659 (1992).

[32] T.L. Carroll & L.M. Pecora, Physica D 67, 126 (1993).

[33] T.L. Carroll, J.F. Heagy & L.M. Pecora, Phys. Lett. A 186, 225 (1994).

[34] Chaos 7 (1997).

[35] G. Chen & X. Dong, Int. J. Bifurc. Chaos 3, 1363 (1993).

[36] L.O. Chua, M. Komuro & T. Matsumoto, IEEE Trans. Circuits Syst. 33, 1072 (1986a).

[37] L.O. Chua, M. Komuro & T. Matsumoto, IEEE Trans. Circuits Syst. 33, 1097 (1986b).

[38] L.O. Chua & L. Yang, IEEE Trans. Circuits Syst. 35, 1257 (1988).

[39] L.O. Chua, Int. J. Elec. and Comm. 46, 250 (1992).

[40] L.O. Chua, IEICE Trans. Fund. Electron., Comm. Compu. Sci. E76-A, 704 (1993).

[41] L.O. Chua (ed.), IEEE Trans. Circuits Syst. I, 42 (1995).

[42] J.J. Collins & I.N. Stewart, J. Nonlinear Sci. 3, 349 (1993).

[43] J.J. Collins & I. Stewart, Biol. Cybern. 71, 95 (1994).

[44] L.M. Cruz, Int. J. Circuit Theory and Applications 21, 309 (1993).

[45] K.M. Cuomo & A.V. Oppenheim, Phys. Rev. Lett. 71, 65 (1993a).

[46] K.M. Cuomo, A.V. Oppenheim & S.H. Strogatz, IEEE Trans. Circuits Syst. 40, 626 (1993b).

[47] K.M. Cuomo, Int. J. Bifurc. Chaos Appl. Sco. Eng. 3, 1327 (1993).

[48] P.F. Curran & L.O. Chua, Int. J. Bifurc. Chaos 7, 1375 (1997).

[49] H. Daido, J. Phys. A: Math Gen 20, L629 (1987).

[50] M. deCastro, V. Perez-Muiiuzuri, L.O. Chua & V. Perez-Villar, Int. J. Bifurc. Chaos 5, 859 (1995).

[51] M. deCastro, V. Pérez-Muñuzuri, I.P. Mariño, M. Gómez-Gesteira, L.O. Chua & V. Perez-Villar, Int. J. Bifurc. Chaos 6, 1725 (1996).

[52] M. deCastro, M. Gomez-Gesteira & V. Perez-Villar, Phys. Rev. E 57, 949 (1998a).

[53] M. deCastro, *Tesis Doctoral: Estudio de Estructuras Biofisicas y sus Comportamientos* (Univ. de Santiago de Compostela, 1998).

[54] M. deCastro, E. Hofer, A.P. Muñuzuri, M. Gomez-Gesteira, G. Plank, I. Schafferhofer, V. Pérez-Muñuzuri & V. Perez-Villar, Phys. Rev. E 59 (in press, 1999a).

[55] M. deCastro, M. Gómez-Gesteira & V. Perez-Villar, IEEE Trans. Circuits Syst. 46 (in press, 199913).

[56] H. Dedieu, M.P. Kennedy & M. Hasler, IEEE Trans. Circuits Syst., II: Analog Digital Signal Process 40, 635 (1993).

[57] W. Ditto, S. N. Rauseo & M. L. Spano, Phys. Rev. Lett. 65, 3211 (1990).

[58] W.L. Ditto & L. Pecora, Sci. Am. (Int. Ed.) 269, *78* (1993).

[59] U. Dressler & G. Nitsche, Phys. Rev. Lett. 68, 1 (1992).

[60] G.B. Ermentrout, Physica D 41, 219 (1990).

[61] D. Fisher, Phys. Rev. Lett. 31, 1486 (1993).

[62] R. Freeman, *Telecommunication System* Engineering, (New York, Wiley, 1989).

[63] H. Fujisaka & T. Yamada, Progr. Theor. Phys. 69, 32 (1983).

[64] A. Garfinkel, M. Spano, W. Ditto & J. Weiss, Science 257, 1230 (1992).

[65] D.J. Gauthier & J.C. Bienfang, Phys. Rev. Lett. 77, 1751 (1996).

[66] Z. Gills, C. Iwata, R. Roy, I. Schwartz & I. Triandaf, Phys. Rev. Lett. 69, 3169 (1992).

[67] L. Glass & M.C. Mackey, From *Clocks to Chaos: The Rythms of Life* (Princeton University Press, Princeton, 1988).

[68] L. Glass, *Chaos in Neural Systems. The Handbook of Brain Theory and Neural Networks,* M. Arbib, (Ed. Cambridge, MIT Press, 1995).

[69] D. Golomb, D. Hansel, B. Shraiman & H. Sompolinsky, Phys. Rev. A 45, 3516 (1992).

[70] M. Golubitsky & I.N. Stewart, Arch. Rat. Mech. Anal. 87, 107 (1985).

[71] M. Golubitsky, I.N. Stewart & D.G. Schaeffer, *Singularities and Groups in Bifurcation Theory*, Vol. II, (Springer, New York 1988).

[72] M. Golubitsky, I. Stewart, P.L. Buono & J.J. Collins, Physica D 115, 56 (1998).

[73] S. Grillner, Physiol. Rev. 55, 247 (1975).

[74] S. Grillner *Control of locomotion in bipeds, tetrapods and fish (Ed.), Handbook of Physiology, Section 1: The Nervous System,* Vol II: Motor Control, American Physiological Society, Bethesda, 1981).

[75] *S.* Grillner & P. Wallén, Annu. Rev. Neurosci. 8, 233 (1985).

[76] *S.* Grillner, Science 228, 143 (1985).

[77] *S.* Grillner, Sci. Am. 274 (l), 48 (1996).

[78] J. Güémez & M.A. Matias, Phys. Rev. E 52, R2145 (1995).

[79] J. Güémez & M.A. Matias, Phys. Rev. E 53, 3059 (1996).

[80] J. Güémez, C. Martin & M.A. Matias, Phys. Rev. E 55, 124 (1997).

[81] J. Giiemez & M.A. Matias, Phys. Lett. A 246, 289 (1998).

[82] H. Haken, Phys. Lett. A 53, 77 (1975).

[83] H. Haken, *Advanced Synergetics* (Springer-Verlag, 1983).

[84] J. Halloy, Y.X. Martiel, B. Wurster & A. Goldbeter, Phys. Lett. A 151, 33 (1990).

[85] KS. Halle, C.W. Wu, M. Itoh & L.O. Chua, Int. J. Bifurc. Chaos 3, 469 (1993).

[86] R.M. Harris, E. Marder, A.I. Selverston & M. Moulins, Dynamic Biological *Networks: The Stomatogastric Nervous System*, (Cambridge, MIT Press, 1992).

[87] H. Hayashi & S. Ishizuka, J. Theor. Biol. 156, 269 (1992).

[88] *S.* Hayes, C. Grebogi & E. Ott, Phys. Rev. Lett. 70, 3031, (1993a).

[89] S. Hayes & C. Grebogi, SPIE 2038, 1 (199313).

[90] S. Hayes & C. Grebogi, Nonlinear Dynamics *in Circuits,325-336* (World 'Scientific, 1995).

[91] *S.* Hayes, C. Grebogi, E. Ott & A. Mark, Phys. Rev. Lett. 73, 1781 (1994).

[92] S. Haykin, *Digital Communications* (John Wiley & Sons, 1988).

[93] R. He & P. G. Vaidya, Phys. Rev. A 46, 7387 (1992).

[94] J.F. Heagy, T.L. Carroll & L.M. Pecora, Phys. Rev. E 50, 1874 (1994a).

[95] J.F. Heagy, N. Platt & SM. Hammel, Phys. Rev. E 49, 1140 (1994b).

[96] J.F. Heagy, T.L. Carroll & L.M. Pecora, Phys. Rev. E 52, R1253 (1995a).

[97] J.F. Heagy, T.L. Carroll & L.M. Pecora, Phys. Rev. Lett. 73, 3528 (1995).

[98] W.F. Heiligenberg, Neural Nets in *Electric Fish*, (MIT Press, Cambridge, MA, 1991).

[99] A.S. Hornby, *Oxford Advanced Dictionary,* (Oxford University Press, 1974).

[100] E.R. Hunt, Phys. Rev. Lett. 47, R2975 (1993).

[101] E.R. Hunt & G. Johnson, IEEE Spectr. 30, 32 (1993).

[102] B.R. Hunt, E. Ott & J.A. Yorke, Phys. Rev. E 55, 4029 (1997).

[103] K. Josic, Phys. Rev. Lett. 80, 3054 (1998).

[104] T. Kapitaniak, Phys. Rev. E 47, R2975 (1993).

[105] M.V. Kapranov, *Interacting multicoupling PLL* in System of phase synchronization, 55-73 (Radio i svjaz, Moscow, 1982).

[106] M. Kawasaki, G. Rose, & W. Heiligenberg, Nature 336, 173 (1988).

[107] E. Knobloch, Phys. Lett. A 82, 439 (1981).

[108] E.I. Knudsen, & M. Konishi, Science 200, 795 (1978).

[109] L. Kocarev, K.S. Halle, K. Eckert, L.O. Chua & U. Parlitz, Int. J. Bifurc. Chaos 2, 709 (1992).

[110] L. Kocarev & U. Parlitz, Phys. Rev. Lett. 74, 5028 (1995).

[111] L. Kocarev & U. Parlitz, Phys. Rev. Lett. 76, 1816 (1996a).

[112] L. Kocarev & U. Parlitz, Phys. Rev. Lett. 77, 2206 (199613).

[113] G. Kolumbán, M.P. Kennedy, IEEE Trans. Circuits Syst. 44, 927 (1997).

[114] M. Konishi, Sci. Am. 268, 34 (1993).

[115] R. Konnur, Phys. Rev. Lett. 77, 2937 (1996).

[116] N. Kopell & G.B. Ermentrout, Commun. Pure Appl. Math. 39, 623 (1986).

[117] N. Kopell & G.B. Ermentrout, Math. Biosci. 90, 87 (1988).

[118] N. Kopell & G.B. Ermentrout, SIAM J. Appl. Math. 50, 1014 (1990).

[119] J.M. Kowalski, G.L. Albert & G.W. Gross, Phys. Rev. A 42, 6260 (1990).

[120] J.M. Kowalski, G.L. Albert, B.K. Rhoades & G.W. Gross, Neural Networks 5, 805 (1992).

[121] V.I. Krinsky, Self- *Organization:* Autowaves and *Structures far from Equilibrium*, (Springer, New York, 1984).

[122] Y. Kuramoto *Chemical Oscillations, Waves, and Turbulence,* (Springer-Verlag, New York, 1984).

[123] Y. Kuramoto & I. Nishikawa, J. Stat. Phys. 49, 569 (1987).

[124] J. Kurths, A. Pikovsky & M. Rosenblum, *Phase synchronization of chaotic self-oscillatory systems* (ICND-96 Proc, Saratov, Russia, 1996).

[125] D.A. Linkens, I. Taylor & H.L. Duthie, IEEE Trans. Biomed. Eng. 23, 101 (1976).

[126] E.N. Lorenz, J. Atmos. Sci. 20, 130 (1963).

[127] E.N. Lorenz, *The Essence of Chaos,* (UCL Press, London, *1993).*

[128] M.N. Lorenzo, I.P. Mariño, V. Perez Muñuzuri, M.A. Matías & V. Perez-Villar, Phys. Rev. E 54, R3094 (1996a).

[129] M.N. Lorenzo, I.P. Mariño, V. Perez Muñuzuri, M.A. Matías & V. Perez-Villar, Nonlinear *Dynamics of Electronic Circuits, IEEE, 223-228* (Sevilla, 199613).

[130] M.N. Lorenzo, *Tesis de Licenciatura: Ondas de* Sincronizacidn en *Sistemas Cao'ticos,* (Univ. de Santiago de Compostela, 1996c)

[131] R. Lozi & L.0. Chua, Int. J. Bifurc. Chaos 3, 1319 (1993).

[132] E.D. Lumer & B.A. Huberman, Neural Comput. 4, 341 (1992).

[133] *The General Problem of the Stabillity of Motion,* edited by A.M. Lyapunov, Taylor & Francis (London, 1992).

[134] R.N. Madan, *Chua's Circuit: A Paradigm* for *Chaos,* (World Scientific, Singapore, 1993).

[135] W.V.R. Malkus, Mempoirs Societe Royale des Sciences de Lige, Series 6, 125 (1972).

[136] I.P. Mariño, M. deCastro, V. Pérez-Muñuzuri, M. Gómez-Gesteira, L.0. Chua & V. Pérez-Villar, IEEE Trans. Circuits Syst. 42, 665 (1995a).

[137] *Mariño Tesis de Licenciatura: Fomacio'n de Reentradas en Fibrus Paralelas* (Univ. de Santiago de Compostela, 1995b).

[138] I.P. Mariño, M.A. Matias & V. Pérez-Muñuzuri, Int. J. Bifurc. and Chaos, 8, 1733 (1998).

[139] I.P. Mariño, E. Rosa, Jr. & C. Grebogi, Int. J. Bifurc. Chaos, (in press, 1999a).

[140] I.P. Mariño, V. Pérez-Muñuzuri, V. Pérez-Villar, E. Sánchez & M.A. Matias, Physica D, (in press, 1999b).

[141] G. Le Masson, S. Le Masson & M. Moulins, Prog. Biophys. Molec. Biol. 64, 201 (1995).

[142] M.A. Matias, *Tesis Doctoral: Control y* Sincronización de *Sistemas Caóticos,* (Univ. de Salamanca, 1996).

[143] M.A. Matias, V. Pérez-Muñuzuri M.N. Lorenzo, I.P. Mariiio, & V. Pérez-Villar, Phys. Rev. Lett. 78, 219 (1997a).

[144] M.A. Matias, J. Güémez, V. Pérez-Muñuzuri, I.P. Mariño, M.N. Lorenzo & V. Pérez-Villar, Europhys. Lett. 37, 379 (1997b).

[145] M.A. Matías, J. Güémez& C. Martin, Phys. Lett. A *226, 264* (1997c).

[146] M.A. Matías & J. Güemez, Phys. Rev. Lett. 81, 4124 (1998).

[147] T. Matsumoto, L.O. Chua & M. Komuro, IEEE Trans. Circuits Syst. 23, 798 (1985).

[148] P.C. Matthews & S. H. Strogatz, Phys. Rev. Lett. 65, 1701 (1990).

[149] A. Mehrotra, GSA4 *System Engineering,* (Artech House, Inc., USA, 1997).

[150] R. Mirollo & S.H. Strogatz, SIAM J. Appl. Math. 50, 1645 (1990).

[151] A. Moiseff, & M. Konishi, J. Neurosci. 1, 40 (1981).

[152] G.J. Mpitsos, R.M. Burton, H.C. Creech & S.S. Soinla, Brain Res. Bull. 21, 529 (1988).

[153] A.P. Muñuzuri, V. Pérez-Muñuzuri, V. Pérez-Villar & L.O. Chua, IEEE Trans. Circuits Syst. 40, 872 (1993).

[154] A.P. Muñuzuri, V. Perez Muñuzuri, M. Gomez-Gesteira, L.O. Chua & V. Pérez-Villar, Int. J. Bifurc. Chaos 5, 17 (1995).

[155] A.P. Muñuzuri, M. DeCastro, V. Perez Muñuzuri, M. Gómez-Gesteira, I.P. Marino, E. Hofer & V. Pérez-Villar, *An Electronic real-time model of one-dimensional discontinuous conduction of the cardiac impulse realized with Chua's circuits,* , 439-442 (In Industrial Applications in Power Systems, Computer Science and Telecomunications, Vol. I., edited by IEEE Central and South Italy section, 1996).

[156] J.D. Murray, *Mathematical Biology* (Springer-Verlag, New York, 1989).

[157] N. Nakagawa. & Y. Kuramoto, Prog. Theor. Phys. 89, 313 (1993).

[158] Y. Nishio, N. Inaba & S. Mori, *Chaotic phenomena in an autonomous circuit with nonlinear inductor,* in ISCAS, 942 (1990).

[159] P. Noll, IEEE Signal Processing Magazine 14, 59 (1997).

[160] H. Nozawa, .Chaos 2, 377 (1992).

[161] M.J. Ogorzalek, IEEE Trans. Circuits Syst. 36, 1221 (1989).

[162] K. Okuda & Y. Kuramoto, Prog. Theor. Phys. 86, 1159 (1991).

[180] V. Pérez-Muñuzuri, M. Gómez-Gesteira, V. Pérez-Villar & L.O. Chua, Int. J. Bifurc. Chaos 3, 211 (1993).

[181] V. Perez-Muñuzuri, M. Alonso, L.O. Chua & V. Pérez-Villar, Int. J. Bifurc. Chaos 4, 1631 (1994).

[182] V. Pérez-Villar, A.P. Pérez-Muñuzuri & V. Pérez-Muñuzuri, Int. J. Bifurc. Chaos 3, 1067 (1993).

[183] E. Peter, Chaos and Order on *Capital Markers,* (John Wiley & Sons, 1991).

[184] V. Petrov, V. Gáspár, J. Masere & K. Showalter, Nature 361, 240 (1993).

[185] A.S. Pikovsky & P. Grassberger, J. Phys. A Math. Gen. 24, 4587 (1991).

[186] J.G. Proakis, *Digital Communications,* (McGraw-Hill Inc., Third Edition, Singapore, 1995).

[187] M.I. Rabinovich & D.I. Trubetskov, *Introduction to the Theory of Oscillations and Waves,* (Kluwer, Amsterdam, 1989).

[188] J. Rifá & LL. Huguet, Comunicución *Digital,* (Masson S.A., Spain, 1991).

[189] E. de1 Rio, M.G. Velarde, A. Rodriguez-Lozano, N.F. Rul'kov & A.R. Volkovskii, Int. J. Bifurc. Chaos 4, 1003 (1994).

[190] F. Romeiras, C. Grebogi, E. Ott & W. P. Dayawansa, Physica D 58, 165 (1992).

[191] E. Rosa, Jr., S. Hayes & C. Grebogi, Phys. Rev. Lett. 78, 1247 (1997).

[192] G. Rose & W. Heiligenberg, Nature 318, 178 (1985).

[193] M.G. Rosenblum, A.S. Pikovsky &J. Kurths, Phys. Rev. Lett. 76, 1804 (1996).

[194] M.G. Rosenblum, A.S. Pikovsky & J. Kurths, Phys. Rev. Lett. 78, 4193 (1997).

[195] R. Roy, Z. Gills & K.S. Thornburg, Opt. Photonics News 5, 8 (1994).

[196] R. Roy & K.S. Thornburg, Phys. Rev. Lett. 72, 2009 (1994).

[197] N.F. Rul'kov, A.R. Volkovskii, A. Rodriguez-Lozano, E. de1 Rio & M.G. Velarde, Int. J. Bifurc. Chaos Appl. Sci. Eng. 2, 669 (1992).

[198] N.F. Rul'kov & A.R. Volkovskii, Tech. Phys. Lett. 19, 97 (1993).

[199] N.F. Rul'kov, A.R. Volkovskii, A. Rodriguez-Lozano, E. del Rio & M.G. Velarde, Chaos, Solitons, Fractals 4, 201 (1994).

[200] N.F. Rul'kov, M.M. Sushckik, L.S. Tsimring & H.D.I. Abarbanel, Phys. Rev. E 51, 980 (1995).

[201] N.F. Rul'kov & M.M. Sushckik, Phys. Lett. A 214, 145 (1996).

[202] N.F. Rul'kov & M.M. Sushckik, Int. J. Bifurc. Chaos 7, 625 (1997).

[203] E. Sánchez, M.A. Matias & V. Pérez-Muñuzuri, Phys. Rev. E 56, 4068 (1997).

[204] E. Sánchez & M.A. Matias, Phys. Rev. E 57, 6184 (1998).

[205] E. Sánchez, M.A. Matias & V. Pérez-Muñuzuri, IEEE Trans. Circuits Syst. I 46 (in press, 1999).

[206] V.V. Shakhgildyan & A.A. Lyahovkin, *Phase-Locked Loops*, (Svjaz, Moscow, 1972).

[207] M.L. Shik, G.N. Orlovsky, Physiol. Rev 56, 465 (1976).

[208] T. Shimizu & N. Morioka, Phys. Lett. A 66, 182 (1978).

[209] T. Shinbrot, E. Ott, C. Grebogi & J. A. Yorke, Nature 363, 411 (1993).

[210] K.M. Short, Int. J. Bifurc. Chaos 4, 959 (1994).

[211] T. Sikora, IEEE Signal Processing Magazine, 14, 82 (1997).

[212] M. Silber, L. Fabiny & K. Wiesenfeld, J. Opt. Soc. Am. B 10, 1121 (1993).

[213] J. Singer, Y.Z. Wang & H.H. Bau, Phys. Rev. Lett. 66, 1123 (1991).

[214] B. Sklar, *Digital Communications, Fundamentals and Applications*, (Prentice-Hall Inc., USA, 1988).

[215] T. Sobrino, M. Alonso, V. Pérez-Muñuzuri & V. Pérez-Villar, Eur. J. Phys. 14, 74 (1993).

[216] H. Sompolinsky, D. Golomb & D. Kleinfeld, Phys. Rev. A 43, 6990 (1991).

[217] C.T. Sparrow, J. Math. Analysis and Applications 83, 275 (1981).

[218] W. Stallings, Data and Computer Communications, (Prentice-Hall Inc., Fourth Edition, Singapore, 1994).

[219] P.S.G. Stein, Ann. Rev. Neurosci. 1, 61 (1978).

[220] S.H. Strogatz, C.M. Marcus, R.M. Westervelt & R.E. Mirollo, Physica D 36, 23 (1989).

[221] S.H. Strogatz & I.N. Stewart, Sci. Am. 269, 102 (1993).

[222] N. Suga, Sci. Am. 262, 34 (1993).

[223] D.Y. Tang, R. Dykstra, M.W. Hamilton & H.R. Heckenberg, Chaos 8, 697 (1998).

[224] D.J. Tritton, Physical Fluid Dynamics (Oxford: Clarendon, 1988).

[225] L.S. Tsimring & M.M. Sushchik, Phys. Lett. A 213, 155 (1996).

[226] A.M. Turing, Phil. Trans. Roy. Soc. Lond. B 237, 37 (1952).

[227] N.N. Verichev, *Mutual synchronizution in chaotic systems,* in Methods of the Qualitative theory of Differential Equations, 47-57 (Gorky University Press, Gorky, 1986).

[228] N.N. Verichev & A.G. Maksimov, Izuv. VUZ Radiofiz. RPQEAC. 32, 713 (1989).

[229] A.R. Volkovskii & N.F. Rul'kov, Sov. Tech. Phys. Lett. 15, 249 (1989).

[230] H. Wang & E.H. Abed, *Bifurcation control of chaotic dynamical systems,* Proceedings of IFAC Nonlinear Control Systems Design Symposium, Bourdeaux (1992).

[231] A.T. Winfree, J. Theor. Biol 16, 15 (1968).

[232] A.T. Winfree, *The geometry of biological time* (Springer, New York, 1980).

[233] A.T. Winfree, *When Time Breaks Down* (Princeton University Press, Princeton, 1987).

[234] H.G. Winful & L. Rahman, Phys. Rev. Lett. 65, 1575 (1990).

[235] A. Wolf, J.B. Swift, H.L. Swinney & J.A. Vastano, Physica D 16 285 (1985).

[236] C.W. Wu & L.O. Chua, Int. J. Bifurc. Chaos 3, 1619 (1993).

[237] C.W. Wu & L.O. Chua, Int. J. Bifurc. Chaos 4, 979 (1994).

[238] J.H. Xiao, G. Hu & Z. Qu, Phys. Rev. Lett. 77, 4162 (1996).

[239] T. Yamada & H. Fujisaka, Prog. Theor. Phys. 70, 1240 (1983).

[240] T. Yang & L.O. Chua, IEEE Trans. Circuits Syst., II: Fundam. Theory AppI. 43, 817 (1996).

[241] E.D. Yorke & J.A. Yorke, J. Stat. Phys. 21, 263 (1979).

[242] M. Yoshimoto, K. Yoshikawa & Y. Mori, Phys. Rev. E 47, 864 (1993).

[243] A.L. Zheleznyak & L.O. Chua, Int. J. Bifurc. Chaos 4, 639 (1994).

[244] G.Q. Zhong & F. Ayrom, Int. J. Cir. Theor. Appl. 13, 93 (1985).

[245] V.S. Zykov, *Simulation of Wave Processes in Excitable Media* (Manchester Univ. Press, 1987).